LATERAL TORSIONAL BUCKLING OF WOODEN BEAM-DECK SYSTEMS

By

Yang Du

A thesis submitted to University of Ottawa
in partial fulfillment of the requirements for
Masters of Applied Science in Civil Engineering

Department of Civil Engineering
Faculty of Engineering
University of Ottawa

Abstract

A theoretical study is conducted for the lateral torsional buckling of wooden beam-deck assemblies consisting of twin beams braced by tongue-and-groove decking at the top. Two models are developed, each with a series of analytical and numerical solutions formulated. The first model targets twin-beam-deck assemblies where deck boards and other components are detailed to provide full continuous lateral restraint while the second model is built for situations where the beams are allowed to sway laterally and the relative lateral movement between the beams is partially restrained by the deck boards. In the first model, focus is on wind uplift while in the second model, both gravity and uplift loading scenarios are investigated.

In the first model, an energy method is adopted and the principle of stationary potential energy is evoked to formulate closed-form solutions, energy-based solutions and a finite element solution. The validity of the present solutions is verified against a finite element based ABAQUS model. Similarly, a family of solutions is developed under the sway model and verified against the ABAQUS. Parametric studies are conducted for both models to examine the effects of various variables on the buckling capacity. A comparative investigation on the behavioral difference between the two models under ABAQUS is also presented.

Overall, the restraining effects of deck boards bracing either on the beam compression or tension side is observed to have a significant influence on the lateral torsional buckling capacity of the twin-beam-deck assemblies.

Acknowledgements

I would like to thank my supervisors Dr. Magdi Mohareb and Dr. Ghasan Doudak for their academic and financial support. It was my great honor to study under your co-supervision. I also want to express my deepest gratitude to Dr. Magdi Mohareb whose profound knowledge and expertise guided me through all the academic challenges and who taught me how to solve problems, write reports and present my ideas to others. Those weekly meetings we had would be one of the greatest memories that I will always cherish.

I would also like to thank my fellow graduate students, Mr. Ye Hu and Mr. Rémi St-Amour Darveau for their guidance and help.

Finally, my deepest thanks go to my parents Zhenwen Du and Hongmei Wan for their sacrifice and encouragement.

TABLE OF CONTENTS

TABLE OF CONTENTS

TABLE OF CONTENTS

TABLE OF CONTENTS

TABLE OF CONTENTS

TABLE OF CONTENTS

LIST OF FIGURES

LIST OF TABLES

CHAPTER 1:Introduction

1.1 Description of the Problem

1.1.1 Material properties of wood

Wood is generally considered as an orthotropic material with properties in longitudinal (*L*), radial (*R*) and tangential (*T*) directions different and independent from each other. The longitudinal axis is parallel to the grain, the radial axis is perpendicular to the grain and normal to the growth rings, and the tangential axis is perpendicular to the grain but tangent to the growth rings (FPL, 2010). These axes are shown in Figure 1.1.

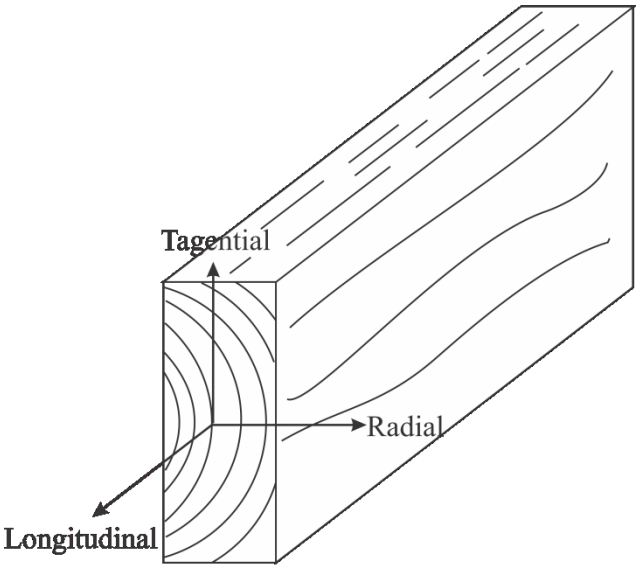

Figure 1.1 Three principal axes of wood

Based on its orthotropic property, the material properties of wood are described by twelve constants, i.e., three moduli of elasticity E, three shear moduli G, and six Poisson's ratios μ. Based on FPL, 2010, the moduli of elasticity E and Poisson's ratios μ are interrelated. Therefore, only nine of the twelve properties are independent.

Xiao (2014) conducted a lateral torsional buckling sensitivity analysis using the finite element software ABAQUS for those independent variables. It was concluded from his study that the modulus of elasticity E_L along the longitudinal direction and transverse shear modulus G_T are the only two variables that affect the lateral torsional buckling capacity. This constitutes the basics of the present investigation.

1.1.2 Lateral torsional buckling of beam-deck assemblies

Practical and aesthetic requirements for modern buildings, public infrastructure, sport stadiums, arenas, etc. involve large spaces with little or no visual obstruction. This prompts the wide use of long and deep beams in engineering practice. Deep beams are efficient in bridging long spans but are prone to lateral torsional buckling as a governing failure mode.

In wood structures, beams are commonly connected to plank deck boards through fasteners. Figure 1.2 shows a typical wooden twin-beam-deck assembly. The deck boards may enhance the lateral torsional buckling capacity by suppressing the lateral displacements (or relative lateral displacements) and reducing the twisting along the longitudinal axis. The restraining action of decking to wooden beams against lateral torsional buckling needs to be quantified. Current wood design standards in North America (e.g., CAN-CSA O86 2014, NDS 2015) recognize the beneficial role of deck boards in improving the lateral torsional buckling capacity. For timber beams, the lateral torsional buckling mode is considered to be suppressed when the deck boards can be assumed to prevent the lateral displacement along the beam compression edge. However, no recommendations are available for cases where (1) the tension edge is restrained, and (2) the deck boards can only provide partial lateral restraint relative to rigid lateral restraint.

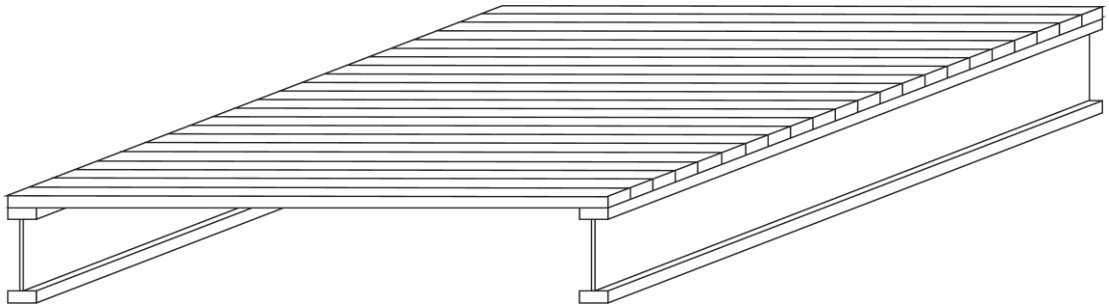

Figure 1.2 Wooden twin-beam-deck system

1.2 Objectives of the Research

Within the above context, the main objective of the present study is to analyze the lateral torsional buckling of wooden floor and roof systems and assess the effects of key variables on the buckling capacity. The main focus is on twin-beam-deck assemblies where two identical beams are braced at their top by individual deck boards. Given the

dimensions of the deck boards and the configurations of the deck connections, twin-beam-deck assemblies can be categorized into (1) non-sway model where the deck boards and other components are detailed to provide full lateral restraint, and (2) sway model where the deck boards are assumed to provide partial lateral restraint. The main research goals include (1) developing analytical and numerical solutions that are capable of predicting lateral torsional buckling capacity for both models, (2) quantitatively assessing the effects of deck bracing on the buckling capacity, and (3) comparing the behavioral difference between the sway and non-sway models. Under both models, wind uplift loads are of primary interest as (1) no guidelines in design standards are available for such loading, and (2) wind uplift is generally considered to be more detrimental than gravity loads simply because under such loading conditions the beams' bottom fibers are in compression and unrestrained. Gravity loads are also investigated in the second series of models for cases where wooden floor system is subjected to service loads.

1.3 Scope of the Research

To achieve the objectives, two finite element models based on the commercial software ABAQUS are developed to assess the behavioral difference between the sway and non-sway models. Then, two series of analytical and numerical solutions, each corresponding to the sway or the non-sway model, are developed and compared against ABAQUS results. The first series is aimed for the buckling analysis of the twin-beam-deck assemblies where deck boards and other components are detailed to provide full lateral restraint, i.e. fully prevent sway at the deck level, while the second series is built for situations where the beams are allowed to sway laterally. In such applications, the deck is assumed to partially restrain the relative lateral displacements between the twin beams. The partial twisting restraint provided by the deck bending stiffness is captured in both series of solutions. Parametric studies are conducted for wooden twin-beam-deck assemblies with practical dimensions and material properties to investigate the effects of key parameters on the buckling capacity.

1.4 Outline of the Thesis

The thesis is organized in a paper format with Chapter 3, Chapter 4 and Chapter 5 as three separate research papers.

Chapter 2 presents a literature review of the lateral torsional buckling of continuously restrained beams.

Chapter 3 presents the sway and non-sway models developed in ABAQUS for twin-beam-deck assemblies under wind uplift. In both models, one-dimensional beam elements are used to represent the twin beams and individual deck boards. A comparative study is conducted to highlight the key behavioral differences between the models.

In Chapter 4, a series of analytical and numerical solutions are developed for the lateral torsional buckling analysis of twin-beam-deck systems under wind uplift. The deck boards are assumed to provide continuous rigid lateral and partial twisting restraints at the top of both beams. Four solutions are developed: (1) a closed-form solution for simply-supported beams under uniform moments, (2) an analytical solution for beams with arbitrary boundary conditions and subjected to uniform moments, (3) an energy-based approximate solution for simply-supported beams under non-uniform moments, (4) a finite element solution (with a programme developed in Matlab) capable of solving general boundary and loading conditions. All solutions are verified against the ABAQUS non-sway model. A parametric study then examines the effects of various parameters on the lateral torsional buckling capacity of wooden twin-beam-deck assemblies.

Chapter 5 presents a series of solutions for the lateral torsional buckling analysis of twin-beam-deck systems where the beams are allowed to sway laterally and the deck boards are assumed to partially restrain the lateral displacements and angles of twist of the beams. Both gravity loading and wind uplift loading are investigated. The characteristics of nail properties in wooden joints are captured in this model. Similar to Chapter 4, closed-form solutions, energy-based approximate solutions, a beam FEA formulation (with a programme developed in Matlab) are developed and the ABAQUS sway model is presented for verification. A parametric study is then conducted to examine the effect of various design parameters on the critical moments of the system.

Chapter 6 provides a summary of the research, outlines the main conclusions, and proposes future extensions of the work.

List of Symbols

E	modulus of elasticity;
E_L	modulus of elasticity along longitudinal direction;
G	shear modulus;
G_T	transverse shear modulus;
L	longitudinal direction;
R	radial direction;
T	tangential direction;
μ	Poisson's ratio.

References

[1] *ABAQUS 6.12-3* [Computer software]. Providence, RI, Dassault Systèmes Simulia.

[2] American Wood Council. (2015). "National Design Specification for Wood Construction." *ANSI/AWC NDS-2015,* Virginia, U.S.

[3] Canadian Standard Association (CSA). (2014). "Engineering design in wood." *O86-14,* Mississauga, Ontario, Canada.

[4] Forest Products Laboratory (FPL). (2010). Wood Handbook-Wood as an Engineering Material. Madison, U.S.

[5] Xiao, Q. (2014). "Lateral Torsional Buckling of Wood Beams", M.A.Sc. thesis, Dept. of Civil Engineering, Uni. of Ottawa, Ontario, Canada.

CHAPTER 2: LITERATURE REVIEW

In this Chapter, previous studies contributing directly to the subject of lateral torsional buckling of continuously restrained beams are of primary interest and are organized chronologically and reviewed in a detailed fashion. Studies that are generally pertinent to the subject of current investigation (i.e., studies involving local and distortional buckling, load-slip relationship for nailed wood connections) are reviewed in a condensed manner in Chapter 3, 4 and 5.

2.1 Detailed Review on Lateral Torsional Buckling of Continuously Restrained Beams

Vlasov (1961) formulated the general differential equations for a beam embedded in an elastic medium. A buckling solution was developed for simply-supported beams under uniform moments with a continuous rigid lateral restraint offset from the shear center and a continuous elastic twisting restraint. The critical moment was also determined for a beam braced by continuous elastic lateral and twisting restraints and subjected to uniform moment.

Zahn (1965) formulated the governing equilibrium conditions for wooden rectangular beams laterally restrained along the beam centroidal axis by the shear action of deck boards. A closed-form solution was developed for a simply-supported beam under uniform moment. Critical moments for simply-supported beams under uniformly distributed loads or cantilevers beams were obtained through a power-series solution.

Taylor and Ojalvo (1966) formulated a buckling solution for doubly-symmetric beams braced by continuous or discrete elastic torsional restraint under various loading cases. For simply-supported beams under uniform moments, a closed-form solution was obtained by assuming sinusoidal for the displacement fields. For the cases of concentrated load or uniformly distributed load, the buckling loads were determined through an iteration process.

Pincus and Fisher (1966) investigated the buckling of two I-section beam-columns laterally braced by a diaphragm. The diaphragm was considered as axially inextensible. Under this assumption, the beams were assumed to undergo the same lateral displacement and angle of twist in the same direction. The in-plane shear stiffness was considered as the principal restraining action within the diaphragm. Using the

Euler-Lagrange Conditions, they formulated the equations of neutral stability and solved them approximately by assuming half-sine waves for the displacement fields. Critical moments for beams were expressed in terms of the shear rigidity of the diagram. The resulting analytical predictions were verified against experimental results.

Errera et al. (1967) extended the solution of Pincus and Fisher (1966) to several cases: (1) beam-columns laterally braced at both flanges by shear diaphragms with or without angles of twist suppressed, (2) beam-columns laterally braced at one flange by the shear stiffness with or without twist suppressed, and (3) beams laterally braced at one flange by a shear diaphragm with fixed boundary conditions. Tests were also conducted for twin-column assemblies under concentric loading with a diaphragm connected to one or both flanges and twin beams assemblies under uniform flexural loading with diaphragm bracing on the compression flange. Experimental results agreed well with theoretical predictions.

Apparao (1968) investigated the lateral torsional buckling of beam-diaphragm assemblies consisting of two beams with I or C section laterally supported at their compression flanges by a shear diaphragm. The equilibrium equations were developed under the condition of uniform moments and distributed longitudinal forces induced by shear action of the diaphragm. For simplicity, the diaphragm transverse bending rigidity was conservatively neglected. Two types of solutions were developed: (1) a load-deformation solution in which initial imperfections were considered, and (2) an eigen-value solution leading to critical moments, which agreed with Errera et al. (1967).

Zahn (1973) analytically investigated the lateral torsional buckling of rectangular timber beams laterally braced by the deck shear action. For a given beam within a floor system, the total potential energy was assumed to consist of two contributions: the beam and the tributary strip of deck boards. The stationarity condition of the total potential energy was evoked to recover the governing differential equations of neutral stability. By enforcing boundary conditions, a closed form solution was obtained for simply-supported beams under uniform moments and the result was shown to agree with that in Errera et al. (1967). For the case of concentrated load or uniformly distributed load, the critical moment was obtained through a power series solution. Cantilever beams were also investigated.

Based on the analytical solution of Apparao (1968), Nethercot and Trahair (1975) proposed a design approach for I-section beams whose top flanges are laterally braced by corrugated steel diagrams. The design procedure quantifies the diaphragm shear stiffness and strength required for beams to attain the yield moment resistance.

Hancock and Trahair (1978) formulated a finite element eigen-value solution for the lateral torsional buckling of continuously braced beam-columns. They characterized the diaphragm as elastic restraints partially restraining lateral displacement, angle of twist, weak-axis rotation and warping. Their solution was an extension of the Barsoum and Ghallagher (1970) finite element based on Hermitian polynomials to interpolate the lateral displacement and twisting fields, in which they added a stiffness matrix contribution which captures continuous elastic restraint.

Trahair (1979) formulated an eigen-value buckling solution for beam-columns of mono-symmetric cross-sections with continuous partial restraints for lateral displacement, angle of twist, weak-axis rotation and warping. The governing equations were obtained through either direct equilibrium or an energy-based approach. A closed-form solution was recovered for uniform moment.

Lawson and Nethercot (1985) proposed a critical moment equation for beams braced by a shear diaphragm, which incorporates the effects of moment gradient and load position. The criteria to assess the adequacy of the diaphragm shear stiffness were also developed.

Using a direct variational approach, Assadi and Roeder (1985) investigated the lateral torsional buckling of cantilevers with continuous elastic lateral restraint. A numerical buckling solution for a fix-free cantilever beam subject to a concentrated load at the free end was obtained. The effects of restraint height and load position were analyzed. It was concluded that in practical situations, the stiffness provided by continuous bracing greatly exceeded the stiffness requirement for achieving rigid lateral restraint.

Albert and Dawe (1990) developed a finite element solution for the stability of two-span continuous I-section beams whose top flanges were restrained by translational and rotational springs. The effects of span length, load condition, and additional web stiffeners were investigated. For the purpose of capturing the interaction between the web and flanges, the flanges were modeled by one-dimensional beam elements while the web was modeled by plate elements. The

inelastic behavior was estimated by neglecting the yielded areas of the beam and computing the stiffness matrices based on the remaining elastic core. The results based on the finite element solution agreed with experimental results.

Lucas et al. (1997a) formulated a non-linear elasto-plastic finite element model with geometric nonlinearity. The model captured purlin-sheeting interaction and successfully modelled cross-sectional distortion and local buckling. In another study, Lucas et al. (1997b) developed a simplified model where the effects of sheeting were idealized as elastic springs.

Helwig and Frank (1999) conducted an eigenvalue finite-element analysis using the commercial software ANSYS on the lateral torsional buckling of twin beams with light-gage metal sheeting acting as a shear diaphragm. Loading cases investigated were uniform moment, uniformly distributed load and mid-span concentrated load. The study also investigated the load position effect. For the case of uniform moment, the finite-element solution agreed well with those obtained by Nethercot and Trahair (1975). They suggested new design equations for transverse loads applied at different heights. Also proposed was the diaphragm shear stiffness required to achieve the design moment resistance.

Park and Kang (2003) developed a shell based finite element model under MSC/NASTRAN for the lateral torsional buckling of an I-section beam with continuous rigid lateral bracing at the top flange subjected to transverse loading applied at beam mid-height and end moments. They proposed simplified design equations based on their model. In a subsequent study conducted by Park et al. (2004), the result based on the finite element model for uniform moment was in agreement with that of Trahair (1979). New design equations for beams subjected to top flange loading were presented based on the results of the finite-element investigation.

Li (2004) performed an energy-based analysis on the lateral torsional buckling of Z-section beams partially restrained by metal sheeting restraining translational and rotational displacements. Based on the principle of minimum potential energy, the pre-buckling displacements and moment distribution were obtained, which were then used in the buckling analysis. For the special case where the translational stiffness is infinite and the rotational stiffness is negligible, the critical loads for various loading cases were obtained by assuming displacement fields to be spline functions. Chu et al.

(2004) expanded the study for channel-section beams.

Larue et al. (2007) conducted an eigenvalue lateral torsional buckling analysis of I-section beams with continuous rigid lateral restraint. Similar to Vlasov (1961), the lateral displacement and twist angle were coupled in the model. A numerical procedure was proposed for solving the partial differential equations in which the displacement fields were approximated by trigonometric functions. The study highlights that the restraint on the beam tension flange is not sufficient to limit lateral buckling.

Helwig and Yura (2008) formulated a finite element model based on the commercial software ANSYS for the lateral torsional buckling of twin beams with a shear diaphragm. In the model, the diaphragm was modeled by truss element which is more computationally effective than shell element used in the previous model (Helwig and Frank 1999). They proposed a moment gradient factor equations for beams with stocky webs and suggested the optimal diaphragm shear stiffness for beams with initial imperfections.

Khelil and Larue (2008) investigated the lateral torsional buckling of I-section beams continuously restrained by elastic lateral restraint at either the beam compression or tension flange. An energy method was adopted in the analysis. The internal strain energy consisted of a beam contribution including linear and non-linear effects, as well as an elastic restraint contribution. The governing differential equations were obtained by evoking Euler-Lagrange conditions and were solved by the Galerkin method. Their solution was capable of predicting the lateral torsional buckling capacity for uniform or non-uniform moment distributions.

2.2 Summary of Literature

Given the main objective of the present study, the literature reviewed above can be categorized into non-sway models where the beam is fully restrained against lateral displacement and sway models where the lateral displacement is partially restrained. For lateral torsional buckling of non-sway models, only Vlasov (1961) and Larue et al. (2007) formulated analytical solutions. However, the Vlasov solution is limited to uniform moment loading, while the Larue et al. solution is restricted to simply-supported boundary conditions. In the present study, a finite element formulation will be developed for the non-sway model to accommodate more general boundary and loading conditions. For studies aimed for sway models, the majority (i.e.,

Zahn 1965, Pincus and Fisher 1966, Errera et al. 1967, Apparao 1968, Zahn 1973, Nethercot and Trahair 1975, Lawson and Nethercot 1985, Helwig and Frank 1999, and Helwig and Yura 2008) considered the diaphragm in-plane shear stiffness as the principal restraining action. In comparison, in the present sway model, the lateral restraint will be based on the combined lateral stiffness of individual deck boards and connectors.

Among all the literature reviewed, only Zahn (1965) and Zahn (1973) focused on the lateral torsional buckling of wooden beams. The present study will go beyond the solutions found in Zahn (1965) and Zahn (1973) in that the current study will (1) investigate both gravity and wind uplift loadings, (2) incorporate the load position effects, (3) capture the partial twisting restraint provided by deck bending action, and (4) assess the effects of various key parameters on the buckling capacity.

Previous lateral torsional buckling investigations were focused on either the non-sway or the sway model. No studies have specifically contributed to the comparison between the two modelling approaches. The present study, comprised of a series of analytical and numerical solutions developed for both the sway and non-sway models and an ABAQUS comparative study highlighting key behavior difference between the two models, is aimed to provide a more comprehensive understanding of the subject.

References

[1] Albert, C., and Dawe, J. (1990). "Buckling of continuous steel girders with flange restraint." *Can. J. Civ. Eng.,* 17(2), 121-128.

[2] Apparao, T. V. S. R. (1968). "Problems in structural diaphragm bracing." *Report No. 331*, *Dept. of Struct. Engrg.,* Cornell Univ., Ithaca, N.Y.

[3] Assadi, M., and Roeder, C. W. (1985). "Stability of continuously restrained cantilevers." *J. Eng. Mech.,* 111(12), 1440-1456.

[4] Barsoum, R. S., and Gallagher, R. H. (1970). "Finite element analysis of torsional and lateral stability problems." Int. J. Numer. Methods Eng., 2(3), 335–352.

[5] Chu, X., Kettle, R., and Li, L. (2004). "Lateral-torsion buckling analysis of partial-laterally restrained thin-walled channel-section beams." *J. Constr. Steel Res.,* 60(8), 1159-1175.

[6] Errera, S. J., Pincus, G., and Fisher, G. P. (1967). "Columns and beams braced by diaphragms." *J. Struct. Div.,* 93(1), 295-318.

[7] Errera, S. J., and Apparao, T. (1976). "Design of I-shaped beams with diaphragm bracing. " *J. Struct. Div.*, 102(4), 769–781.

[8] Hancock, G. J., and Trahair, N. S. (1978). "Finite element analysis of the lateral buckling of continuously restrained beam-columns." *Civ. Engrg. Trans*., Institution of Engineers, Australia, CE20, 120-127.

[9] Helwig, T. A., and Frank, K. H. (1999). "Stiffness requirements for diaphragm bracing of beams." *J. Struct. Eng.,* 125(11), 1249-1256.

[10] Helwig, T. A., and Yura, J. A. (2008). "Shear diaphragm bracing of beams. I: Stiffness and strength behavior." *J. Struct. Eng.,* 134(3), 348-356.

[11] Khelil, A., and Larue, B. (2008). "Simple solutions for the flexural-torsional buckling of laterally restrained I-beams." *Eng. Struct.,* 30(10), 2923-2934.

[12] Larue, B., Khelil, A., and Gueury, M. (2007). "Elastic flexural–torsional buckling of steel beams with rigid and continuous lateral restraints." *J. Constr. Steel Res.,* 63(5), 692-708.

[13] Lawson, R., and Nethercot, D. (1985). "Lateral stability of I-beams restrained by profiled sheeting." *The Struct. Engr*., London, 63B(1), 3–13.

[14] Li, L. (2004). "Lateral–torsional buckling of cold-formed zed-purlins partial-laterally restrained by metal sheeting." *Thin-Walled Struct.,* 42(7), 995-1011.

[15] Lucas, R., Al-Bermani, F., and Kitipomchai, S. (1997). "Modelling of cold-formed

purlin-sheeting systems—Part 1: Full model." *Thin-Walled Struct.,* 27(3), 223-243.

[16] Nethercot, D. A., and Trahair, N. S. (1975). "Design of diaphragm-braced I-beams." *J. Struct. Div.,* 101(10), 2045-2061.

[17] Park, J., and Kang, Y. (2003). "Lateral buckling of beams with top bracing." *Struct.Eng.Mech.,* 16(5), 613-625.

[18] Park, J. S., Stallings, J. M., and Kang, Y. J. (2004). "Lateral–torsional buckling of prismatic beams with continuous top-flange bracing." *J. Constr. Steel Res.,* 60(2), 147-160.

[19] Pincus, G., and Fisher, G. P. (1966). "Behavior of diaphragm-braced columns and beams." *J. Struct. Div.,* 92(2), 323-370.

[20] Taylor, A. C., and Ojalvo, M. (1966). "Torsional restraint of lateral buckling." *J. Struct. Div.,* 92(2), 115-130.

[21] Trahair, N. S. (1979). “Elastic lateral buckling of continuously restrained beam columns.” *The profession of a civil engineer*, D. Campbell-Allen and E. H. Davis, eds., Sydney University Press, Sydney, Australia, 61–73.

[22] Vlasov, V. Z. (1961). *Thin-walled elastic beams*. 2nd. ed., Israel Program for Scientific Translations, Jerusalem.

[23] Zahn, J. (1965). "Lateral stability of deep beams with shear-beam support." *U.S.D.A. Forest Service Research Paper FPL 43.*

[24] Zahn, J. J. (1973). "Lateral stability of wood beam-and-deck systems." *J. Struct. Div.,* 99(7), 1391-1408.

CHAPTER 3: LATERAL TORSIONAL BUCKLING OF TWIN-BEAM-DECK ASSEMBLIES UNDER WIND UPLIFT – SWAY VERSUS NON-SWAY MODELS

Abstract

Simply-supported wooden beams nailed to deck boards subjected to wind uplift forces are subjected to compressive stresses at their bottom fibers. Because the bracing action of the decking is provided to the top fibers, it is unclear to what extent such restraints are effective in controlling lateral torsional buckling as a possible mode of failure. Thus, the present study aims to quantify the effects of restraints provided by deck boards on the lateral torsional buckling capacity of beams under wind uplift. Towards this goal, two finite element models based on ABAQUS are developed for a twin-beam-deck assembly. Both models capture the continuous partial twisting restraint provided by the deck bending action. In the first model, the deck is assumed to provide full lateral restraint to the twin beams so as to prevent sway while in the second model, the assembly is allowed to sway laterally. Comparisons between the results of both models are presented and key behavioral differences are highlighted. Both models show that the lateral torsional buckling capacity of twin-beam-deck assemblies under uplift is significantly enhanced by the deck restraining effects.

KEYWORDS: Lateral torsional buckling, beam-deck assembly, finite element analysis

3.1 Introduction

Timber roof structures typically consist of parallel deep beams braced on top by tongue-and-groove wood deck boards through nail connections. Deep beams are efficient in bridging long spans in such structures but are prone to lateral torsional buckling as a possible mode of failure. Deck boards can potentially improve the buckling capacity by partially restraining the twisting and lateral displacements. When subjected to wind uplift, simply-supported beams are subjected to compressive

stresses at their bottom fibers. The beneficial effect caused by the presence of bracing on the tension side of the beam has not been quantified in North American Standards (CSA O86 (2014), NDS 2015). Within this context, the present study develops two finite element models based on the commercial software ABAQUS for twin-beam-deck systems to quantitatively examine the deck restraining effects on the lateral torsional buckling of the beams. Both models capture the continuous partial twisting restraint provided by the deck bending action. In the first model, the deck is assumed to provide full lateral restraint to the twin beams so as to prevent sway at beams top while in the second model, the assembly is allowed to sway laterally and the relative partial lateral bracing is provided by a deck-joint assembly. The lateral stiffness of the deck-joint assembly incorporates the flexibility of the nailed joints in shear and the longitudinal flexibility of the deck boards. Parametric studies are performed under both models to investigate the effects of key parameters on the lateral torsional buckling capacity of the twin-beam-deck assemblies: beam and deck span, lateral restraint height and stiffness, and the contributions of lateral and twisting restraints. Comparisons between the predictions of both models are presented and key behavioral differences are highlighted.

3.2 Literature Review

Previous analytical studies on the stability of continuously restrained beams can be categorized into two types: (1) non-sway models (Section 3.2.1) where the beam is prevented from lateral movement at the top, and (2) sway models (Section 3.2.2) where the top of the beam is allowed to sway laterally and is partially restrained against lateral movement and/or angle of twist. Consistent with the objective of the study, only studies involving wind uplift are reviewed in the paper. Also, a review of relevant numerical studies based on finite element models under existing FEA software are provided in Section 3.2.3.

3.2.1 Non-sway models

Only a few studies have considered the case where the beam is restrained from swaying. This includes the work of Vlasov (1961) who formulated a lateral torsional buckling solution for simply-supported beams with a continuous rigid later restraint and a continuous elastic twisting restraint under uniform moments. An experimental verification of the Vlasov equation was provided by Roeder and Assadi (1982). Larue

et al. (2007) further generalized the buckling solution of Vlasov (1961) for linear and parabolic bending moment distributions with moment reversal.

3.2.2 Sway models

Vlasov (1961) also formulated a buckling solution for beams braced by continuous elastic lateral and twisting restraints and subjected to uniform moments. Taylor and Ojalvo (1966) extended Vlasov's work for beams with continuous or discrete elastic twisting restraint under uniform and non-uniform moments. Using the Euler-Lagrange Conditions, Errera et al. (1967) developed solutions for twin beams braced by the shear action of diaphragm and subjected to uniform moments. Hancock and Trahair (1978) formulated a finite element solution for continuously braced beam-columns where the deck is characterized as elastic restraints partially restraining lateral displacement, twisting along beam longitudinal axis, weak-axis rotation and warping. A closed-form solution for uniform moment was also developed by Trahair (1979). Khelil and Larue (2008) developed an energy-based solution for simply-supported beams with continuous relative partial lateral restraint. The solution was able to predict buckling capacity of beams with uniform and non-uniform moment distributions.

Pekoz and Soroushian (1982) modelled steel purlin-sheeting systems as beams on elastic foundation. Sokol (1996) modelled restrained purlins using elastic rotational foundation. Jiang and Davies (1997) studied the buckling behavior of purlin-sheeting systems based on the Generalized Beam Theory (GBT). Lucas et al. (1997a) formulated a non-linear elasto-plastic finite element model with geometric nonlinearity. The model captured purlin-sheeting interaction and successfully modelled cross-sectional distortion and local buckling. In another study, Lucas et al. (1997b) developed a simplified model where the effects of sheeting were idealized as elastic springs. Ye et al. (2002) adopted a finite strip method to investigate the local, distortional and lateral torsional buckling of zed-purlins restrained by steel sheeting. The lateral torsional buckling capacity of channel purlins laterally braced by sheeting was investigated by Chu et al. (2004). Li (2004) and Chu et al. (2005) expanded the study for zed sections. Basaglia et al. (2013) developed a GBT solution for the local, distortional and lateral torsional buckling of channel and zed purlins restrained by sheeting and subjected to uplift loading.

3.2.3 Finite element models

Helwig and Frank (1999) presented a finite element model based on ANSYS for twin I-section beams braced by a shear diaphragm. The beams were modelled by eight-node shell elements and the diaphragm was modelled by four-node shell elements to capture its shear action. Park and Kang (2003) as well as Park et al. (2004) developed a model under MSC/NASTRAN where an I-section beam was modelled by four-node shell elements and was rigidly restrained along the beam top flange. Helwig and Yura (2008) modified the model of Helwig and Frank (1999) by replacing the four-node shell elements with two-node truss elements to model the diaphragm shear action.

Compared with the models mentioned above, the present models capture the lateral (either rigid or partial) and partial twisting restraints provided by deck boards. In contrast, Park and Kang (2003) and Park et al. (2004) focused solely on rigid lateral restraints, while Helwig and Frank (1999) and Helwig and Yura (2008) focused on beams laterally braced by the diaphragm shear action. Another distinctive feature of the present models is that they specifically target wood beams while incorporating the unique characteristics of wood nailed connections.

3.3 FEA Model Description

3.3.1 Non-sway model

The finite element program ABAQUS 6.12-3 was used to perform the lateral torsional buckling analysis of the twin-beam-deck assemblies. The two-node B31OS element within the ABAQUS library was used to model the twin beams. Each node has seven degrees of freedom (i.e., three translations, three rotations, and one warping deformation). The B31 element was chosen to model the deck boards. The B31 element has two nodes with six degrees of freedom per node (i.e., three translations, and three rotations). Figure 3.1 shows the twin-beam-deck model developed in ABAQUS with B31OS elements depicted at the centroidal axes of twin beams (lying on Line 1) and B31 elements at the height of beam-deck interface (Line 2). The number of B31OS elements used in each beam was chosen to be consistent with the number of deck boards. Each centroidal node (Line 1 in Figure 3.1) was tied to the deck node (Line 2 in Figure 3.1) using a rigid link as defined by the BEAM type multi-point constraint (*MPC) feature in ABAQUS. Then, the *EQUATION feature

was used to activate only the transverse bending of the deck boards. Also, the lateral displacement of each deck node was restrained. The above kinematic constraints enforce continuous full lateral restraint while accounting for the partial twisting restraint provided by the deck bending action.

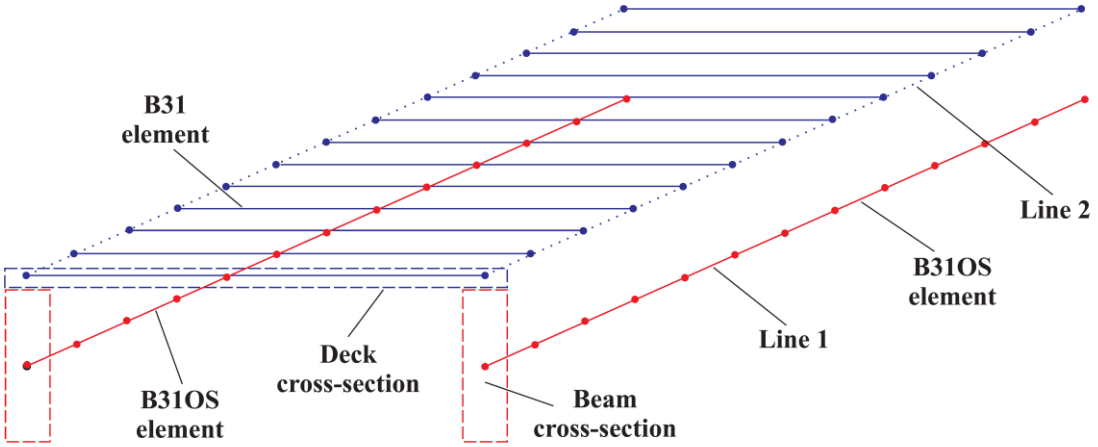

Figure 3.1 ABAQUS non-sway model

3.3.2 Sway model

Figure 3.2 shows the sway model of the twin-beam-deck assembly. Similar to the non-sway model, the B31OS and B31 elements were respectively chosen to model the twin beams and deck bending action. In addition, the two-node SPRING2 element was employed to model the relative partial lateral restrain between the top of both beams provided by the deck-joint assembly. The lateral stiffness k of a single deck board nailed at each end can be conceived to be that of three springs in tandem (i.e., two springs, each representing the shear stiffness of the joint k_j at the beam-deck interface, and another spring representing the deck axial stiffness k_d at the height of the beam-deck interface). By adding the flexibility of the three components, one obtains the equivalent stiffness k as $k = k_d k_j / 2k_d + k_j$. The shear stiffness of the nailed joint k_j was taken as the initial stiffness (i.e., gradient that joins the origin and 10% of lateral strength resistance governed by the smallest capacities amongst different failure modes) from the load-displacement equation recommended by CSA-O86 (2014) as

$$\Delta = 0.5 d K_m \left(\frac{F}{F_u} \right)^{1.7} \tag{3.1}$$

where Δ is the shear deformation of a single-nail joint, d is the nail diameter in mm, K_m is the service creep factor accounting for load duration and moisture level, F is the lateral load, and F_u is the lateral strength resistance as governed by the smallest capacities amongst different failure modes. In the present study, the value $K_m = 1$ was used.

For the sway model, each deck node on Line 2 in Figure 3.2 was tied to the centroidal node (Line 1). Also, each spring node (Line 3) was tied to the corresponding centroidal node (on Line 1). Both rigid links were defined using the BEAM type multi-point constraint (*MPC) feature in ABAQUS. Similarly, the *EQUATION feature was then used to activate only the transverse bending of the deck boards represented by B31 elements.

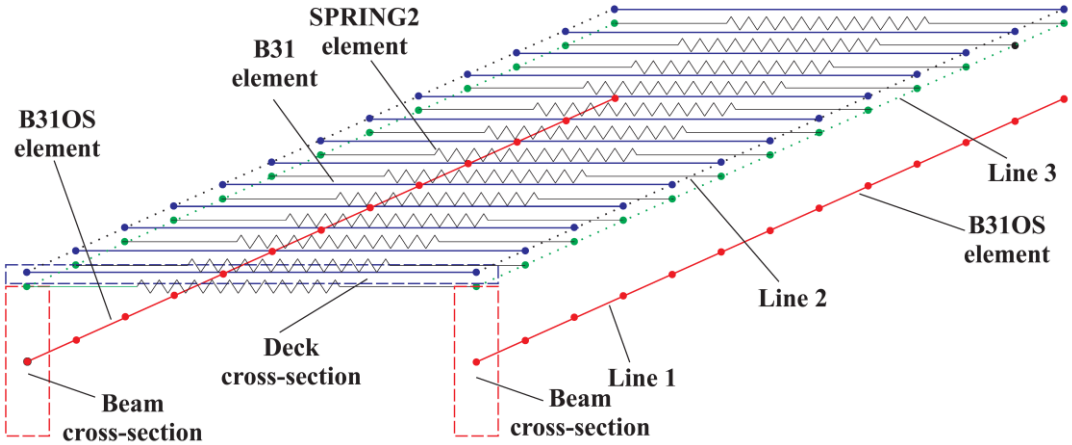

Figure 3.2 ABAQUS sway model

3.4 Parametric Study and Results

A twin-beam-deck assembly with 6 m beam span and 2 m deck span was chosen as a reference case. Beam material was assumed to be glu-laminated Spruce-Lodgepole Pine-Jack Pine 20f-EX with a 570 mm deep and 80 mm wide cross-section. The modulus of elasticity and shear modulus were assumed to be 10,300 MPa and 474 MPa, respectively. Based on a material failure mode, the nominal bending moment resistance for the beams as determined from CSA-O86 (2014) is 270 kNm. The deck boards were 38 mm thick and were assumed to be Spruce-Pine-Fir No. 2 grade with a modulus of elasticity of 10,000 MPa. Two 3.76 mm nails were assumed to be installed at each beam-deck interface. All material properties are based on CSA-O86 (2014) and FPL (2010).

For the reference case, a mesh sensitivity analysis was conducted for the sway and non-sway models to determine the number of elements required for convergence. Parametric studies were then conducted to examine the effect of various parameters on the lateral torsional buckling capacity by varying one parameter at a time. Since only uplift loading cases are investigated, the absolute value of critical moments is reported in the results.

3.4.1 Mesh sensitivity analysis

For the reference case, Figure 3.3(a,b) shows the results of the mesh study for the non-sway and sway models under three loading types: uniform moments, uniformly distributed loads (UDL) and mid-span concentrated loads. For the non-sway model (Figure 3.3a), the critical moment under uniform moments exhibits an oscillating behavior as the number of beam elements is increased and attains convergence at 80 elements per beam. In contrast, for the other two loading types, only 10 to 12 elements per beam were found to be needed for convergence. For the sway model, Figure 3.3b suggests that 12 elements per beam are enough for all three loading cases investigated. To ensure convergence, 80 elements per beam were used in all subsequent runs. For both models, a single B31 element was found to be adequate to represent the deck bending action.

3.4.2 Comparison of mode shapes

For the reference case, the buckling modes of the two models under UDL or mid-span concentrated loads are shown in Figure 3.4(a,b), respectively. For the case of UDL, Figure 3.4a indicates that the non-sway model is able to better control the beam lateral displacement than the sway model. For the case of mid-span concentrated loads, Figure 3.4b verified the above observation. Also, the non-sway model shows a better control of both displacement fields near the beam end supports.

3.4.3 Effect of beam span

For the twin-beam-deck assembly, the beam span was varied from 4 m to 10 m. All spans correspond either to an elastic or inelastic governing buckling failure mode. The deck span was kept constant at 2 m. The critical moments as predicted by both models under UDL and mid-span concentrated loads are shown in Figure 3.5(a,b), respectively. For the case of UDL, the non-sway model (Figure 3.5a) predicts a critical moment of 240 kNm for 4 m beam span. This compares with a slightly lower

238 kNm obtained from the sway model for the same span. As the beam span is increased, the non-sway model shows no significant capacity decrease while a 37.4% capacity decline is observed for the sway model when the span is 10 m. Similar conclusions can be drawn for the case of mid-span concentrated loading (Figure 3.5b). The above observations suggest no clear trend between critical moment and beam span for the non-sway model. Also, the buckling capacity predicted from the sway model is marginally lower than that based on the non-sway model for short beam spans.

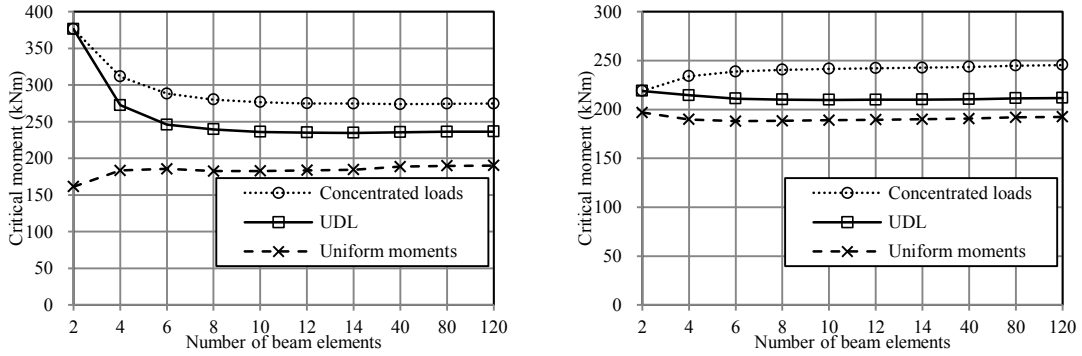

Figure 3.3 Mesh study for (a) non-sway model, (b) sway model

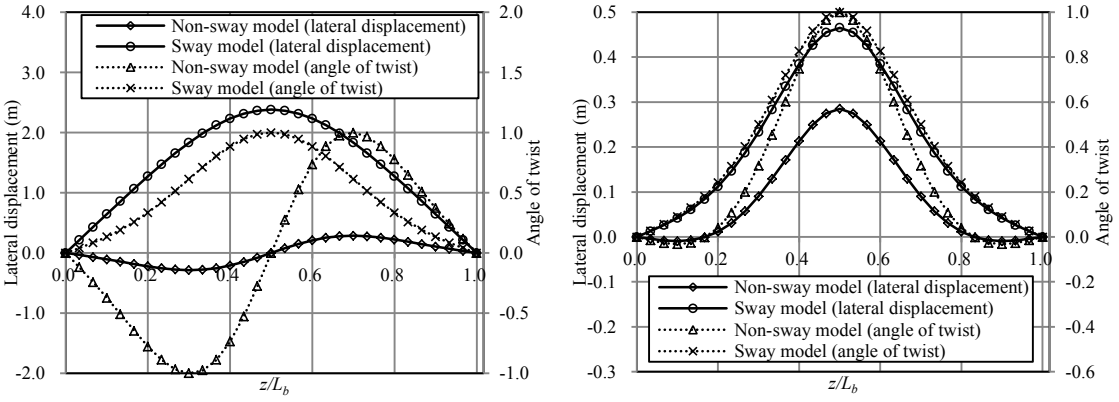

Figure 3.4 Buckling modes for (a) UDL, (b) mid-span concentrated loads

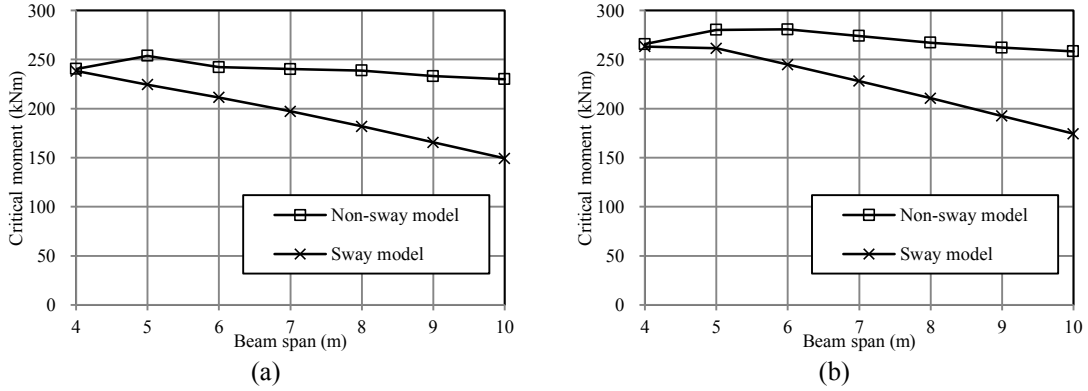

Figure 3.5 Effect of beam span on critical moment for (a) UDL, (b) mid-span concentrated loads

3.4.4 Effect of deck span

Two loading patterns (i.e., UDL and mid-span concentrated loads) were investigated for the twin-beam-deck assembly where the deck span was varied from 1 m to 5 m and the beam span was at a constant 6 m. For the case of UDL (Figure 3.6a), the non-sway model predicts a steady decline in critical moment as the deck span is

increased. In contrast, the sway model shows a slight capacity increase as the span increases from 1.0 m to 1.5 m, after which the critical moment exhibit a moderate drop. Similar conclusion is observed from the case of mid-span concentrated loads in Figure 3.6b. For both loading conditions, the buckling capacity difference between the sway and non-sway model is less when the deck span exceeds 2 m.

3.4.5 Effect of lateral restraint stiffness

For the twin-beam-deck assembly under UDL, Figure 3.7a depicts the critical moment as a function of the relative lateral stiffness per unit deck width $\bar{k}$, defined as $\bar{k} = k/b$, where b is the width of a single deck board. Four beam spans (i.e., 4, 6, 8 and 10 m) were studied while the deck span was kept constant at 2 m. For a beam span of 4 m, the critical moment increases steadily as the relative lateral stiffness $\bar{k}$ increases. When the beam span is 6 or 8 m, the critical moment is observed to increase before $\bar{k}$ reaches a threshold value, after which the critical moment remains constant, i.e., independent to the magnitude of $\bar{k}$. For a beam span of 10 m, the critical moment remains constant, irrespective of the magnitude of $\bar{k}$. For the reference deck-joint assembly, the relative lateral stiffness $\bar{k}$ corresponding to a single nail per joint is 5572 kN/m/m, while that based on two nails per joint is 9974 kN/m/m (Details are shown in Chapter 5). Both values are depicted by vertical lines on Figure 3.7a. For beam spans of 6 and 8 m, both values far exceed the threshold stiffness, thus ensuring that the critical moment is maximized. For a beam span of 4 m, the critical moment based on $\bar{k}$ corresponding to double nails per joint is marginally below the threshold, but is enough to develop nearly the full critical moment capacity. Thus, for the beam spans investigated, it is concluded that beam-deck connections with two nails are sufficient to develop full critical moment capacity.

3.4.6 Effect of lateral restraint height

For the case of UDL loading, Figure 3.7b shows the buckling capacity for the reference twin-beam-deck system as the lateral restraint is hypothetically moved from the beam shear center to the beam-deck interface. The non-sway model shows a steep capacity decline as the lateral restraint height moves upward. In contrast, the results from the sway model where the lateral stiffness per unit deck width $\bar{k}$ exceeds the

threshold value remain constant. Insight on the above observations can be provided by examining the associated mode shapes. For a relative lateral stiffness below the threshold value, the modes are observed to be symmetric. In contrast, when the relative lateral stiffness is beyond the threshold value, the modes become anti-symmetric, thus eliminating the dependence of the solution on the restraint height (Details are shown in Chapter 5).

3.4.7 Contributions of continuous lateral and twisting restraints

For the twin-beam-deck assembly where the beam span was varied from 4 to 10 m and deck span was kept constant at 2 m, three restraint scenarios are considered for the case of UDL loading in both models: (1) lateral and twisting restraints, (2) no lateral or twisting restraint, and (3) no restraints. For the non-sway model (Figure 3.8a), the large difference between the upper and lower solid lines indicates that the critical loads for laterally and torsionally restrained beams are several times higher than those based on unrestrained beams. For example, for a beam span of 10 m, the critical moment ratio between restrained and unrestrained beams is 6.3. In the non-sway model, the contribution of the partial twisting restraint is illustrated by the gap between the upper solid line and the dotted line. Also, the effect of rigid lateral restraint is illustrated by the gap between the dotted line and the lower solid line. The above comparison suggests that, for all the beam spans investigated, the partial twisting restraint is the prime contributor to the buckling capacity increase with the rigid lateral restraint playing only a minor role.

For the sway model, Figure 3.8b illustrates the important role of the partial twisting restraint in enhancing the buckling capacity. Interestingly, in Figure 3.8b, the dotted line corresponding to the case of no twisting restraint coincides with the lower solid line for the case of no twisting and lateral restraints, suggesting that the presence of relative lateral restraint only has no beneficial contribution for equally loaded twin beams. Also, the gap between the upper solid line and the dashed line suggests that the relative partial lateral restraint contributes to the buckling capacity only when the twisting restraint is also provided.

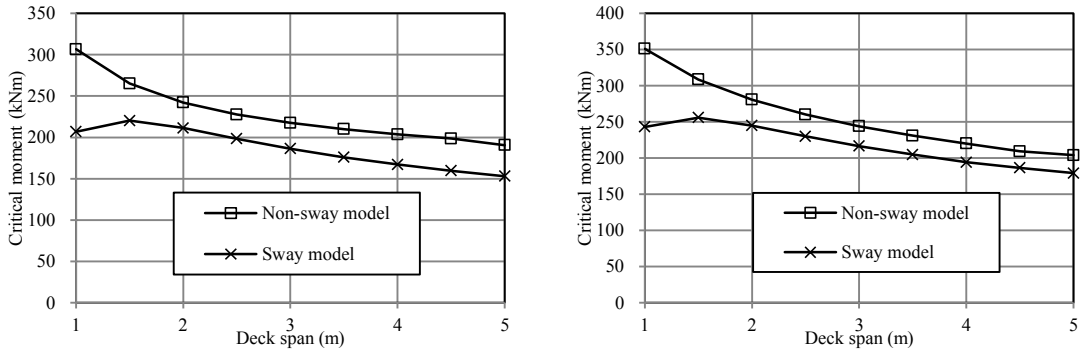

Figure 3.6 Effect of deck span on critical moment for (a) UDL, (b) mid-span concentrated loads

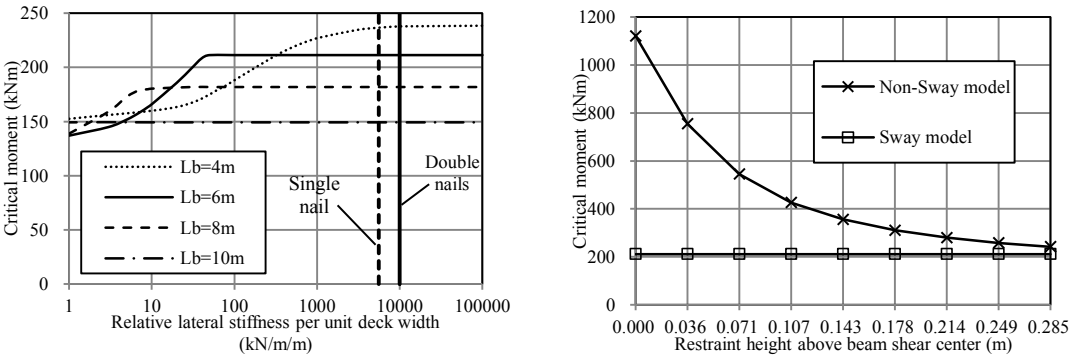

Figure 3.7 Effect of (a) lateral restraint stiffness on the sway model, (b) lateral restraint height on sway and non-sway models

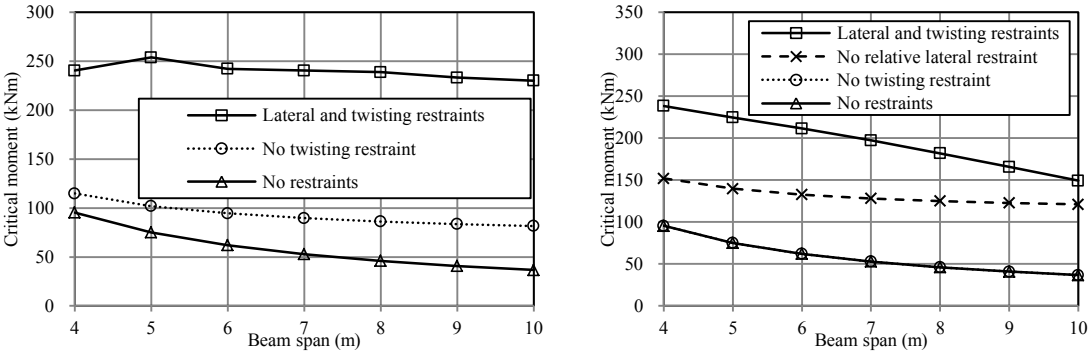

Figure 3.8 Buckling capacity as influenced by inclusion/exclusion of lateral and twisting restraints in (a) the non-sway model, (b) sway model

3.5 Conclusions

Two finite-element models based on ABAQUS were developed for the lateral torsional buckling investigation of twin-beam-deck assemblies under wind uplift. Parametric studies were conducted to (1) investigate the effects of various parameters on the buckling capacity, (2) quantitatively compare the difference between the sway and non-sway models. The key engineering observations are:

1. For both sway and non-sway models, the buckling capacity can be several times higher than unrestrained beams and most of the additional capacity is attributed to the continuous partial twisting restraint. For the sway model, the present comparison shows that results based only on relative lateral restraint are ineffective.
2. In general, the non-sway model consistently predicts critical moments higher than those based on the sway model. Large differences are observed for long beam span or short deck span.
3. Unlike the sway model which has a clear downward trend between critical moment and beam span, the results from the non-sway model indicate that, in general, there is no clear trend between the buckling capacity and beam span.
4. For the deck span examined, both models show an overall buckling capacity decline as the span is increased.
5. For the sway model, the lateral stiffness of the deck-joint assembly with two nails at each joint is shown to provide enough lateral stiffness to maximize (or nearly maximize) the lateral torsional buckling capacity.
6. The lateral restraint height has a significant influence on the buckling capacity for the non-sway model. However, for the sway model where the lateral stiffness exceeds the threshold value, the lateral restraint height has no effect on buckling capacity.

References

[1] *ABAQUS 6.12-3* [Computer software]. Providence, RI, Dassault Systèmes Simulia.

[2] American Wood Council. (2015). "National Design Specification for Wood Construction." *ANSI/AWC NDS-2015,* Virginia, U.S.

[3] Basaglia, C., Camotim, D., Gonçalves, R., and Graça, A. (2013). "GBT-based assessment of the buckling behaviour of cold-formed steel purlins restrained by sheeting." *Thin-Walled Struct.,* 72, 217-229.

[4] Canadian Standard Association (CSA). (2014). "Engineering design in wood." *O86-14,* Mississauga, Ontario, Canada.

[5] Chu, X., Kettle, R., and Li, L. (2004). "Lateral-torsion buckling analysis of partial-laterally restrained thin-walled channel-section beams." *J. Constr. Steel Res.,* 60(8), 1159-1175

[6] Chu, X., Rickard, J., and Li, L. (2005). "Influence of lateral restraint on lateral-torsional buckling of cold-formed steel purlins." *Thin-Walled Struct.,* 43(5), 800-810.

[7] Errera, S. J., Pincus, G., and Fisher, G. P. (1967). "Columns and beams braced by diaphragms." *J. Struct. Div.,* 93(1), 295-318.

[8] Forest Products Laboratory (FPL). (2010). *Wood Handbook-Wood as an Engineering Material*. Madison, U.S.

[9] Hancock, G. J., and Trahair, N. S. (1978). "Finite element analysis of the lateral buckling of continuously restrained beam-columns." *Civ. Engrg. Trans*., Institution of Engineers, Australia, CE20, 120-127.

[10] Helwig, T. A., and Frank, K. H. (1999). "Stiffness requirements for diaphragm bracing of beams." *J. Struct. Eng.,* 125(11), 1249-1256.

[11] Helwig, T. A., and Yura, J. A. (2008). "Shear diaphragm bracing of beams. I: Stiffness and strength behavior." *J. Struct. Eng.,* 134(3), 348-356.

[12] Khelil, A., and Larue, B. (2008). "Simple solutions for the flexural-torsional buckling of laterally restrained I-beams." *Eng. Struct.,* 30(10), 2923-2934.

[13] Larue, B., Khelil, A., and Gueury, M. (2007). "Elastic flexural–torsional buckling of steel beams with rigid and continuous lateral restraints." *J. Constr. Steel Res.,* 63(5), 692-708.

[14] Li, L. (2004). "Lateral–torsional buckling of cold-formed zed-purlins partial-laterally restrained by metal sheeting." *Thin-Walled Struct.,* 42(7), 995-1011.

[15] Lucas, R., Al-Bermani, F., and Kitipomchai, S. (1997a). "Modelling of cold-formed purlin-sheeting systems—Part 1: Full model." *Thin-Walled Struct.,* 27(3), 223-243.

[16] Lucas, R., Al-Bermani, F., and Kitipornchai, S. (1997b). "Modelling of cold-formed purlin-sheeting systems—Part 2. Simplified model." *Thin-Walled Struct.,* 27(4), 263-286.

[17] Park, J., and Kang, Y. (2003). "Lateral buckling of beams with top bracing." *Struct.Eng.Mech.,* 16(5), 613-625.

[18] Park, J. S., Stallings, J. M., and Kang, Y. J. (2004). "Lateral–torsional buckling of prismatic beams with continuous top-flange bracing." *J. Constr. Steel Res.,* 60(2), 147-160.

[19] Peköz, T., and Soroushian, P. (1982). “Behaviour of C- and Z-purlins under wind uplift.” *Proc., 6th Int. Specialty Conf. on Cold-Formed Steel Structures,* 409–429.

Roeder, C. W., and Assadi, M. (1982). "Lateral stability of I-beams with partial support." *J. Struct. Div.,* 108(8), 1768-1780.

[20] Sokol L. (1996). "Stability of cold formed purlins braced by steel sheeting. " *Thin-Walled Struct.,* 25(4),247–268.

[21] Taylor, A. C., and Ojalvo, M. (1966). "Torsional restraint of lateral buckling." *J. Struct. Div.,* 92(2), 115-130.

[22] Trahair, N. S. (1979). “Elastic lateral buckling of continuously restrained beam columns.” *The profession of a civil engineer*, D. Campbell-Allen and E. H. Davis, eds., Sydney University Press, Sydney, Australia, 61–73.

[23] Vlasov, V. Z. (1961). *Thin-walled elastic beams*. 2nd. ed., Israel Program for Scientific Translations, Jerusalem.

[24] Ye, Z., Kettle, R. J., Li, L., and Schafer, B. W. (2002). "Buckling behavior of cold-formed zed-purlins partially restrained by steel sheeting." *Thin-Walled Struct.,* 40(10), 853-864.

CHAPTER 4:NON-SWAY MODEL FOR THE LATERAL TORSIONAL BUCKLING OF WOODEN BEAMS UNDER WIND UPLIFT

Abstract

Simply-supported wooden beams nailed to deck boards subjected to wind uplift forces are subjected to compressive stresses at their bottom fibers. Because the restraining action provided by decking is at the top fibers, it is unclear to what extent such restraints are effective in controlling lateral torsional buckling as a possible mode of failure under wind uplift. Present design standards do not have provisions for such cases. Thus, the present study aims to quantify the effect of restraints provided by the deck boards on the lateral torsional buckling capacity of twin-beam-deck systems under wind uplift. Towards this goal, a series of analytical and numerical models were formulated. All models capture the continuous rigid lateral restraint and partial twisting restraint provided by the deck boards. The effects of load type and load position were investigated. The bending stiffness of deck boards was observed to have a significant influence on the lateral torsional buckling capacity of twin-beam-deck systems.

4.1 Introduction

A typical timber roof system consists of a set of parallel beams with continuous lateral bracing at the top by tongue-and-groove wood decking. When subjected to wind uplift, and given the typically low self-weight of such systems, the net bending moments may induce compression at the bottom fibers of the beams which are laterally unrestrained. Such beams have a tendency to undergo a lateral torsional buckling mode of failure.

Depending on the configuration of the decking, lateral displacements may be either fully or partially restrained at the beam top. Also, the deck boards typically placed perpendicular to the beams are expected to partially restrain the beams' twisting, thus contributing to its lateral torsional buckling resistance. However, it is unclear to what extent these restraints are effective in increasing the lateral torsional buckling capacity of such systems. Current standard provisions CAN/CSA O86 (2014) and NDS (2015) ignore such contributions. Within this context, the present study develops a family of solutions for predicting the lateral torsional buckling capacity of twin-beam-deck systems. A finite element model is also developed under ABAQUS 6.12-3 to assess the

validity of the solutions.

4.2 Literature Review

4.2.1 Overview of the stability research on wood members

The lateral torsional buckling of wood beams has been experimentally investigated by Hooley and Madsen (1964), Hindman et al. (2005a), Hindman et al. (2005b), Burow et al. (2006), and Xiao (2014) with emphasis on comparing experimental results with design codes. Buchanan (1986), Zahn (1986), Koka (1987), Zahn (1988), Bell and Eggen (2001), Steiger and Fontana (2005), Song and Lam (2006), Song and Lam (2009), and Song and Lam (2010) investigated the buckling behavior of beam-columns. Zahn (1965), Zahn (1973), and Zahn (1984) developed analytical solutions for the lateral torsional buckling of wood beam-deck systems. Most studies on lateral torsional buckling of beam-deck systems involve steel beams. A review of such studies is provided in the following subsections.

4.2.2 Sway models under gravity loads

Timoshenko and Gere (1961) developed a buckling solution for columns continuously braced by eccentric elastic lateral and twisting restraints. Vlasov (1961) formulated the general differential equations for a beam embedded in an elastic medium. The critical moment was determined for a beam braced by continuous elastic lateral and twisting restraints and subjected to uniform moment. Taylor and Ojalvo (1966) formulated a buckling solution for doubly-symmetric I-section beams with continuous or discrete elastic twisting restraint. Pincus and Fisher (1966) developed an energy-based solution for two simply-supported I-section beams braced by the deck subjected to uniform moments. The solution accounted for the shear and twisting actions of the deck. Errera et al. (1967) extended the solutions of Pincus and Fisher (1966) to accommodate other bracing scenarios. Apparao (1968) investigated floor assemblies consisting of two beams of channel, zed and I-sections laterally braced at their compression flanges by the shear action of the deck. Two types of solutions were developed: (1) A load-deformation solution, in which initial imperfections were considered, and (2) a lateral torsional buckling eigen-value solution. Zahn (1965) formulated equilibrium equations for wooden rectangular beams that are laterally restrained by the shear action of deck boards. The buckling capacity was estimated for various loading and boundary conditions. Jenkinson and Zahn (1972) experimentally verified the validity of the

solutions of Zahn (1965). In another study, Zahn (1972) conducted a series of experiments to quantify the shear stiffness of wooden deck boards, to be used as input in the analytical solutions. An energy solution was also developed (Zahn 1973) by expressing the total potential energy for a beam within a floor system and that of its tributary strip of decking. The stationarity conditions of the total potential energy were evoked to recover the governing differential equations of neutral stability. Solutions were provided for simply-supported beams under uniform moments, concentrated load, uniformly distributed load and cantilevers. Zahn (1984) further analyzed the effects of additional discrete lateral and twisting restraints on the buckling capacity of the floor system. Trahair (1979) formulated a closed-form buckling solution for beam-columns of mono-symmetric cross-sections with continuous elastic restraints restraining lateral displacement, angle of twist, weak-axis rotation and warping. For the case of doubly-symmetric I-beams, the author investigated the effects of the height of lateral and twisting restraints on the critical moments.

4.2.3 Sway models under uplift loads

A non-exhaustive review of sway models under uplift loads includes the work of Pekoz and Soroushian (1982) who developed a solution for critical uplift load of purlin-sheeting system, by modelling the system as a beam on elastic foundation. Lucas et al. (1997a) formulated a non-linear elasto-plastic finite element model with geometric nonlinearity for purlin-sheeting systems. The model captured purlin-sheeting interaction and successfully modelled cross-sectional distortion and local buckling. Lucas et al. (1997b) also developed a simplified model where the effects of sheeting were idealized as elastic springs. The lateral torsional buckling capacity of channel purlins laterally braced by sheeting was investigated by Chu et al. (2004). Li (2004) and Chu et al. (2005) expanded the study for zed sections. Ye et al. (2002) adopted a finite strip method to investigate the local, distortional and lateral torsional buckling of zed-purlins restrained by steel sheeting. Basaglia et al. (2013) developed a Generalized Beam Theory (GBT) solution for the local, distortional and lateral torsional buckling of channel and zed purlins restrained by sheeting and subjected to uplift loading. Apart from the studies of Chu et al. (2004), Li (2004) and Chu et al. (2005), the above studies have focused on the distortional buckling of thin cold-formed sections.

4.2.4 Non-sway models under gravity and uplift loads

In the above studies, the beams were assumed to be free to sway laterally. Only a few studies have considered the case where the beams are restrained from lateral sway. This includes the work of Vlasov (1961) who formulated a buckling solution for a simply-supported beam under uniform moments with a continuous rigid later restraint offset from the shear center and a continuous elastic twisting restraint. Roeder and Assadi (1982) provided an experimental study which verified the Vlasov Model. Park and Kang (2003) developed a shell based finite element model under MSC/NASTRAN for the lateral torsional buckling analysis of I-section beams with continuous lateral bracing at the top flange subjected to mid-height loading and end moments. They developed simplified design equations based on their model. In a subsequent study (Park et al. 2004), they extended the previous work to account for top flange loading. Using a trigonometric series solution, Larue et al. (2007) further generalized the buckling solution of Vlasov (1961) for linear and parabolic bending moment distributions with moment reversal.

For relatively light wooden beams under wind uplift, the net vertical load may be upwards. In such cases, decking mounted on the top face of the beam would provide restraint to the tension flange of the simply-supported beam. Within this context, the present study aims at developing solutions for examining the critical moment capacity for twin-beam-deck systems under wind uplift. Focus is on wood material. In this respect, only the studies by Zahn (1965), Zahn (1973) and Zahn (1984) were focused on wood members. The present study targets cases where the decking details provide continuous rigid lateral restraint preventing the system from swaying laterally, and elastic twisting restraint (in a manner similar to Vlasov 1961). However, the field equations and boundary conditions and the finite element formulation developed as part of the present study are able to go beyond the Vlasov solution in that they can accommodate the general load distributions and boundary conditions by formulating a series of general analytical and numerical solutions.

4.3 Assumptions

The following assumptions are adopted:

1. The deck boards are assumed to provide rigid lateral restraint, i.e., the system is prevented from swaying laterally, in line with the studies of Vlasov (1961) and Laure et al. (2007).

2. Elastic twisting restraint is provided by the deck bending action, in a manner consistent with the Vlasov (1961).
3. The in-plane elastic shear restraint provided by the deck boards is negligible.
4. Throughout deformation, beam cross-sections remain rigid in their own plane, i.e., distortional effects are neglected.
5. Shear deformation effects within the beams are negligible.
6. Beam and decking materials are linearly elastic.
7. Pre-buckling deformation effects are neglected, and
8. Both beams are subjected to general loading (unlike the Vlasov solution which is confined to uniform moments).

4.4 Formulation

4.4.1 Problem description and notation

The model considered in the present study consists of two identical parallel beams with doubly symmetric sections (either rectangular or I-shaped) braced by individual deck boards. For the twin-beam-deck system, each of the twin beams is assumed to be subjected to transverse load $q(z)$ applied at a distance $h(z)$ below the deck centerline (Figure 4.1). Under such external loads, the system is assumed to deform from Configuration 1 to 2 where both beams undergo vertical displacements $v_p(z)$. As a convention, subscript *p* represents pre-buckling displacements. The applied loads are then assumed to increase by a factor λ and attain the value of $\lambda q(z)$ at the onset of buckling (Configuration 3). Under the load increase, it is assumed that pre-buckling deformation linearly increases to $\lambda v_p(z)$. The system then undergoes lateral torsional buckling (Configuration 4) manifested by beam lateral displacements $u_1(z), u_2(z)$ and angles of twist $\theta_1(z), \theta_2(z)$, where subscripts 1 and 2 denote the generalized displacements for the first and second beam, respectively. A left-hand coordinate system is used, with *z* axis being along the longitudinal direction of the beam, and *x* and *y* axes taken in the plane of the cross-section. The positive sign convention adopted is consistent with that in Trahair (1993) where the angle of twist is clockwise. Since the lateral displacement along the deck centerline is assumed to be rigidly restrained, the lateral displacements $u_i \quad (i = 1, 2)$ can be related to the angles of twist θ_i as

$$u_i = -a\theta_i \tag{4.1}$$

where a is the vertical distance between beam shear center and deck centerline.

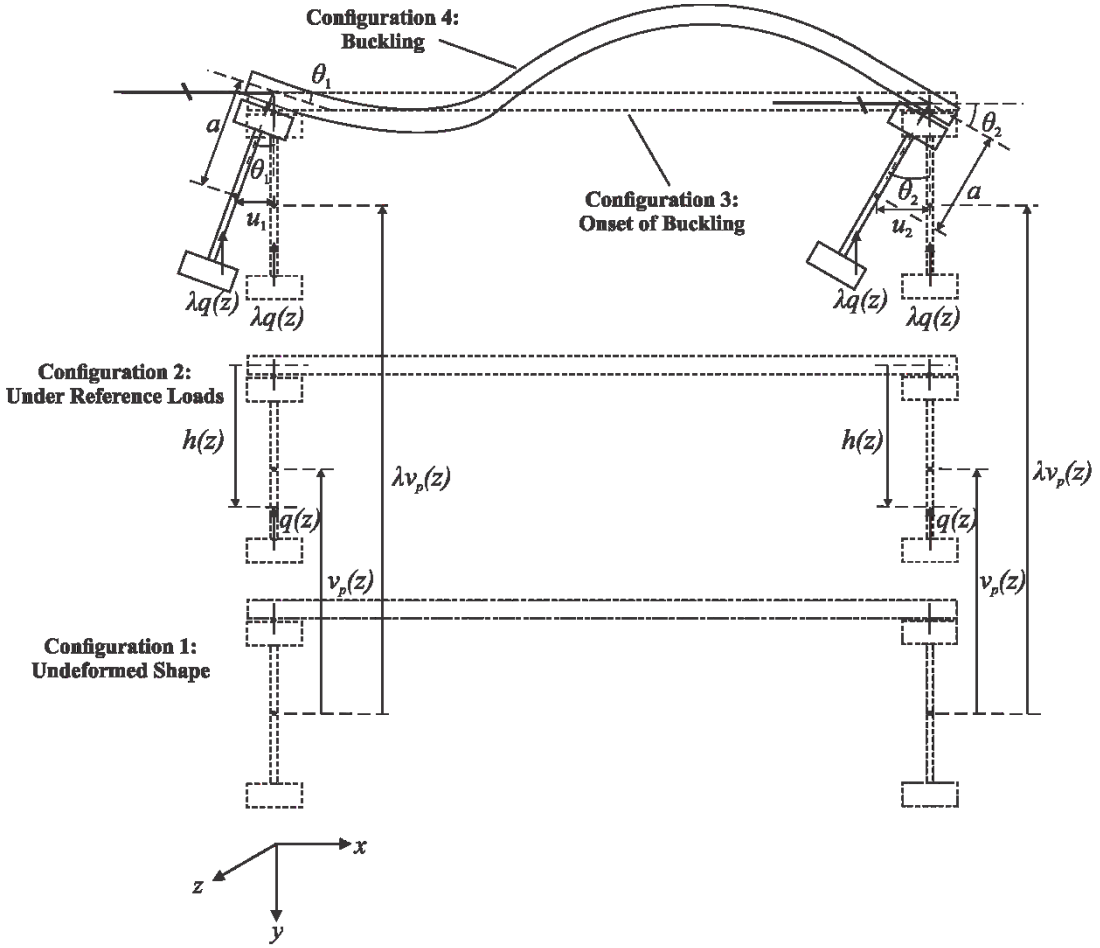

Figure 4.1 Different stages of deformation

4.4.2 Total potential energy

The total potential energy of the twin-beam-deck system Π is the summation of the internal strain energy U and the load potential energy V

$$\Pi = U + V \tag{4.2}$$

where the internal strain energy has three contributions $U = U_{b1} + U_{b2} + U_d$, and U_{bi} are the internal strain energies stored in beam i $(i = 1, 2)$ and U_d is the internal strain energy stored in the deck boards as they undergo transverse bending. The load potential energy has two components $V = V_{b1} + V_{b2}$, one for external loads applied at each beam. For beam i, the internal strain energy is given by Trahair (1993) as

$$U_{bi} = \frac{1}{2}\int_0^{L_b} E_b I_y u_i''^2 dz + \frac{1}{2}\int_0^{L_b} G_b J_b \theta_i'^2 dz + \frac{1}{2}\int_0^{L_b} E_b C_w \theta_i''^2 dz \tag{4.3}$$

where, for a solid beam, E_b is the beam modulus of elasticity, I_y is the moment of inertia about beam weak-axis, G_b is the beam shear modulus, J_b is the Saint-Venant torsional constant, C_w is the warping constant, and L_b is the beam span. All primes denote differentiation with respect to coordinate z along the beam longitudinal axis. For I-section members where the web and flanges have different materials, E_b and G_b become the properties of the flanges, and the properties I_y, C_w, J_b are the corresponding transformed section properties. Expressions of the transformed section properties have been provided in Appendix 4A. The load potential energy for beam i is

$$V_{bi} = \lambda\left(\int_0^{L_b} M\theta_i u_i'' dz + \frac{1}{2}\int_0^{L_b} qh\theta_i^2 dz\right) \tag{4.4}$$

where $M(z)$ is the reference strong-axis moment by reference transverse loads $q(z)$ along the beam span (taken positive when acting downwards), and one recalls that λ is the load multiplier to be solved and $h(z)$ is the distance between the loading point and deck centerline (taken positive when the loading point is below deck centerline). The first term in Eq. (4.4) is the destabilizing term due to strong-axis flexure while the second term accounts for the load potential energy gain induced by the load height effect relative to deck centerline. From Eq. (4.1), by substituting into Eqs. (4.3) and (4.4), one obtains

$$U_{bi} = \frac{1}{2}\int_0^{L_b} E_b C\theta_i''^2 dz + \frac{1}{2}\int_0^{L_b} G_b J_b \theta_i'^2 dz \tag{4.5}$$

$$V_{bi} = \frac{\lambda}{2}\int_0^{L_b} \left(hq\theta_i - 2aM\theta_i''\right)\theta_i dz \tag{4.6}$$

where the property $C = I_y a^2 + C_w$ has been introduced.

For a deck board at a distance z_0 from beam end support, the end moments M_{e1} and M_{e2} are expressed in terms of angles of twist θ_1, θ_2 as

$$\begin{Bmatrix} M_{e1}(z_0) \\ M_{e2}(z_0) \end{Bmatrix} = \frac{2E_d I_d}{L_d} \begin{bmatrix} 2 & 1 \\ 1 & 2 \end{bmatrix} \begin{Bmatrix} \theta_1(z_0) \\ \theta_2(z_0) \end{Bmatrix} \tag{4.7}$$

where E_d and I_d are the deck modulus of elasticity and the moment of inertia about deck strong-axis, respectively, and L_d is the deck board span. The internal strain energy U_d^* stored in this deck board is

$$U_d^* = \frac{1}{2} M_{e1}(z_0)\theta_1(z_0) + \frac{1}{2} M_{e2}(z_0)\theta_2(z_0) \tag{4.8}$$

From Eq. (4.7), by substituting into Eq. (4.8), one rewrites the internal strain energy as

$$U_d^* = \frac{E_d I_d}{L_d} \langle \theta_1(z_0) \quad \theta_2(z_0) \rangle \begin{bmatrix} 2 & 1 \\ 1 & 2 \end{bmatrix} \begin{Bmatrix} \theta_1(z_0) \\ \theta_2(z_0) \end{Bmatrix} \tag{4.9}$$

The internal strain energy U_d in the whole decking is the summation of energy stored in each deck board, which can be approximately written in an integration form as

$$U_d = \sum U_d^* \approx \frac{E_d h_d^3}{12 L_d} \int_0^{L_b} \langle \theta_1 \quad \theta_2 \rangle \begin{bmatrix} 2 & 1 \\ 1 & 2 \end{bmatrix} \begin{Bmatrix} \theta_1 \\ \theta_2 \end{Bmatrix} dz \tag{4.10}$$

in which h_d is the deck board thickness.

The total potential energy of the twin-beam-deck assembly is obtained by summation of the internal strain energies for the twin beams, deck boards, and the load potential energy gains, i.e.,

$$\begin{aligned} \Pi = {} & \frac{1}{2}\int_0^{L_b} E_b C \theta_1''^2 dz + \frac{1}{2}\int_0^{L_b} G_b J_b \theta_1'^2 dz + \frac{\lambda}{2}\int_0^{L_b} \left(hq\theta_1 - 2aM\theta_1'' \right)\theta_1 dz + \frac{1}{2}\int_0^{L_b} E_b C \theta_2''^2 dz \\ & + \frac{1}{2}\int_0^{L_b} G_b J_b \theta_2'^2 dz + \frac{\lambda}{2}\int_0^{L_b} \left(hq\theta_2 - 2aM\theta_2'' \right)\theta_2 dz + \frac{E_d h_d^3}{6 L_d}\int_0^{L_b} \left(\theta_1^2 + \theta_1\theta_2 + \theta_2^2 \right) dz \end{aligned} \tag{4.11}$$

where the fields $\theta_1(z), \theta_2(z), q(z), M(z)$ are dependent on the z coordinate.

4.4.3 General conditions of neutral stability and boundary conditions

The conditions of neutral stability are obtained by setting the variation of the total potential energy to zero, i.e., $\delta\Pi = 0$. By performing integration by parts (Appendix 4B), one recovers the equilibrium equations

$$\begin{aligned}
&\left(E_bC\theta_1''-a\lambda M\theta_1\right)''-G_bJ_b\theta_1''+\lambda\left(hq\theta_1-aM\theta_1''\right)+\frac{E_dh_d^{\,3}}{6L_d}\left(2\theta_1+\theta_2\right)=0\\
&\left(E_bC\theta_2''-a\lambda M\theta_2\right)''-G_bJ_b\theta_2''+\lambda\left(hq\theta_2-aM\theta_2''\right)+\frac{E_dh_d^{\,3}}{6L_d}\left(\theta_1+2\theta_2\right)=0
\end{aligned}\tag{4.12}$$

and the corresponding boundary conditions

$$\begin{aligned}
&\left[\left(G_bJ_b\theta_1'-\left(E_bC\theta_1''-a\lambda M\theta_1\right)'\right)\delta\theta_1\right]_0^{L_b}=0,\ \left[\left(E_bC\theta_1''-a\lambda M\theta_1\right)\delta\theta_1'\right]_0^{L_b}=0\\
&\left[\left(G_bJ_b\theta_2'-\left(E_bC\theta_2''-a\lambda M\theta_2\right)'\right)\delta\theta_2\right]_0^{L_b}=0,\left[\left(E_bC\theta_2''-a\lambda M\theta_2\right)\delta\theta_2'\right]_0^{L_b}=0
\end{aligned}\tag{4.13}$$

4.5 Closed-form Solutions for Uniform Moments

4.5.1 Solution for general boundary conditions

For twin beams with general boundary conditions under uniform moments, the angles of twist are assumed as exponentials, i.e., $\theta_1=A_je^{m_jz}$ and $\theta_2=B_je^{m_jz}$ ($j=1,2,\ldots$.

By substituting into Eq. (4.12), one obtains

$$\begin{bmatrix}
E_bCm_j^{\,4}-\left(2a\lambda M+G_bJ_b\right)m_j^{\,2}+\dfrac{E_dh_d^{\,3}}{3L_d} & \dfrac{E_dh_d^{\,3}}{6L_d}\\
\dfrac{E_dh_d^{\,3}}{6L_d} & E_bCm_j^{\,4}-\left(2a\lambda M+G_bJ_b\right)m_j^{\,2}+\dfrac{E_dh_d^{\,3}}{3L_d}
\end{bmatrix}\begin{Bmatrix}A_j\\B_j\end{Bmatrix}=\begin{Bmatrix}0\\0\end{Bmatrix}\tag{4.14}$$

For a non-trivial solution, the determinant of the matrix of coefficients should vanish, which leads to

$$\begin{aligned}
m_j&=\pm\sqrt{\frac{-\left(2a\lambda M+G_bJ_b\right)\pm\sqrt{\left(2a\lambda M+G_bJ_b\right)^2-\dfrac{2E_dh_d^{\,3}E_bC}{3L_d}}}{2E_bC}}\\
m_j&=\pm\sqrt{\frac{-\left(2a\lambda M+G_bJ_b\right)\pm\sqrt{\left(2a\lambda M+G_bJ_b\right)^2-\dfrac{2E_dh_d^{\,3}E_bC}{L_d}}}{2E_bC}}
\end{aligned}\tag{4.15}$$

Since all eight roots are distinct, the angles of twist θ_1 and θ_2 can be expressed as

$$\{\theta(z)\}_{2\times1}=\begin{Bmatrix}\theta_1(z)\\ \theta_2(z)\end{Bmatrix}=\sum_{j=1}^{8}\begin{Bmatrix}A_j\\ B_j\end{Bmatrix}e^{m_j z} \tag{4.16}$$

From Eq. (4.14), one express B_j in terms of A_j as

$$B_j=\overline{A}_j A_j \tag{4.17}$$

where $\overline{A}_j=-6L_d\left[E_bCm_j^{\,4}-\left(2a\lambda M+G_bJ_b\right)m_j^{\,2}+E_dh_d^{\,3}/3L_d\right]\Big/E_dh_d^{\,3}$. From Eq. (4.17), by substituting into Eq. (4.16), one obtains

$$\{\theta(z)\}_{2\times1}=\sum_{j=1}^{8}A_j\begin{Bmatrix}1\\ \overline{A}_j\end{Bmatrix}e^{m_i z}=[H]_{2\times8}\left[E_m(z)\right]_{8\times8}\{D\}_{8\times1} \tag{4.18}$$

where

$$[H]_{2\times8}=\begin{bmatrix}1 & 1 & \cdots\\ \overline{A}_1 & \overline{A}_2 & \cdots\end{bmatrix}$$

$$\left[E_m(z)\right]_{8\times8}=Diag\left(e^{m_1 z},e^{m_2 z},\cdots\right.$$

$$\{D\}_{8\times1}=\begin{Bmatrix}A_1 & A_2 & \cdots\end{Bmatrix}$$

The angles of twist as given in Eq. (4.18) and their derivatives can then be used to express the eight boundary conditions of the problem. The resulting system of equations is then placed in a matrix form and the smallest critical moment λM which vanishes the determinant of the matrix of coefficient is extracted to yield the critical moment of the system.

4.5.2 Solution for simply-supported boundary conditions

For the case where the twin beams are simply-supported relative to the angle of twist and free to warp at the supports, the applicable boundary conditions as extracted from Eq. (4.13) lead to

$$\begin{aligned}&\theta_1(0)=\theta_2(0)=\theta_1(L_b)=\theta_2(L_b)=0\\ &\theta_1''(0)=\theta_2''(0)=\theta_1''(L_b)=\theta_2''(L_b)=0\end{aligned} \tag{4.19}$$

Assuming the angles of twist as sinusoidal functions, i.e., $\theta_i=A_i\sin\left(n\pi z/L_b\right)\left(i=1,2\right)$, $\left(n=1,2,3,\cdots\right.$, which satisfiy all the boundary conditions in Eq. (4.19), and substituting into the Eq. (4.12), one obtains

$$\begin{bmatrix} E_b C\lambda_n^4 + \left(G_b J_b + 2a\lambda M\right)\lambda_n^2 + \dfrac{E_d h_d^3}{3L_d} & E_d h_d^3/6L_d \\ E_d h_d^3/6L_d & E_b C\lambda_n^4 + \left(G_b J_b + 2a\lambda M\right)\lambda_n^2 + \dfrac{E_d h_d^3}{3L_d} \end{bmatrix} \begin{Bmatrix} A_1 \\ A_2 \end{Bmatrix}_n = \begin{Bmatrix} 0 \\ 0 \end{Bmatrix} \tag{4.20}$$

where $l_n = n\pi/L_b$. For a non-trivial solution, the determinant of the matrix should vanish, leading to the following roots (Appendix 4C)

$$\begin{aligned} \left(\lambda M\right)_{1n} &= -\left[\frac{E_b C}{2a}\left(\frac{n\pi}{L_b}\right)^2 + \frac{G_b J_b}{2a} + \frac{E_d h_d^3}{12aL_d}\left(\frac{L_b}{n\pi}\right)^2\right], \\ \left(\lambda M\right)_{2n} &= -\left[\frac{E_b C}{2a}\left(\frac{n\pi}{L_b}\right)^2 + \frac{G_b J_b}{2a} + \frac{E_d h_d^3}{4aL_d}\left(\frac{L_b}{n\pi}\right)^2\right] \end{aligned} \tag{4.21a,b}$$

It is noted that both roots are negative, signifying that, under the proposed assumptions, only negative moments (moments that create compression at beam bottom fibers) can induce lateral torsional buckling of the system. For the two roots obtained, the first one corresponds to a symmetric buckling mode and the second one corresponds to an antisymmetric buckling mode. Among the two roots, it is clear $\left|\left(\lambda M\right)_{1n}\right| < \left|\left(\lambda M\right)_{2n}\right|$, which means the symmetric buckling mode governs the capacity of the system. The critical moment $M_{cr} = \left(\lambda M\right)_{1n}$ coincides with that in Vlasov (1961). Introducing the notation $M_\alpha = G_b J_b/2a$, one can rewrite the critical moment in a dimensionless form as

$$m_r\left(n\right) = -\left(1 + n^2\alpha + \frac{\beta}{n^2}\right) \tag{4.22}$$

where $m_r\left(n\right) = M_{cr}/M_\alpha$, $\alpha = \pi^2 E_b C/G_b J_b L_b^2$ and $\beta = \left(E_d h_d^3/L_d\right)\left(L_b^2/G_b J_b\right)/6\pi^2$. Setting the first derivative of Eq. (4.22) to zero yields $n = \sqrt[4]{\beta/\alpha}$, which provides an indication of the mode number corresponding to the smallest critical moment m_r. Since n is an integer value, one should consider the roots based on $\mathrm{int}\left(n\right)$ and $\mathrm{int}\left(n+1\right)$. For specific values of α and β, the relationship between β/α ratio and the governing mode number n are determined (Appendix 4D). The results are summarized in Table 4.1.

Table 4.1 Relationship between β/α and the governing mode number

Range of β/α	Governing Mode Number n	Critical moment equation
$\beta/\alpha \le 4$	1	$M_{cr}/M_{\alpha} = -\left(1+\alpha+\beta\right)$
$4 < \beta/\alpha \le 36$	2	$M_{cr}/M_{\alpha} = -\left(1+4\alpha+\beta/4\right)$
$36 < \beta/\alpha \le 144$	3	$M_{cr}/M_{\alpha} = -\left(1+9\alpha+\beta/9\right)$
$\left(i-1\right)^2 i^2 < \beta/\alpha \le i^2(i+1)^2$	i	$M_{cr}/M_{\alpha} = -\left(1+i^2\alpha+\beta/i^2\right)$

4.6 Approximate Energy-based Solutions

4.6.1 Simply-supported boundary conditions

Two loading types are considered: (1) a uniformly distributed load q along beams span, and (2) a mid-span concentrated load P for both beams. The angles of twist are assumed as $\theta_i = A_i' \sin\left(l_n z\right)\ \ (i=1,2)$. Substituting the assumed functions into Eq. (4.11), one obtains

$$\begin{aligned}\Pi = {} & \frac{1}{2}E_b C A_1'^2 l_n^{\,4}\int_0^{L_b}\sin^2\left(l_n z\right)dz + \frac{1}{2}G_b J_b A_1'^2 l_n^{\,2}\int_0^{L_b}\cos^2\left(l_n z\right)dz \\ & + a\lambda A_1'^2 l_n^{\,2}\int_0^{L_b} M\sin^2\left(l_n z\right)dz + \frac{1}{2}\lambda h A_1'^2\int_0^{L_b} q\sin^2\left(l_n z\right)dz + \frac{1}{2}E_b C A_2'^2 l_n^{\,4}\int_0^{L_b}\sin^2\left(l_n z\right)dz \\ & + \frac{1}{2}G_b J_b A_2'^2 l_n^{\,2}\int_0^{L_b}\cos^2\left(l_n z\right)dz + a\lambda A_2'^2 l_n^{\,2}\int_0^{L_b} M\sin^2\left(l_n z\right)dz + \frac{1}{2}\lambda h A_2'^2\int_0^{L_b} q\sin^2\left(l_n z\right)dz \\ & + \frac{E_d h_d^{\,3}}{6L_d}\left(A_1'^2 + A_1'A_2' + A_2'^2\right)\int_0^{L_b}\sin^2\left(l_n z\right)dz\end{aligned} \tag{4.23}$$

4.6.1.1 Uniformly distributed loads (UDL)

The strong-axis moment distribution induced by reference UDL q along beams span is $M = q\left(L_b z - z^2\right)/2$. By applying the principle of stationary total potential energy $\partial\pi/\partial A_1' = \partial\pi/\partial A_2' = 0$, one recovers two algebraic equations. The determinant of the resulting matrix of coefficients is set to zero to recover the critical loads (Appendix 4E), yielding

$$\left(\lambda q\right)_{1n} = -\frac{6n^4\pi^4 E_b C L_d + 6n^2\pi^2 G_b J_b {L_b}^2 L_d + E_d {H_d}^3 {L_b}^4}{{L_b}^4 L_d \left(6h + n^2\pi^2 a + 3a\right)}$$
$$\left(\lambda q\right)_{2n} = -\frac{6n^4\pi^4 E_b C L_d + 6n^2\pi^2 G_b J_b {L_b}^2 L_d + 3E_d {H_d}^3 {L_b}^4}{{L_b}^4 L_d \left(6h + n^2\pi^2 a + 3a\right)} \quad (4.24a,b)$$

Both roots are negative, i.e., only uplift loads can buckle the twin-beam-deck assembly. It is evident that $\left|\left(\lambda q\right)_{1n}\right| < \left|\left(\lambda q\right)_{2n}\right|$, signifying that the governing buckling mode is always symmetric.

4.6.1.2 Mid-span concentrated loads

For a reference concentrated load P applied at the beams mid-span, the strong-axis moment is $M = Pz/2 \quad \left(0 < z \le L_b/2\right)$ and $M = P\left(L_b - z\right)/2 \quad \left(L_b/2 < z \le L_b\right)$. Substituting $M\left(z\right)$ into Eq. (4.23) and applying the principle of stationary total potential energy, one obtains the following roots (Appendix 4F)

$$\left(\lambda P\right)_{1n} = -\frac{12n^4\pi^4 E_b C L_d + 12n^2\pi^2 G_b J_b {L_b}^2 L_d + 2E_d {h_d}^3 {L_b}^4}{3{L_b}^3 L_d \left(4a + 8h + an^2\pi^2\right)}$$
$$\left(\lambda P\right)_{2n} = -\frac{4n^4\pi^4 E_b C L_d + 4n^2\pi^2 G_b J_b {L_b}^2 L_d + E_d {h_d}^3 {L_b}^4}{{L_b}^3 L_d \left(4a + 8h + an^2\pi^2\right)} \quad (4.25a,b)$$

Similarly, only upward loads can buckle the system and $\left|\left(\lambda P\right)_{1n}\right| < \left|\left(\lambda P\right)_{2n}\right|$, signifying that the governing buckling mode is always symmetric.

4.6.2 Fixed boundary conditions

For the twin-beam-deck systems where both beams are fixed against the twist angle, assume the angles of twist as $\theta_i = D_i\left[1 - \cos\left(l_n z\right)\right] \quad \left(i = 1, 2\right)$, which satisfy all the boundary conditions in Eq. (4.13). Substituting the assumed angles of twist functions into the total potential energy, one obtains

$$\Pi = D_1^{\,2} E_b C l_n^{\,4} \frac{1}{2}\int_0^{L_b} \cos^2\left(l_n z\right) dz + D_1^{\,2} G_b J_b l_n^{\,2} \frac{1}{2}\int_0^{L_b} \sin^2\left(l_n z\right) dz$$
$$+ D_1^{\,2} \frac{\lambda}{2}\int_0^{L_b} \left\{hq\left[1-\cos\left(l_n z\right)\right] - 2aMl_n^{\,2}\cos\left(l_n z\right)\right\}\left[1-\cos\left(l_n z\right)\right] dz$$
$$+ D_2^{\,2} E_b C l_n^{\,4} \frac{1}{2}\int_0^{L_b} \cos^2\left(l_n z\right) dz + D_2^{\,2} G_b J_b l_n^{\,2} \frac{1}{2}\int_0^{L_b} \sin^2\left(l_n z\right) dz \qquad (4.26)$$
$$+ D_2^{\,2} \frac{\lambda}{2}\int_0^{L_b} \left\{hq\left[1-\cos\left(l_n z\right)\right] - 2aMl_n^{\,2}\cos\left(l_n z\right)\right\}\left[1-\cos\left(l_n z\right)\right] dz$$
$$+ \frac{E_d h_d^{\,3}}{6L_d}\left(D_1^{\,2} + D_1 D_2 + D_2^{\,2}\right)\int_0^{L_b}\left[1-\cos\left(l_n z\right)\right]^2 dz$$

4.6.2.1 UDL

From the strong-axis moment $M(z)$ induced by UDL, by substituting into Eq. (4.26) and applying the principle of stationary total potential energy $\partial\pi/\partial D_1 = \partial\pi/\partial D_2 = 0$, one obtains the following critical loads (Appendix 4G)

$$\left(\lambda q\right)_{3n} = \frac{-3\left(E_d L_b^{\,4} h_d^{\,3} + 2n^2\pi^2 G_b J_b L_b^{\,2} L_d + 2n^4\pi^4 E_b C L_d\right)}{L_b^{\,4} L_d\left(18h - 3a + an^2\pi^2\right)}$$
$$\left(\lambda q\right)_{4n} = \frac{-3\left(3E_d L_b^{\,4} h_d^{\,3} + 2n^2\pi^2 G_b J_b L_b^{\,2} L_d + 2n^4\pi^4 E_b C L_d\right)}{L_b^{\,4} L_d\left(18h - 3a + an^2\pi^2\right)}$$
$$n = 1,3,5,\ldots \qquad (4.27a,b,c,d)$$
$$\left(\lambda q\right)_{5n} = \frac{-3\left(E_d L_b^{\,4} h_d^{\,3} + 2n^2\pi^2 G_b J_b L_b^{\,2} L_d + 2n^4\pi^4 E_b C L_d\right)}{L_b^{\,4} L_d\left(21a + 18h + an^2\pi^2\right)}$$
$$\left(\lambda q\right)_{6n} = \frac{-3\left(3E_d L_b^{\,4} h_d^{\,3} + 2n^2\pi^2 G_b J_b L_b^{\,2} L_d + 2n^4\pi^4 E_b C L_d\right)}{L_b^{\,4} L_d\left(21a + 18h + an^2\pi^2\right)}$$
$$n = 2,4,6,\ldots$$

4.6.2.2 Mid-span concentrated loads

Substituting the moment distribution $M(z)$ for mid-span concentrated loads into Eq. (4.26) and applying the principle of stationary total potential energy, one obtains the following critical loads (Appendix 4G)

$$(\lambda P)_{3n} = -\frac{2\left(2n^4\pi^4 E_b C L_d + 2n^2\pi^2 G_b J_b {L_b}^2 L_d + E_d {L_b}^4 {h_d}^3\right)}{{L_b}^3 L_d\left(8h - 4a + an^2\pi^2\right)}$$

$$(\lambda P)_{4n} = -\frac{2\left(2n^4\pi^4 E_b C L_d + 2n^2\pi^2 G_b J_b {L_b}^2 L_d + 3E_d {L_b}^4 {h_d}^3\right)}{{L_b}^3 L_d\left(8h - 4a + an^2\pi^2\right)}$$

$n = 1,3,5,\ldots$

$$(\lambda P)_{5n} = -\frac{2\left(2n^4\pi^4 E_b C L_d + 2n^2\pi^2 G_b J_b {L_b}^2 L_d + E_d {L_b}^4 {h_d}^3\right)}{{L_b}^3 L_d\left(32h + 32a + an^2\pi^2\right)}$$

$$(\lambda P)_{6n} = -\frac{2\left(2n^4\pi^4 E_b C L_d + 2n^2\pi^2 G_b J_b {L_b}^2 L_d + 3E_d {L_b}^4 {h_d}^3\right)}{{L_b}^3 L_d\left(32h + 32a + an^2\pi^2\right)} \qquad (4.28a,b,c,d,e,f)$$

$n = 2,6,10,\ldots$

$$(\lambda P)_{7n} = -\frac{2\left(2n^4\pi^4 E_b C L_d + 2n^2\pi^2 G_b J_b {L_b}^2 L_d + E_d {L_b}^4 {h_d}^3\right)}{n^2\pi^2 a {L_b}^3 L_d}$$

$$(\lambda P)_{8n} = -\frac{2\left(2n^4\pi^4 E_b C L_d + 2n^2\pi^2 G_b J_b {L_b}^2 L_d + 3E_d {L_b}^4 {h_d}^3\right)}{n^2\pi^2 a {L_b}^3 L_d}$$

$n = 4,8,12,\ldots$

4.7 Finite Element Formulation

The angles of twist $\theta_i(z)$ are related to the generalized nodal displacements as

$$\theta_i(z) = \left\langle L(z)\right\rangle^T_{1\times 4}\left\{\theta_i\right\}_{4\times 1} \qquad (i = 1,2) \qquad (4.29)$$

where $\left\langle\theta_i\right\rangle^T_{1\times 4} = \left\langle \theta_0 \quad \theta_0' \quad \theta_l \quad \theta_l' \right\rangle_i$ is the generalized nodal angle of twist vector, subscripts 0 and l denote the nodal points, and

$\left\langle L(z)\right\rangle^T_{1\times 4} = \left\langle \left(1 - 3z^2/l^2 + 2z^3/l^3\right) \quad \left(z - 2z^2/l + z^3/l^2\right) \quad \left(3z^2/l^2 - 2z^3/l^3\right) \quad \left(z^3/l^2 - z^2/l\right)\right\rangle$ is the vector of Hermitian interpolation functions and l is the element length. From Eq. (4.29), by substituting into the total potential energy expression in Eq. (4.11), one obtains

$$\Pi = \frac{1}{2}\left\langle \left\langle\theta_1\right\rangle^T_{1\times 4} \quad \left\langle\theta_2\right\rangle^T_{1\times 4}\right\rangle\left(\left[K_e\right]_{8\times 8} - \lambda\left[K_g\right]_{8\times 8}\right)\begin{Bmatrix}\left\{\theta_1\right\}_{4\times 1}\\ \left\{\theta_2\right\}_{4\times 1}\end{Bmatrix} \qquad (4.30)$$

in which the elastic stiffness matrix is

$$\left[K_e\right]=\begin{bmatrix}\left[K_b\right]+2\left[K_d\right] & \left[K_d\right] \\ \left[K_d\right]^T & \left[K_b\right]+2\left[K_d\right]\end{bmatrix}_{8\times 8}$$

and $\left[K_b\right]=E_bC\left[B_1\right]+G_bJ_b\left[B_2\right]$ is the beam stiffness matrix and $\left[K_d\right]=\left(E_dh^3{}_d/6L_d\right)\left[B_3\right]$ is the deck stiffness matrix. Also, in Eq. (4.30), the geometric stiffness matrix $\left[K_g\right]$ is

$$\left[K_g\right]=\begin{bmatrix}2a\left[B_4\right]-h\left[B_5\right] & \left[0\right] \\ \left[0\right] & 2a\left[B_4\right]-h\left[B_5\right]\end{bmatrix}_{8\times 8}$$

and submatrices $\left[B_1\right],\left[B_2\right],\left[B_3\right],\left[B_4\right],\left[B_5\right]$ have been defined in Appendix 4I. By evoking the stationarity conditions for the total potential energy $\delta\Pi=0$ to the discretized system, one obtains

$$\left(\left[K_e\right]_{8\times 8}-\lambda\left[K_g\right]_{8\times 8}\right)\begin{Bmatrix}\{\theta_1\}_{4\times 1} \\ \{\theta_2\}_{4\times 1}\end{Bmatrix}=\{0\}_{8\times 1} \tag{4.31}$$

4.8 Verification

A finite element model based on the commercial software ABAQUS is adopted to verify the validity of present solutions for a selected reference case. Both beams are simply supported. The beam and deck spans are 6 m and 2 m, respectively. Beam material is taken to be glu-laminated Spruce-Lodgepole Pine-Jack Pine 20f-EX. Cross-section depth is 570 mm and its width is 80 mm. The modulus of elasticity and shear modulus are 10,300 MPa and 474 MPa, respectively (CAN/CSA O86-14 and FPL 2010). The nominal bending resistance for the beam due to material failure is 270 kNm. The Spruce-Pine-Fir No. 2 grade deck boards are assumed to be 38 mm thick with a modulus of elasticity of 10,000 MPa.

4.8.1 Details of the ABAQUS model

The finite-element program ABAQUS 6.12-3 was used to perform an eigen-value lateral torsional buckling analysis of the twin-beam-deck. The two-node B31OS elements within the ABAQUS library were selected to model the twin beams. Each node has seven degrees of freedom (i.e., three translations, three rotations, and one warping deformation). The element accounts for transverse shear deformation. Also, the element does not capture distortional effects. The B31 elements were chosen to

model the deck boards. The B31 element has two nodes with six degrees of freedom per node (i.e., three translations, and three rotations). Figure 4.2 shows the twin-beam-deck model developed in ABAQUS with B31OS elements located at the height of beam shear center and B31 elements at the height of deck centerline. The number of B31OS elements used in each beam was chosen so that the number of nodes forming these elements matches the number of deck boards. For each pair of beam and deck nodes, the following kinematic relationships were enforced:

(1) the vertical displacement of a beam node $(v_b)_i$ was equated to the corresponding vertical displacement of the deck node $(v_d)_i$, i.e., $(v_b)_i = (v_d)_i$;

(2) the angle of twist of a beam node was equated to that of the corresponding deck node, i.e., $(\theta_b)_i = (\theta_d)_i$; and

(3) the lateral displacement of a beam node $(u_b)_i$ was related to the twist angle $(\theta_b)_i$ through $(u_b)_i = -a(\theta_b)_i$, where a was previously defined as the distance between beam shear center and deck centerline. Also, the lateral degree of freedom for each of the deck nodes was restrained, i.e., $(u_d)_i = 0$. The above constraints were enforced through the *EQUATION keyword in ABAQUS. The above kinematic constraints enforced the rigid lateral restraint condition while accounting for the partial twisting restraint provided by the deck bending action.

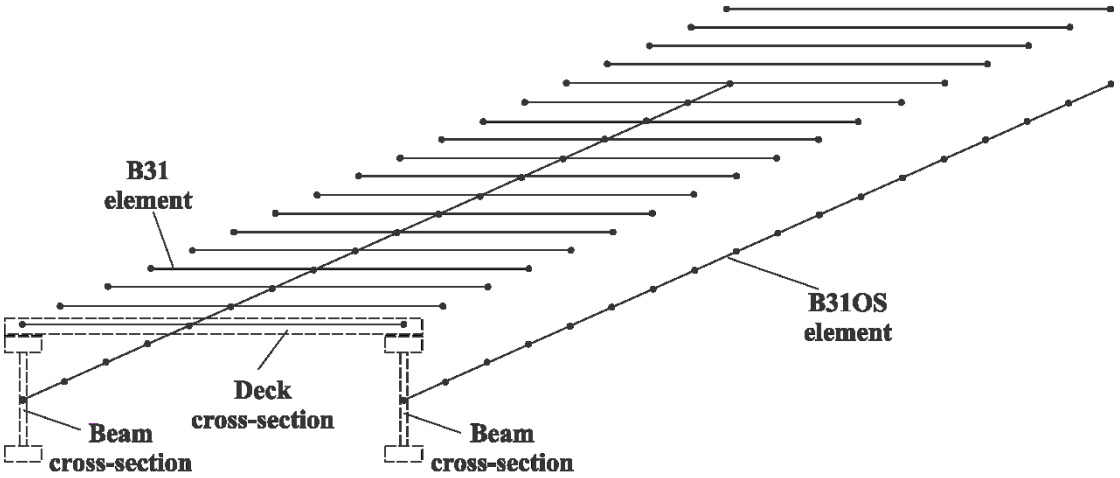

Figure 4.2 ABAQUS twin-beam-deck model

4.8.2 Mesh sensitivity analysis of present FEA and ABAQUS

In addition to uniform moments, two types of transverse loading were considered in the investigation: (1) A UDL applied along the beams span, and (2) a mid-span concentrated load for both beams. For the three loading types, the critical moments as determined by present FEA and ABAQUS are shown in Figure 4.3(a,c,e). For uniform moments (Figure 4.3a), the present FEA requires less than 6 beam elements to converge. The ABAQUS solution exhibits an oscillating behavior as the number of beam elements is increased and achieves convergence at 160 beam elements per beam. For the other two loading cases, 10 to 12 elements are shown to achieve convergence for both formulations. Under all three loading types, the present FEA converges from above and a coarser mesh tends to overestimate the buckling capacity. To ensure convergence, 30 elements per beam were used under the present model and 160 elements per beam under the ABAQUS model in all subsequent runs. Under both solutions, a single element per deck board is found to be enough to achieve convergence. For example, under uniform moments, the present FEA corresponding to two elements per deck yields the same critical moment of 192 kNm as that corresponding to one element per deck.

4.8.3 Verification of results

To validate the present solutions, comparisons between the closed-form solution in Eq. (4.21a,b), energy-based formulations in Eqs. (4.24a,b),(4.25a,b), the present FEA, and ABAQUS are presented for the reference twin-beam-deck assembly. As discussed, only negative moments and uplift loads can induce lateral torsional buckling of the simply-supported single-span twin-beam-deck system. For clarity, the absolute values of critical moments are presented below.

For uniform moments (Figure 4.3a), the closed-form formulation and present FEA yield identical critical moments of 192 kNm while the ABAQUS model predicts a slightly lower value of 190 kNm. All three solutions predict the identical buckling mode shape (Figure 4.3b). For UDL (Figure 4.3c), the approximate energy-based formulation predicts a higher capacity of 267 kNm, compared with 247 kNm as predicted by present FEA and 237 kNm as predicted by ABAQUS. This difference is attributed to the fact that the assumed sinusoidal displacement function in the energy-based formulation does not exactly represent the actual mode shape (Figure

4.3d) and thus provides a stiffer representation of the system, and hence overestimates the critical moments. The difference between present FEA and ABAQUS is possibly due to the fact that the ABAQUS B31OS elements capture the shear deformation effects due to flexure while the present FEA neglects the effects, resulting in a slightly stiffer representation. For mid-span concentrated loads (Figure 4.3e), the critical moments based on the energy-based solution are 508 kNm for $n=1$ and 348 kNm for $n=2$. In both cases, the energy solution over-predicts the critical moment as expected. Although the mode shape corresponding to $n=1$ is somewhat closer to those predicted by the FEA and ABAQUS (Figure 4.3f), the critical moment corresponding to $n=2$ is closer to the critical moment than that based on $n=1$. The difference in results is attributed to the fact the assumed sinusoidal functions represent the actual mode shape for non-uniform moment loading only in an approximate manner. In such a case, the energy-based solution is expected to provide an upper bound prediction of the critical moments. Indeed, Figure 4.3(g,h) confirm that under the cases of UDL and mid-span concentrated loads, the approximate energy-based solutions consistently predict higher critical moments than those based on the present FEA and ABAQUS model for various beam spans. Also evident is the fact that the approximate solutions are more accurate for shorter beam spans. The present FEA model, thus validated, is subsequently used to investigate the effects of various parameters on critical moments.

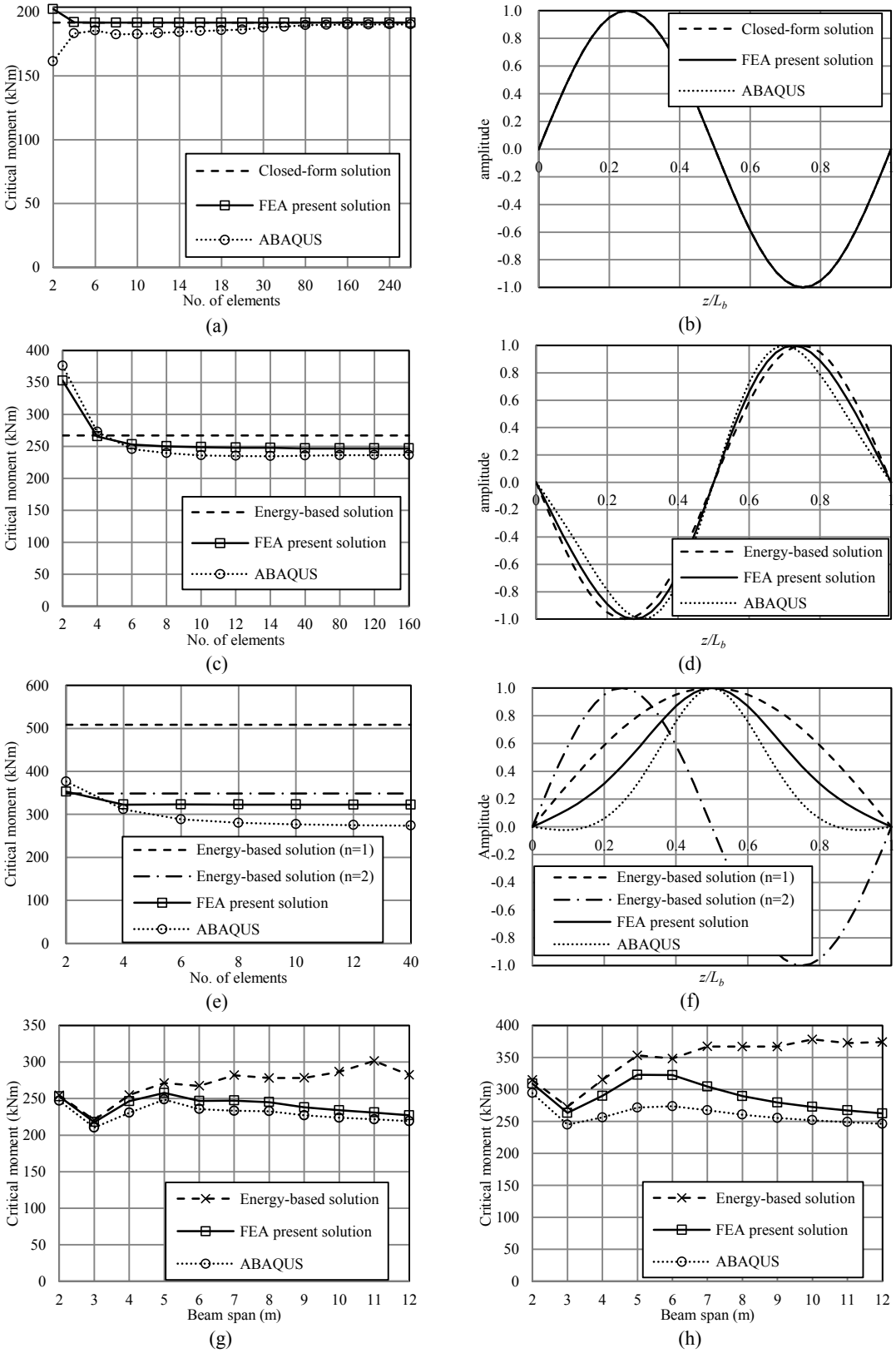

Figure 4.3 (a) Convergence study for uniform moments, (b) mode shapes for uniform moments, (c) convergence study for UDL, (d) mode shapes for UDL, (e) convergence study for mid-span concentrated loads, (f) mode shapes for mid-span concentrated loads, (g) critical moments for UDL with varying beam span, (h) critical moments for mid-span concentrated loads with varying beam span

4.9 Parametric Study

A parametric study has been conducted by varying one parameter at a time from the reference case defined in the verification study and observing the critical moments and buckling mode shapes as predicted by the present solutions. Nine sets of parametric studies are considered by varying loading types, beam and deck span, lateral restraint height, load position, number of spans and whether the deck lateral or twisting restraint is included in the analysis (Table 4.2).

Table 4.2 Summary of parametric runs

Case No.	Closed-form or energy-based solution	FEA present solution	ABAQUS	Load type	Beam span (m)	Deck span (m)	Loading point	No. of spans	Height of lateral restraint	Lateral or twisting restraints included	Figure or table link
Reference	✓	✓	✓	UM/UDL/CL	6	2	/	1	DC	Y	Figure 4.3 (a,b,c,d,e,f)
1	✓	✓	✓	UDL/CL	2-12	2	DC	1	DC	Y	Figure 4.3(g,h)
2	✓			UM	2-12	2	DC	1	DC	Y	Figure 4.4a
3		✓		UM/UDL/CL	6	1-5	DC	1	DC	Y	Figure 4.4b
4	✓			UM	2-12	2	/	1	DC	N	Figure 4.4c
5	✓			UM	6	1-5	/	1	DC	N	Figure 4.4d
6		✓		UDL	4,6,8	2	DC	1	BSC-DC	Y	Figure 4.4e
7	✓	✓		UDL	4,6,8	2	DC/BSC/BB	1	DC	Y	Table 4.3
8	✓	✓		UDL	6	1,3,5	DC/BSC/BB	1	DC	Y	Table 4.4
9		✓		UDL/CL	4-12	2	DC	2	DC	Y	Figure 4.5(a,b)

Note:
UM=uniform moments; UDL=uniformly distributed loads; CL= mid-span concentrated loads;
DC=deck centerline; BSC=beam shear center; BB=beam bottom;
Y=yes; N=no.

4.9.1 Effects of beam and deck span

Figure 4.4a shows the critical moments for both beams under uniform moments. The beam span was varied from 2 m to 12 m, all in the elastic or inelastic buckling range. The critical moments corresponding to modes 1 to 4 are shown in the figure. It is observed that mode 1 provides the lowest critical moment for spans ranging from 2 m to 4 m. From 4 m to 7 m, mode 2 corresponds to the lowest critical moment while mode 3 provides the lowest critical moment from 7 m to 10 m and mode 4 is the governing mode of buckling for spans larger than 10 m. As the beam span increases, the critical moments are observed to be nearly constant while the governing mode number n

changes with the beam span. For the cases of UDL and mid-span concentrated loads (Figure 4.3g,h), the critical moments from all three solutions show an oscillating behavior as the beam span is increased. In contrast, as the deck span increases from 1 m to 5 m, the buckling capacity is observed to decrease (Figure 4.4b) for all three loading types investigated.

4.9.2 Effects of deck lateral and twisting restraints

For uniform moments, Figure 4.4c shows three solutions: (1) the classical solution, which is based on laterally unrestrained beam, gives the lowest buckling capacity; (2) the solution by Roeder and Assadi (1982), which recognizes the rigid lateral restraint provided by decking but neglects its partial twisting restraint, and thus gives a higher critical moment prediction than that based on the classical solution; and (3) the present solution, i.e., Eq. (4.21a,b), which assumes the deck boards to provide rigid lateral restraint and partial twisting restraint, gives the highest buckling predictions among the three solutions. Figure 4.4c shows that the effects of both types of restraints is small for short span but becomes more substantial in long span. Also, the critical moments obtained from the present study can be several folds higher than values of unrestrained beams. For deck span increasing from 1 m to 5 m (Figure 4.4d), the contribution of elastic twisting restraint declines. This reflects on the observed critical moments which reduce with deck span. By comparing the solid and dashed lines, the rigid lateral restraint contributes a constant 68.3 kNm towards the total capacity.

4.9.3 Effect of lateral restraint height

Figure 4.4e shows the critical moments as predicted by the present FEA for the twin-beam-deck system under UDL with rigid lateral restraint height varying from the beam shear center to deck centerline. Three beam spans were investigated (i.e., 4, 6, 8 m). The results suggest that for each span, there is an optimal lateral bracing height which corresponds to a peak moment.

4.9.4 Effect of load position

To assess the effect of load position, a UDL was applied at three different heights (i.e., deck centerline, beam shear center and beam bottom). The critical moments as predicted by the approximate energy-based solution and the present FEA are summarized in Table 4.3 for three beam spans (i.e., 4, 6, 8 m). No ABAQUS results were provided since the B31OS solution does not support the feature for load position

effect. For all three spans investigated, both the energy-based solution and the present FEA predict a decrease in critical moments as the point of load application moves downwards. Also, it is observed that the load position effect is particularly significant for the shorter beam span of 4 m. Compared with the case of beam shear center loading, both solutions predict a more than 40% capacity increase for the case of deck centerline loading and more than a 20% capacity decrease for the case of beam bottom loading. In contrast, for the case of longer beam spans, the load position effect is observed to be less substantial. It is of interest to note that the percentage increase or decrease of critical moments due to load position effect based on the energy solution reasonably agree well with those based on the finite element solution.

The effect is also investigated under three deck spans (i.e., 1, 3, 5 m) and is summarized in Table 4.4. The load position effect is observed to be more substantial for long deck span.

4.9.5 Effect of beam span on two-span twin-beam-deck systems

The buckling capacity obtained from the present FEA for a two-span twin-beam-deck system under UDL and a mid-span concentrated load are shown in Figure 4.5(a,b). Contrary to the case of single-span beams where lateral torsional buckling is associated solely with negative moments or upward loading, the buckling resistance of continuous beams is found possible under upward and downward acting loading. For downward acting loadings, the critical moments observed at mid-spans decrease significantly as the beam span increases from 4 m to 12 m. In contrast, for upward acting loading, the critical moments remain essentially constant and are insensitive of the span. Table 4.5 provides a comparison of the critical moments for single-span and two-span twin-beam-deck systems with an uplift UDL applied at the deck centerline. The results suggest that the critical moments for two-span twin-beam-deck assemblies are generally higher than those based on single-span assemblies of the same span.

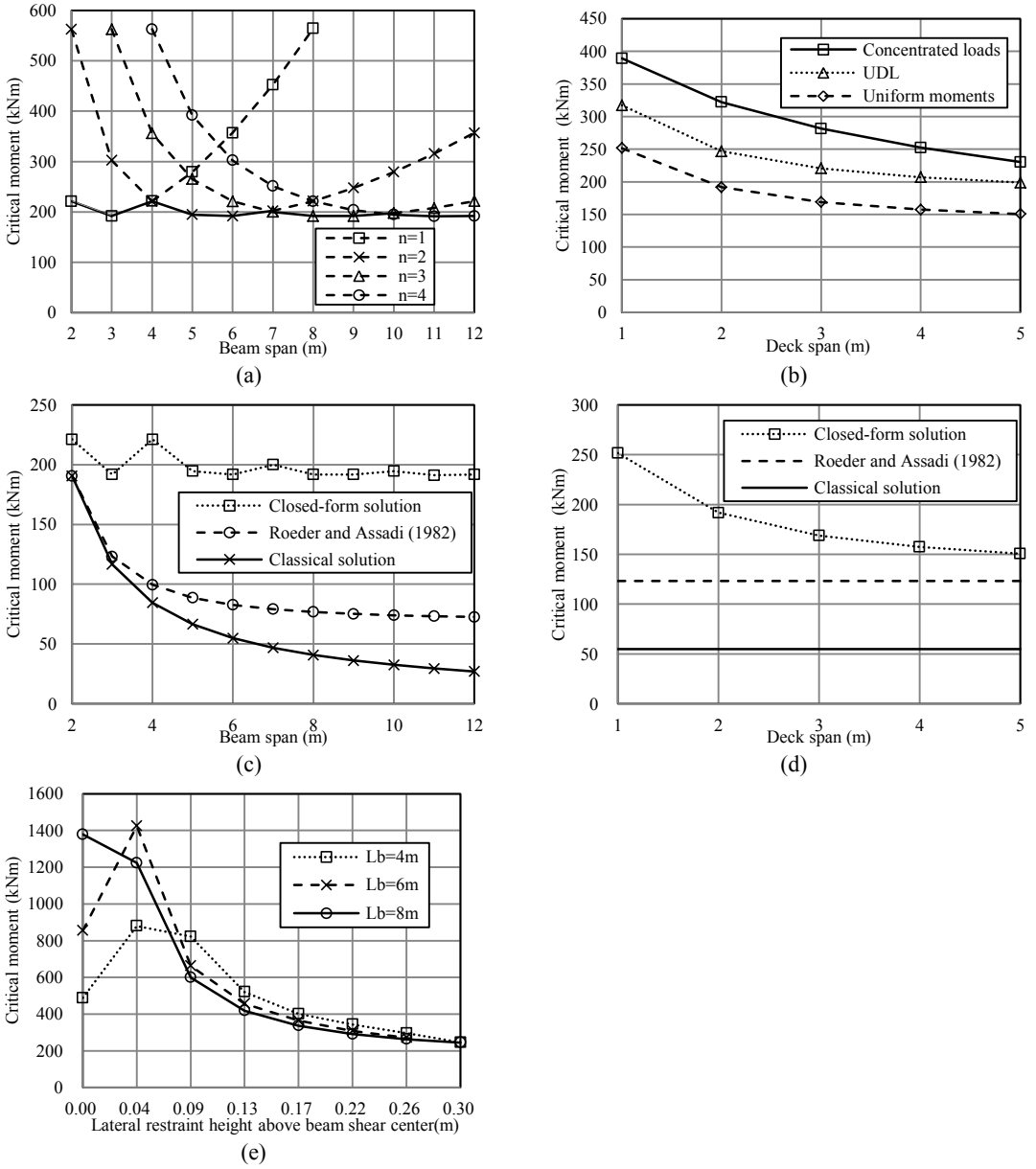

Figure 4.4 (a) Effect of beam span on buckling capacity under uniform moments, (b) effect of deck span on buckling capacity; buckling capacity as influenced by inclusion/exclusion of lateral and twisting restraints under uniform moments (c) with varying beam span, (d) with varying deck span; (e) effect of lateral restraint height under UDL

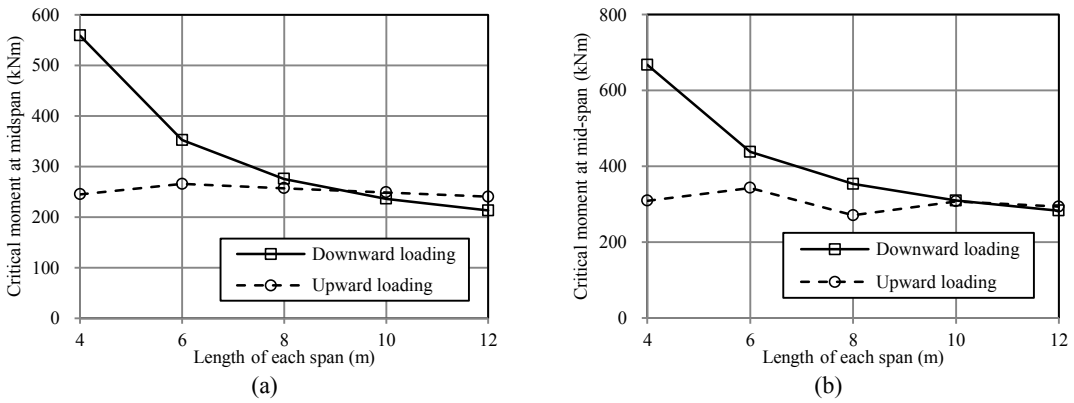

Figure 4.5 Buckling capacity for two-span continuous beams under (a) UDL, (b) mid-span concentrated loads

Table 4.3 Load position effect for different beam spans under UDL

Beam span (m)	Load position	Energy-based solution		FEA present	
		Critical moment (kNm)	Difference	Critical moment (kNm)	Difference
4	Deck centerline	255	46.6%	246	43.0%
	Beam shear center	174	/	172	/
	Beam bottom	134	-23.0%	133	-22.7%
6	Deck centerline	268	14.5%	247	12.3%
	Beam shear center	234	/	220	/
	Beam bottom	210	-10.3%	200	-9.09%
8	Deck centerline	278	6.51%	245	6.06%
	Beam shear center	261	/	231	/
	Beam bottom	242	-7.28%	215	-6.93%

Table 4.4 Load position effect for different deck spans under UDL

Deck span (m)	Load position	Energy-based solution		FEA present	
		Critical moment (kNm)	Difference	Critical moment (kNm)	Difference
1	Deck centerline	363	14.2%	317	9.69%
	Beam shear center	318	/	289	/
	Beam bottom	285	-10.4%	265	-8.30%
3	Deck centerline	236	14.6%	221	12.2%
	Beam shear center	206	/	197	/
	Beam bottom	161	-21.8%	157	-20.3%
5	Deck centerline	210	39.1%	199	35.4%
	Beam shear center	151	/	147	/
	Beam bottom	116	-23.2%	115	-21.8%

Table 4.5 Comparison of critical moments between single-span and two-span beams

Beam span/ length of each span (m)	Critical moment for upward UDL (kNm)		Ratio
	Single-span system	Two-span system	
4	246	245	0.99
6	247	266	1.08
8	245	257	1.05
10	234	249	1.06
12	227	240	1.06

4.10 Summary and Conclusions

1. Four solutions were developed, formulated, and implemented for investigating the lateral torsional buckling capacity of wooden twin-beam-deck assembles: (1) a closed-form solution for simply-supported beams under uniform moments, (2) an analytical solution for generic boundary conditions under uniform moments, (3) an energy based approximate solution for non-uniform moments, and (4) a FEA solution.
2. The validity of the solutions was assessed by comparison to the results based on ABAQUS, and to a close-form solution available in the literature for the special case involving uniform moments.
3. The verified solutions were then used to provide a comprehensive parametric study to investigate the effects of load types, beam and deck spans, height of lateral restraint, load position relative to deck centerline, number of spans and whether the deck lateral or twisting restraint is included in the analysis.

For single-span simply-supported twin-beam-deck system, the key engineering observations are:

1. Only net uplift loads are found to be able to induce lateral torsional buckling.
2. The approximate energy-based solutions provide predictions in excellent agreement with the present FEA and ABAQUS for short beams span. For long spans, the solution slightly overestimates the critical moments.
3. Unlike laterally unsupported beams which has clear downward trend between critical moment and beam span, both the present solutions and ABAQUS indicate that, in general, there is no clear trend for the buckling capacity and span.

4. The lateral torsional buckling capacity for laterally and rotationally restrained twin beams can be much higher than unrestrained beams. The presence of lateral and twisting restrains is strongly influential in increasing the lateral torsional buckling capacity of the system, especially for long beams span.
5. The height of lateral restraint has a significant influence on the buckling capacity of the system. For a given beam span, there is an optimal lateral restraint height that maximizes the buckling load capacity.
6. The buckling capacity was observed to decrease as the point of application of the applied upward load moves downwards and such effect is particularly significant for *short beam* span or *long deck* span.

For two-span twin-beam-deck systems, both upward and downward loading are observed to be able to induce lateral torsion buckling. For upward loading, the buckling capacity remains nearly constant irrespective of the beam span. The buckling capacity for two-span systems is slightly higher than that of a single-span system with the same span. For downward loading, the buckling capacity is observed to significantly decrease as the span increases.

Appendix 4A Transformed Section Properties for Composed I-section Beams

Consider a composite I-section beam with both flanges having different material from the web. Assume the flanges have a modulus of elasticity E_b and shear modulus G_b with a total area for both flanges A_f. The web is assumed to have a modulus of elasticity E_w, a shear modulus G_w and an area A_w. The internal strain energy stored in the beam U_b can be expressed as

$$U_b = U_L + U_{sv} = \frac{1}{2}\int_0^{L_b}\left(\int_{A_f}\sigma\varepsilon dA_f + \int_{A_w}\sigma\varepsilon dA_w\right)_b dz + \frac{1}{2}\int_0^{L_b}\left(G_bJ_f + G_wJ_w\right)_b\theta'^2 dz \quad (4.A.1)$$

in which U_L and U_{sv} are the internal strain energy expressions due to longitudinal strain ε and Saint-Venant torsion, respectively, σ is the longitudinal stress, and J_f, J_w are the Saint-Venant torsional constants for both flanges and the web, respectively and subscript b denotes variables pertaining to the beam. Defining the modular ratio for shear moduli $n_1 = G_w/G_b$ and introducing the transformed Saint-Venant torsional constant $J_b = J_f + n_1J_w$, Eq. (4.A.1) can be rewritten as

$$U_b = \frac{1}{2}\int_0^{L_b}\left(\int_{A_f}\sigma\varepsilon dA_f + \int_{A_w}\sigma\varepsilon dA_w\right)_b dz + \frac{1}{2}\int_0^{L_b}G_bJ_b\theta'^2 dz \quad (4.A.2)$$

Assuming compatibility of strains at the web-flange interfaces, the longitudinal stress is expressed in terms of the strains as

$$\sigma = \begin{cases} E_b\varepsilon & ....A_f \\ E_w\varepsilon & ....A_w \end{cases} \quad (4.A.3)$$

Introducing the modular ratio $n_2 = E_w/E$ for the moduli of elasticity, one rewrites Eq. (4.A.2) as

$$U_b = \frac{E_b}{2}\int_0^{L_b}\left(\int_{A_f}\varepsilon^2 dA_f + n_2\int_{A_w}\varepsilon^2 dA_w\right)_b dz + \frac{1}{2}\int_0^{L_b}G_bJ_b\theta'^2 dz \quad (4.A.4)$$

According to the Vlasov theory (Vlasov 1961), the longitudinal displacement field

$\overline{w}(s,z)$ at a generic point is

$$\overline{w}(s,z)=\left\langle w(z) \quad -u'(z) \quad -v'(z) \quad -\theta'(z)\right\rangle \begin{Bmatrix} 1 \\ x(s) \\ y(s) \\ \omega(s) \end{Bmatrix} \tag{4.A.5}$$

in which $w(z)$ is the average longitudinal displacement, and one recalls that $u(z)$ is the lateral displacement, $v(z)$ is the vertical displacement, $\theta(z)$ is the angle of twist. Symbols $x(s)$, $y(s)$ denote the coordinates along x and y axes of a point $B(s)$ located at a circumferential distance s from the sectorial origin B_1, and $\omega(s)=\int_{B_1}^{B(s)} d\omega(s)$ is the sectorial coordinate based on a fixed radius taken from the shear center to the sectorial origin B_1. All primes denote differentiation with respect to coordinate z along the beam longitudinal axis. The longitudinal strain $\varepsilon(s,z)$ is obtained by differentiation of the longitudinal displacement $\overline{w}(s,z)$ as given in Eq. (4.A.5)

$$\varepsilon(s,z)=\frac{\partial}{\partial z}\overline{w}(z,s)=\left\langle w'(z) \quad -u''(z) \quad -v''(z) \quad -\theta''(z)\right\rangle \begin{Bmatrix} 1 \\ x(s) \\ y(s) \\ \omega(s) \end{Bmatrix} \tag{4.A.6}$$

From Eq. (4.A.6), by substituting into Eq. (4.A.4), one obtains

$$U_L=\frac{E}{2}\int_0^{L_b}\left\langle w' \quad -u'' \quad -v'' \quad -\theta''\right\rangle \times$$
$$\begin{bmatrix} A_f+n_2A_w & -S_{x,f}-n_2S_{x,w} & -S_{y,f}-n_2S_{y,w} & -S_{\omega,f}-n_2S_{\omega,w} \\ -S_{x,f}-n_2S_{x,w} & I_{yy,f}+n_2I_{yy,w} & I_{xy,f}+n_2I_{xy,w} & I_{\omega x,f}+n_2I_{\omega x,w} \\ -S_{y,f}-n_2S_{y,w} & I_{xy,f}+n_2I_{xy,w} & I_{xx,f}+n_2I_{xx,w} & I_{\omega y,f}+n_2I_{\omega y,w} \\ -S_{\omega,f}-n_2S_{\omega,w} & I_{\omega x,f}+n_2I_{\omega x,w} & I_{\omega y,f}+n_2I_{\omega y,w} & I_{\omega\omega,f}+n_2I_{\omega\omega,w} \end{bmatrix}_b \begin{Bmatrix} w' \\ -u'' \\ -v'' \\ -\theta'' \end{Bmatrix} dz \tag{4.A.7}$$

where

$$S_{x,f}=\int_{A_f} xdA_f, S_{x,w}=\int_{A_w} xdA_w, S_{y,f}=\int_{A_f} ydA_f, S_{y,w}=\int_{A_w} ydA_w, S_{\omega,f}=\int_{A_f} \omega dA_f,$$

$$S_{\omega,w}=\int_{A_w} \omega dA_w, I_{xx,f}=\int_{A_f} y^2 dA_f, I_{xx,w}=\int_{A_w} y^2 dA_w, I_{yy,f}=\int_{A_f} x^2 dA_f, I_{yy,w}=\int_{A_w} x^2 dA_w,$$

$$I_{xy,f}=\int_{A_f} xydA_f, I_{xy,w}=\int_{A_w} xydA_w, I_{\omega x,f}=\int_{A_f} \omega xdA_f, I_{\omega x,w}=\int_{A_w} \omega xdA_w, I_{\omega y,f}=\int_{A_f} \omega ydA_f,$$

$$I_{\omega y,w}=\int_{A_w} \omega ydA_w, I_{\omega\omega,f}=\int_{A_f} \omega^2 dA_f, I_{\omega\omega,w}=\int_{A_w} \omega^2 dA_w$$

For doubly-symmetric I-section beam, by choosing the origin O to coincide with the section centroid, one obtains

$$-S_{x,f}-n_2 S_{x,w}=0,\ -S_{y,f}-n_2 S_{y,w}=0 \tag{4.A.8}$$

Also, orienting x and y axes along the principal directions gives

$$I_{xy,f}+n_2 I_{xy,w}=0 \tag{4.A.9}$$

By selecting the pole N at the section centroid, one has

$$I_{\omega x,f}+n_2 I_{\omega x,w}=0,\quad I_{\omega y,f}+n_2 I_{\omega y,w}=0 \tag{4.A.10}$$

Also, by selecting the sectorial origin B_1 at the section centroid, one obtains

$$-S_{\omega,f}-n_2 S_{\omega,w}=0 \tag{4.A.11}$$

Eq. (4.A.7) simplifies to

$$U_L=\frac{E}{2}\int_0^{L_b}\left\langle w'(z)\quad -u''(z)\quad -v''(z)\quad -\theta''(z)\right\rangle$$

$$\begin{bmatrix} A_f+n_2A_w & 0 & 0 & 0\\ 0 & I_{yy,f}+n_2I_{yy,w} & 0 & 0\\ 0 & 0 & I_{xx,f}+n_2I_{xx,w} & 0\\ 0 & 0 & 0 & I_{\omega\omega,f}+n_2I_{\omega\omega,w}\end{bmatrix}\begin{Bmatrix} w'(z)\\ -u''(z)\\ -v''(z)\\ -\theta''(z)\end{Bmatrix}dz \tag{4.A.12}$$

$$=\frac{1}{2}\int_0^{L_b} E_b\left(A_f+n_2A_w\right)w'^2dz+\frac{1}{2}\int_0^{L_b} E_b\left(I_{yy,f}+n_2I_{yy,w}\right)u''^2dz$$

$$+\frac{1}{2}\int_0^{L_b} E_b\left(I_{xx,f}+n_2I_{xx,w}\right)v''^2dz+\frac{1}{2}\int_0^{L_b} E_b\left(I_{\omega\omega,f}+n_2I_{\omega\omega,w}\right)\theta''^2dz$$

In lateral torsional buckling analysis, only the third and fourth terms in Eq. (4.A.12) contribute to the internal strain energy for the I cross-section beam can be written as

$$U_b = \frac{1}{2}\int_0^{L_b} E_b I_y u''^2 dz + \frac{1}{2}\int_0^{L_b} E_b C_w \theta''^2 dz + \frac{1}{2}\int_0^{L_b} G_b J_b \theta'^2 dz \tag{4.A.13}$$

In Eq. (4.A.13), one recapitulates that E_b and G_b are the modulus of elasticity and shear modulus of the flange, and the following transformed sections have been defined

$$J_b = J_f + n_1 J_w$$
$$I_y = I_{yy,f} + n_2 I_{yy,w}$$
$$C_w = I_{\omega\omega,f} + n_2 I_{\omega\omega,w}$$

in which J_f and J_w are the Saint-Venant torsional constants for both flanges, and the web, respectively, $n_1 = G_w/G_b$ is the ratio of shear modulus G_w for the web to that of the flange, $n_2 = E_w/E_b$ is the ratio of Young modulus E_w of the web to that of the flange.

Appendix 4B Derivation of Equilibrium Equations and Boundary Conditions

Starting from the total potential energy expression Eq. (4.11), this appendix shows the details of deriving the equilibrium equations and associated boundary conditions. By imposing the stationarity condition, one obtains

$$\delta\pi = \frac{\partial\pi}{\partial\theta_1}\delta\theta_1 + \frac{\partial\pi}{\partial\theta_1'}\delta\theta_1' + \frac{\partial\pi}{\partial\theta_1''}\delta\theta_1'' + \frac{\partial\pi}{\partial\theta_2}\delta\theta_2 + \frac{\partial\pi}{\partial\theta_2'}\delta\theta_2' + \frac{\partial\pi}{\partial\theta_2''}\delta\theta_2'' = 0 \quad (4.B.1)$$

which leads to

$$\begin{aligned}\delta\Pi = {} & \lambda\int_0^{L_b}\left(hq\theta_1 - aM\theta_1''\right)\delta\theta_1 dz + \frac{E_d h_d^{\,3}}{6L_d}\int_0^{L_b}\left(2\theta_1+\theta_2\right)\delta\theta_1 dz + \int_0^{L_b} G_b J_b\theta_1'\delta\theta_1' dz \\ & + \int_0^{L_b}\left(E_b C\theta_1'' - a\lambda M\theta_1\right)\delta\theta_1'' dz + \lambda\int_0^{L_b}\left(hq\theta_2 - aM\theta_2''\right)\delta\theta_2 dz + \frac{E_d h_d^{\,3}}{6L_d}\int_0^{L_b}\left(\theta_1+2\theta_2\right)\delta\theta_2 dz \\ & + \int_0^{L_b} G_b J_b\theta_2'\delta\theta_2' dz + \int_0^{L_b}\left(E_b C\theta_2'' - a\lambda M\theta_2\right)\delta\theta_2'' dz = 0\end{aligned} \quad (4.B.2)$$

Through integration by parts, one obtains

$$\begin{aligned}&\int_0^{L_b} G_b J_b\theta_1'\delta\theta_1' dz = \left[G_b J_b\theta_1'\delta\theta_1\right]_0^{L_b} - \int_0^{L_b} G_b J_b\theta_1''\delta\theta_1 dz \\ &\int_0^{L_b}\left(E_b C\theta_1'' - a\lambda M\theta_1\right)\delta\theta_1'' dz = \left[\left(E_b C\theta_1'' - a\lambda M\theta_1\right)\delta\theta_1'\right]_0^{L_b} - \int_0^{L_b}\left(E_b C\theta_1'' - a\lambda M\theta_1\right)'\delta\theta_1' dz \\ &= \left[\left(E_b C\theta_1'' - a\lambda M\theta_1\right)\delta\theta_1'\right]_0^{L_b} - \left[\left(E_b C\theta_1'' - a\lambda M\theta_1\right)'\delta\theta_1\right]_0^{L_b} + \int_0^{L_b}\left(E_b C\theta_1'' - a\lambda M\theta_1\right)''\delta\theta_1 dz \\ &\int_0^{L_b} G_b J_b\theta_2'\delta\theta_2' dz = \left[G_b J_b\theta_2'\delta\theta_2\right]_0^{L_b} - \int_0^{L_b} G_b J_b\theta_2''\delta\theta_2 dz \\ &\int_0^{L_b}\left(E_b C\theta_2'' - a\lambda M\theta_2\right)\delta\theta_2'' dz = \left[\left(E_b C\theta_2'' - a\lambda M\theta_2\right)\delta\theta_2'\right]_0^{L_b} - \int_0^{L_b}\left(E_b C\theta_2'' - a\lambda M\theta_2\right)'\delta\theta_2' dz \\ &\left[\left(E_b C\theta_2'' - a\lambda M\theta_2\right)\delta\theta_2'\right]_0^{L_b} - \left[\left(E_b C\theta_2'' - a\lambda M\theta_2\right)'\delta\theta_2\right]_0^{L_b} + \int_0^{L_b}\left(E_b C\theta_2'' - a\lambda M\theta_2\right)''\delta\theta_2 dz\end{aligned} \quad (4.B.3)$$

Substituting the above expressions into Eq. (4.B.2), one obtains

$$
\begin{aligned}
\delta\Pi = & \int_0^{L_b}\left[\left(E_bC\theta_1'' - a\lambda M\theta_1\right)'' - G_bJ_b\theta_1'' + \lambda\left(hq\theta_1 - aM\theta_1''\right) + \frac{E_d{h_d}^3}{6L_d}\left(2\theta_1+\theta_2\right)\right]\delta\theta_1 dz \\
& + \int_0^{L_b}\left[\left(E_bC\theta_2'' - a\lambda M\theta_2\right)'' - G_bJ_b\theta_2'' + \lambda\left(hq\theta_2 - aM\theta_2''\right) + \frac{E_d{h_d}^3}{6L_d}\left(\theta_1+2\theta_2\right)\right]\delta\theta_2 dz \\
& + \left[\left(G_bJ_b\theta_1' - \left(E_bC\theta_1'' - a\lambda M\theta_1\right)'\right)\delta\theta_1\right]_0^{L_b} + \left[\left(E_bC\theta_1'' - a\lambda M\theta_1\right)\delta\theta_1'\right]_0^{L_b} \\
& + \left[\left(G_bJ_b\theta_2' - \left(E_bC\theta_2'' - a\lambda M\theta_2\right)'\right)\delta\theta_2\right]_0^{L_b} + \left[\left(E_bC\theta_2'' - a\lambda M\theta_2\right)\delta\theta_2'\right]_0^{L_b} \\
= & 0
\end{aligned}
\tag{4.B.4}
$$

Therefore, the equilibrium equations take the form

$$
\begin{aligned}
&\left(E_bC\theta_1'' - a\lambda M\theta_1\right)'' - G_bJ_b\theta_1'' + \lambda\left(hq\theta_1 - aM\theta_1''\right) + \frac{E_d{h_d}^3}{6L_d}\left(2\theta_1+\theta_2\right) = 0 \\
&\left(E_bC\theta_2'' - a\lambda M\theta_2\right)'' - G_bJ_b\theta_2'' + \lambda\left(hq\theta_2 - aM\theta_2''\right) + \frac{E_d{h_d}^3}{6L_d}\left(\theta_1+2\theta_2\right) = 0
\end{aligned}
\tag{4.B.5}
$$

Also, the boundary conditions are

$$
\begin{aligned}
&\left[\left(G_bJ_b\theta_1' - \left(E_bC\theta_1'' - a\lambda M\theta_1\right)'\right)\delta\theta_1\right]_0^{L_b} = 0,\ \left[\left(E_bC\theta_1'' - a\lambda M\theta_1\right)\delta\theta_1'\right]_0^{L_b} = 0 \\
&\left[\left(G_bJ_b\theta_2' - \left(E_bC\theta_2'' - a\lambda M\theta_2\right)'\right)\delta\theta_2\right]_0^{L_b} = 0,\ \left[\left(E_bC\theta_2'' - a\lambda M\theta_2\right)\delta\theta_2'\right]_0^{L_b} = 0
\end{aligned}
\tag{4.B.6}
$$

Appendix 4C Derivation of Critical Moment for Simply-supported Beams under Uniform Moments

Based on Eq. (4.20), this appendix shows the details of deriving the critical moment expression for a simply-supported twin-beam-deck system under uniform moments. For a non-trivial solution, the determinant of the matrix of coefficient must vanish yielding

$$\begin{vmatrix} E_b C l_n^4 + \left(G_b J_b + 2a\lambda M\right) l_n^2 + \dfrac{E_d h_d^3}{3L_d} & E_d h_d^3 / 6L_d \\ E_d h_d^3 / 6L_d & E_b C l_n^4 + \left(G_b J_b + 2a\lambda M\right) l_n^2 + \dfrac{E_d h_d^3}{3L_d} \end{vmatrix} = 0 \quad \text{(4.C.1)}$$

which leads to

$$E_b C l_n^4 + \left(G_b J_b + 2a\lambda M\right) l_n^2 + \frac{E_d h_d^3}{3L_d} = \pm \frac{E_d h_d^3}{6L_d} \quad \text{(4.C.2)}$$

From Eq. (4.C.2) , one obtains the following two roots

$$\begin{aligned} \left(\lambda M\right)_{1n} &= -\left[\frac{E_b C}{2a} \left(\frac{n\pi}{L_b} \right)^2 + \frac{G_b J_b}{2a} + \frac{E_d h_d^3}{12aL_d} \left(\frac{L_b}{n\pi} \right)^2 \right], \\ \left(\lambda M\right)_{2n} &= -\left[\frac{E_b C}{2a} \left(\frac{n\pi}{L_b} \right)^2 + \frac{G_b J_b}{2a} + \frac{E_d h_d^3}{4aL_d} \left(\frac{L_b}{n\pi} \right)^2 \right] \end{aligned} \quad \text{(4.C.3)}$$

By substituting the first root into Eq. (4.C.1), one obtains the amplitude ratio $A_1 / A_2 = -1$, which corresponds to a symmetric mode. Also, by substituting the second root into Eq. (4.C.1), one obtains $A_1 / A_2 = 1$, which corresponds to an anti-symmetric buckling mode.

Appendix 4D Relationship between β/α Ratio and Buckling Mode Number

Based on Eq. (4.22), for combinations of dimensionless parameters α and β, the relationship between β/α ratio and the corresponding buckling mode number n is derived in this appendix. From Eq. (4.22), when the mode number is $n=1$, the dimensionless critical moment is $m_r(1)=-\left(1+\alpha+\beta\right)$. When $n=2$, the corresponding dimensionless critical moment $m_r(2)=-\left(1+4\alpha+\beta/4\right)$. By setting $\left|m_r(1)\right|\le\left|m_r(2)\right|$, one obtains $\beta/\alpha\le 4$. For $n=3$, the dimensionless critical moment $m_r(3)=-\left(1+9\alpha+\beta/9\right)$. By setting $\left|m_r(2)\right|\le\left|m_r(3)\right|$, one obtains $\beta/\alpha\le 36$. Similarly, by setting $\left|m_r(3)\right|\le\left|m_r(4)\right|$ leads to $\beta/\alpha\le 144$. For the mode number $n=i$, $m_r(i)=-\left(1+i^2\alpha+\beta/i^2\right)$ and for $n=i+1$, $m_r(i+1)=-\left[1+\left(i+1\right)^2\alpha+\beta/\left(i+1\right)^2\right]$. By Setting $\left|m_r(i)\right|\le\left|m_r(i+1)\right|$, one otbains $\beta/\alpha\le i^2(i+1)^2$. The above relationship is summarized in Table 4.D.1.

Table 4.D.1 Relationship between β/α and the governing mode number

Range of β/α	Governing Mode Number n	Critical moment equation
$\beta/\alpha\le 4$	1	$M_{cr}/M_{\alpha}=-\left(1+\alpha+\beta\right)$
$4<\beta/\alpha\le 36$	2	$M_{cr}/M_{\alpha}=-\left(1+4\alpha+\beta/4\right)$
$36<\beta/\alpha\le 144$	3	$M_{cr}/M_{\alpha}=-\left(1+9\alpha+\beta/9\right)$
$\left(i-1\right)^2 i^2<\beta/\alpha\le i^2(i+1)^2$	i	$M_{cr}/M_{\alpha}=-\left(1+i^2\alpha+\beta/i^2\right)$

Appendix 4E Derivation of Critical Load for Simply-supported Beams under UDL

Based on Eq.(4.23), this appendix shows the details of deriving the critical UDL for the twin-beam-deck system. Substituting the strong-axis bending moment $M = q\left(L_b z - z^2\right)/2$ into Eq.(4.23), one obtains

$$\begin{aligned}\Pi = {} & \frac{1}{2}E_b C A_1'^2 l_n^4 \int_0^{L_b} \sin^2\left(l_n z\right) dz + \frac{1}{2}G_b J_b A_1'^2 l_n^2 \int_0^{L_b} \cos^2\left(l_n z\right) dz \\ & + a\lambda A_1'^2 l_n^2 \int_0^{L_b} M \sin^2\left(l_n z\right) dz + \frac{1}{2}\lambda h A_1'^2 \int_0^{L_b} q \sin^2\left(l_n z\right) dz + \frac{1}{2}E_b C A_2'^2 l_n^4 \int_0^{L_b} \sin^2\left(l_n z\right) dz \\ & + \frac{1}{2}G_b J_b A_2'^2 l_n^2 \int_0^{L_b} \cos^2\left(l_n z\right) dz + a\lambda A_2'^2 l_n^2 \int_0^{L_b} M \sin^2\left(l_n z\right) dz + \frac{1}{2}\lambda h A_2'^2 \int_0^{L_b} q \sin^2\left(l_n z\right) dz \\ & + \frac{E_d h_d^3}{6L_d}\left(A_1'^2 + A_1' A_2' + A_2'^2\right) \int_0^{L_b} \sin^2\left(l_n z\right) dz\end{aligned} \tag{4.E.1}$$

By applying the principle of stationary potential energy, i.e., $\partial\pi/\partial A_1' = \partial\pi/\partial A_2' = 0$, one obtains

$$\begin{aligned}\delta\Pi = {} & \delta A_1' \left[E_b C A_1' l_n^4 \int_0^{L_b} \sin^2\left(l_n z\right) dz + G_b J_b A_1' l_n^2 \int_0^{L_b} \cos^2\left(l_n z\right) dz + a\lambda q A_1' l_n^2 L_b^3 \frac{n^2\pi^2 + 3}{12n^2\pi^2} \right. \\ & \left. + h\lambda q A_1' \int_0^{L_b} \sin^2\left(l_n z\right) dz + \frac{E_d h_d^3}{6L_d}\left(2A_1' + A_2'\right) \int_0^{L_b} \sin^2\left(l_n z\right) dz \right] \\ & + \delta A_2' \left[E_b C A_2' l_n^4 \int_0^{L_b} \sin^2\left(l_n z\right) dz + G_b J_b A_2' l_n^2 \int_0^{L_b} \cos^2\left(l_n z\right) dz + a\lambda q A_2' l_n^2 L_b^3 \frac{n^2\pi^2 + 3}{12n^2\pi^2} \right. \\ & \left. + h\lambda q A_2' \int_0^{L_b} \sin^2\left(l_n z\right) dz + \frac{E_d h_d^3}{6L_d}\left(A_1' + 2A_2'\right) \int_0^{L_b} \sin^2\left(l_n z\right) dz \right] \\ = {} & 0\end{aligned} \tag{4.E.2}$$

The following equilibrium equations are recovered

$$\begin{bmatrix} \psi_n + \lambda q\left(h + a l_n^2 L_b^2 \dfrac{n^2\pi^2 + 3}{6n^2\pi^2}\right) & \dfrac{E_d h_d^3}{6L_d} \\ \dfrac{E_d h_d^3}{6L_d} & \psi_n + \lambda q\left(h + a l_n^2 L_b^2 \dfrac{n^2\pi^2 + 3}{6n^2\pi^2}\right) \end{bmatrix} \begin{Bmatrix} A_1' \\ A_2' \end{Bmatrix}_n = \{0\}$$

(4.E.3)

in which $\psi_n = E_b C l_n^4 + G_b J_b l_n^2 + E_d h_d^3 / 3L_d$ has been defined. For a non-trivial solution in Eq.(4.E.3), the determinant should vanish, which leads to

$$\begin{aligned}
(\lambda q)_{1n} &= -\frac{6n^4\pi^4 E_b C L_d + 6n^2\pi^2 G_b J_b L_b^2 L_d + E_d H_d^3 L_b^4}{L_b^4 L_d \left(6h + n^2\pi^2 a + 3a\right)} \\
(\lambda q)_{2n} &= -\frac{6n^4\pi^4 E_b C L_d + 6n^2\pi^2 G_b J_b L_b^2 L_d + 3E_d H_d^3 L_b^4}{L_b^4 L_d \left(6h + n^2\pi^2 a + 3a\right)}
\end{aligned} \tag{4.E.4}$$

Substituting $(\lambda q)_{1n}$ into Eq. (4.E.3), one obtains the buckling amplitude ratio $A_1' / A_2' = -1$, which corresponds to a symmetric mode. Also, by substituting $(\lambda q)_{2n}$ into Eq. (4.E.3), one obtains $A_1' / A_2' = 1$, corresponding to an anti-symmetric buckling mode.

Appendix 4F Derivation of Critical Load for Simply-supported Beams under Mid-span Concentrated Loads

Starting with Eq.(4.23), this appendix shows the details of deriving the critical load for a twin-beam-deck system subjected to a mid-span point load. Substituting the expression for the strong-axis bending moments $M(z)$ induced by a mid-span concentrated load into Eq. (4.23), one obtains

$$\begin{aligned}\Pi = {} & \frac{1}{2}E_b C A_1'^2 l_n^4 \int_0^{L_b} \sin^2(l_n z)\,dz + \frac{1}{2}G_b J_b A_1'^2 l_n^2 \int_0^{L_b} \cos^2(l_n z)\,dz + \frac{a\lambda P A_1'^2\left(\pi^2 n^2+4\right)}{16} \\ & + \frac{h\lambda P A_1'^2}{2} + \frac{1}{2}E_b C A_2'^2 l_n^4 \int_0^{L_b} \sin^2(l_n z)\,dz + \frac{1}{2}G_b J_b A_2'^2 l_n^2 \int_0^{L_b} \cos^2(l_n z)\,dz + \frac{a\lambda P A_2'^2\left(\pi^2 n^2+4\right)}{16} \\ & + \frac{h\lambda P A'^2}{2} + \frac{E_d h_d^3}{6L_d}\left(A_1'^2 + A_1' A_2' + A_2'^2\right)\int_0^{L_b} \sin^2(l_n z)dz\end{aligned} \tag{4.F.1}$$

By applying the principle of stationary potential energy, one obtains

$$\begin{aligned}\delta\Pi = {} & \delta A_1'\left[E_b C A_1' l_n^4 \int_0^{L_b} \sin^2(l_n z)\,dz + G_b J_b A_1' l_n^2 \int_0^{L_b} \cos^2(l_n z)\,dz + \lambda P A_1' \frac{\left(\pi^2 n^2+4\right)a+8h}{8}\right. \\ & \left. + \frac{E_d h_d^3}{6L_d}\left(2A_1' + A_2'\right)\int_0^{L_b} \sin^2(l_n z)dz\right] \\ & + \delta A_2'\left[E_b C A_2' l_n^4 \int_0^{L_b} \sin^2(l_n z)\,dz + G_b J_b A_2' l_n^2 \int_0^{L_b} \cos^2(l_n z)\,dz + \lambda P A_2' \frac{\left(\pi^2 n^2+4\right)a+8h}{8}\right. \\ & \left. + \frac{E_d h_d^3}{6L_d}\left(A_1' + 2A_2'\right)\int_0^{L_b} \sin^2(l_n z)dz\right] \\ = {} & 0\end{aligned} \tag{4.F.2}$$

The equilibrium equations take the form

$$\begin{bmatrix} \psi_n + \lambda P\dfrac{\left(\pi^2 n^2+4\right)a+8h}{4L_b} & \dfrac{E_d h_d^3}{6L_d} \\ \dfrac{E_d h_d^3}{6L_d} & \psi_n + \lambda P\dfrac{\left(\pi^2 n^2+4\right)a+8h}{4L_b} \end{bmatrix} \begin{Bmatrix} A_1' \\ A_2' \end{Bmatrix}_n = \{0\} \tag{4.F.3}$$

in which $\psi_n = E_b C l_n^4 + G_b J_b l_n^2 + E_d h_d^3/3L_d$ has been defined previously. For

non-trivial solutions, the determinant of the matrix of coefficients should vanish. This leads to the following two roots

$$\begin{aligned}(\lambda P)_{1n} &= -\frac{12n^4\pi^4 E_b C L_d + 12n^2\pi^2 G_b J_b {L_b}^2 L_d + 2E_d {h_d}^3 {L_b}^4}{3{L_b}^3 L_d\left(4a + 8h + an^2\pi^2\right)} \\ (\lambda P)_{2n} &= -\frac{4n^4\pi^4 E_b C L_d + 4n^2\pi^2 G_b J_b {L_b}^2 L_d + E_d {h_d}^3 {L_b}^4}{{L_b}^3 L_d\left(4a + 8h + an^2\pi^2\right)}\end{aligned} \tag{4.F.4}$$

By substituting the expression for $(\lambda P)_{1n}$ into Eq. (4.F.3), one obtains the buckling amplitude ratio $A_1' / A_2' = -1$, which corresponds to a symmetric mode. Also, by substituting the expression for $(\lambda P)_{2n}$ into Eq. (4.F.3), one obtains $A_1' / A_2' = 1$, corresponding to an anti-symmetric buckling mode.

Appendix 4G Derivation of Critical Load for fixed Beams under Non-uniform Moments

Evoking the stationarity conditions $\partial\pi/\partial D_1 = \partial\pi/\partial D_2 = 0$, one recovers the following equations

$$\begin{aligned} &D_1 E_b C l_n^{\,4} \int_0^{L_b} \cos^2(l_n z)\,dz + D_1 G_b J_b l_n^{\,2} \int_0^{L_b} \sin^2(l_n z)\,dz \\ &+ D_1 \lambda \int_0^{L_b} \left\{ hq\left[1-\cos(l_n z)\right] - 2aMl_n^{\,2}\cos(l_n z)\right\}\left[1-\cos(l_n z)\right]dz \\ &+ \frac{E_d h_d^{\,3}}{6L_d}(2D_1 + D_2)\int_0^{L_b}\left[1-\cos(l_n z)\right]^2 dz = 0 \end{aligned} \tag{4.G.1}$$

$$\begin{aligned} &D_2 E_b C l_n^{\,4} \int_0^{L_b} \cos^2(l_n z)\,dz + D_2 G_b J_b l_n^{\,2} \int_0^{L_b} \sin^2(l_n z)\,dz \\ &+ D_2 \lambda \int_0^{L_b} \left\{ hq\left[1-\cos(l_n z)\right] - 2aMl_n^{\,2}\cos(l_n z)\right\}\left[1-\cos(l_n z)\right]dz \\ &+ \frac{E_d h_d^{\,3}}{6L_d}(D_1 + 2D_2)\int_0^{L_b}\left[1-\cos(l_n z)\right]^2 dz = 0 \end{aligned} \tag{4.G.2}$$

Substituting $\int_0^{L_b} \cos^2(l_n z)\,dz = \int_0^{L_b} \sin^2(l_n z)\,dz = L_b/2$, $\int_0^{L_b}\left[1-\cos(l_n z)\right]^2 dz = 3L_b/2$ and rewriting the equations in an matrix form, one obtains

$$\begin{bmatrix} \frac{L_b}{2}\left(E_b C l_n^{\,4} + G_b J_b l_n^{\,2} + \frac{E_d h_d^{\,3}}{L_d}\right) + H(M) & \frac{E_d h_d^{\,3} L_b}{4L_d} \\ \frac{E_d h_d^{\,3} L_b}{4L_d} & \frac{L_b}{2}\left(E_b C l_n^{\,4} + G_b J_b l_n^{\,2} + \frac{E_d h_d^{\,3}}{L_d}\right) + H(M) \end{bmatrix} \begin{Bmatrix} D_1 \\ D_2 \end{Bmatrix} = \begin{Bmatrix} 0 \\ 0 \end{Bmatrix} \tag{4.G.3}$$

where $H(M) = \lambda \int_0^{L_b} \left\{ hq\left[1-\cos(l_n z)\right] - 2aMl_n^{\,2}\cos(l_n z)\right\}\left[1-\cos(l_n z)\right]dz$ has been defined.

Case 1: Uniformly Distributed loads

The strong-axis moment distribution induced by reference UDL q along beams span is $M = q\left(L_b z - z^2\right)/2$. Therefore, $H = \lambda q L_b\left(3a/4 \pm a + 3h/2 + an^2\pi^2/12\right)$ (adopt

positive sign when $n=2,4,6,\ldots$ and negative sign when $n=1,3,5,\ldots$). Substituting H into Eq. (4.G.3) and setting the determinant of the matrix of coefficient to zero, one obtains the following critical loads

$$
\begin{aligned}
\left(\lambda q\right)_{3n} &= \frac{-3\left(E_d {L_b}^4 {h_d}^3 + 2n^2\pi^2 G_b J_b {L_b}^2 L_d + 2n^4\pi^4 E_b C L_d\right)}{{L_b}^4 L_d\left(18h - 3a + an^2\pi^2\right)} \\
\left(\lambda q\right)_{4n} &= \frac{-3\left(3E_d {L_b}^4 {h_d}^3 + 2n^2\pi^2 G_b J_b {L_b}^2 L_d + 2n^4\pi^4 E_b C L_d\right)}{{L_b}^4 L_d\left(18h - 3a + an^2\pi^2\right)} \\
& n = 1,3,5,\ldots \\
\left(\lambda q\right)_{5n} &= \frac{-3\left(E_d {L_b}^4 {h_d}^3 + 2n^2\pi^2 G_b J_b {L_b}^2 L_d + 2n^4\pi^4 E_b C L_d\right)}{{L_b}^4 L_d\left(21a + 18h + an^2\pi^2\right)} \\
\left(\lambda q\right)_{6n} &= \frac{-3\left(3E_d {L_b}^4 {h_d}^3 + 2n^2\pi^2 G_b J_b {L_b}^2 L_d + 2n^4\pi^4 E_b C L_d\right)}{{L_b}^4 L_d\left(21a + 18h + an^2\pi^2\right)} \\
& n = 2,4,6,\ldots
\end{aligned}
\qquad \text{(4.G.4a,b,c,d)}
$$

Case 2: Mid-span concentrated loads

For a reference mid-span concentrated load P applied at both beams, the strong-axis moment is $M = Pz/2 \quad \left(0 < z \le L_b/2\right)$ and $M = P\left(L_b - z\right)/2 \quad \left(L_b/2 < z \le L_b\right)$. Substituting the moment distribution M, one obtains

$$
H = \begin{cases} \lambda P\left[h + a\left(n^2\pi^2 - 4\right)/8\right], & n = 1,3,5,\ldots \\ \lambda P\left[4h + a\left(n^2\pi^2 + 32\right)/8\right], & n = 2,6,10,\ldots \\ P\lambda a n^2\pi^2/8, & n = 4,8,12,\ldots \end{cases} \qquad \text{(4.G.5)}
$$

Substituting H into Eq. (4.G.3) and setting the determinant of the matrix of coefficient to zero, one obtains the following critical loads

$$(\lambda P)_{3n} = -\frac{2\left(2n^4\pi^4 E_b C L_d + 2n^2\pi^2 G_b J_b {L_b}^2 L_d + E_d {L_b}^4 {h_d}^3\right)}{{L_b}^3 L_d\left(8h - 4a + an^2\pi^2\right)}$$

$$(\lambda P)_{4n} = -\frac{2\left(2n^4\pi^4 E_b C L_d + 2n^2\pi^2 G_b J_b {L_b}^2 L_d + 3E_d {L_b}^4 {h_d}^3\right)}{{L_b}^3 L_d\left(8h - 4a + an^2\pi^2\right)}$$

$n = 1,3,5,\ldots$

$$(\lambda P)_{5n} = -\frac{2\left(2n^4\pi^4 E_b C L_d + 2n^2\pi^2 G_b J_b {L_b}^2 L_d + E_d {L_b}^4 {h_d}^3\right)}{{L_b}^3 L_d\left(32h + 32a + an^2\pi^2\right)}$$

$$(\lambda P)_{6n} = -\frac{2\left(2n^4\pi^4 E_b C L_d + 2n^2\pi^2 G_b J_b {L_b}^2 L_d + 3E_d {L_b}^4 {h_d}^3\right)}{{L_b}^3 L_d\left(32h + 32a + an^2\pi^2\right)}$$

(4.G.6a,b,c,d,e,f)

$n = 2,6,10,\ldots$

$$(\lambda P)_{7n} = -\frac{2\left(2n^4\pi^4 E_b C L_d + 2n^2\pi^2 G_b J_b {L_b}^2 L_d + E_d {L_b}^4 {h_d}^3\right)}{n^2\pi^2 a {L_b}^3 L_d}$$

$$(\lambda P)_{8n} = -\frac{2\left(2n^4\pi^4 E_b C L_d + 2n^2\pi^2 G_b J_b {L_b}^2 L_d + 3E_d {L_b}^4 {h_d}^3\right)}{n^2\pi^2 a {L_b}^3 L_d}$$

$n = 4,8,12,\ldots$

Appendix 4H Pre-buckling Analysis

For a beam element under transverse load $q(z)$ along the element span, the total potential energy Π stored in the pre-buckling stage is

$$\Pi = \frac{1}{2}\int_0^l E_b I_x v''^2 dz - \int_0^l q(z) v dz \tag{4.H.1}$$

where I_x is the moment of inertia about beam strong-axis, and one recalls v_p is the pre-buckling vertical displacement. All primes denote differentiation with respect to coordinate z along the beam longitudinal axis. Relate the pre-buckling vertical displacement v_p to the generalized nodal displacements as

$$v_p(z) = \langle L(z) \rangle_{1\times 4}^T \{v_p\}_{4\times 1} \tag{4.H.2}$$

in which the components of the generalized nodal displacements vector $\{v_p\}_{4\times 1} = \langle v_0 \quad \varphi_0 \quad v_l \quad \varphi_l \rangle^T$ are the nodal vertical displacements and nodal rotations at $z = 0, l$, and one recalls $\langle L(z) \rangle^T$ is the vector of Hermitian interpolation functions defined previously. Substituting Eq. (4.H.2) into Eq. (4.H.1) yields

$$\Pi = \frac{1}{2}\langle v_p \rangle_{1\times 4} [K_p]_{4\times 4} \{v_p\}_{4\times 1} - \langle v_p \rangle_{1\times 4} \{Q\}_{4\times 1} \tag{4.H.3}$$

in which the pre-buckling elastic stiffness matrix $[K_p]$ is

$$[K_p] = \int_0^l E_b I_x \{L''(z)\}_{4\times 1} \langle L''(z) \rangle_{1\times 4}^T dz = \frac{E_b I_x}{l^3} \begin{bmatrix} 12 & 6l & -12 & 6l \\ 6l & 4l^2 & -6l & 2l^2 \\ -12 & -6l & 12 & -6l \\ 6l & 2l^2 & -6l & 4l^2 \end{bmatrix}$$

and the energy equivalent load vector $\{Q\}$ is

$$\langle Q \rangle^T = \int_0^l q(z) \langle L_1(z) \quad L_2(z) \quad L_3(z) \quad L_4(z) \rangle_{1\times 4} dz$$

Applying the principle of minimum potential energy $\partial \pi / \partial \{v\} = 0$, one obtains the following force-displacement relationship at the element level

$$\left[K_p\right]_{4\times4}\{v\}_{4\times1}=\{Q\}_{4\times1} \tag{4.H.4}$$

Assembling $\left[K_p\right]$, $\left\{v_p\right\}$ and $\{Q\}$ from element level yields the following global force-displacement relationship

$$\left[K_p\right]_{2m\times2m}\left\{v_p\right\}_{2m\times1}=\{Q\}_{2m\times1} \tag{4.H.5}$$

where m is the number of elements per beam. After enforcing the boundary conditions, the global nodal displacement vector $\left\{v_p\right\}_{2m\times1}$ is recovered. The nodal reaction vector $\{R\}_{4\times1}$ is

$$\{R\}_{4\times1}=\left[K_p\right]_{4\times4}\{\Delta\}_{4\times1}-[Q]_{4\times1} \tag{4.H.6}$$

where $\{R\}_{4\times1}=\langle P_0 \quad M_0 \quad P_l \quad M_l\rangle^T$, P_0, P_l are the nodal shear forces and M_0, M_l are the nodal strong-axis bending moments, $\{\Delta\}_{4\times1}$ is the element nodal displacements vector directly extracted from global nodal displacement vector $\left\{v_p\right\}_{2m\times1}$.

Appendix 4I Expressions for Submatrices in Elastic and Geometric Stiffness Matrices

This appendix provides the expressions for submatrices $[B_1],[B_2],[B_3],[B_4],[B_5]$ introduced after Eq. (4.30)

$$[B_1]=\int_0^l \{L''(z)\}_{4\times1}\langle L''(z)\rangle_{1\times4}^T dz=\frac{1}{l^3}\begin{bmatrix}12 & 6l & -12 & 6l\\ 6l & 4l^2 & -6L & 2l^2\\ -12 & -6l & 12 & -6l\\ 6l & 2l^2 & -6l & 4l^2\end{bmatrix},$$

$$[B_2]=\int_0^l \{L'(z)\}_{4\times1}\langle L'(z)\rangle_{1\times4}^T dz=\frac{1}{30l}\begin{bmatrix}36 & 3l & -36 & 3l\\ 3l & 4l^2 & -3l & -l^2\\ -36 & -3l & 36 & -3l\\ 3l & -l^2 & -3l & 4l^2\end{bmatrix},$$

$$[B_3]=\int_0^l \{L(z)\}_{4\times1}\langle L(z)\rangle_{1\times4}^T dz=\frac{l}{420}\begin{bmatrix}156 & 22l & 54 & -13l\\ 22l & 4l^2 & 13l & -3l^2\\ 54 & 13l & 156 & -22l\\ -13l & -3l^2 & -22l & 4l^2\end{bmatrix},$$

$$[B_4]=\int_0^l M(z)\{L(z)\}_{4\times1}\langle L''(z)\rangle_{1\times4}^T dz,\quad [B_5]=\int_0^l q(z)\{L(z)\}_{4\times1}\langle L(z)\rangle_{1\times4}^T dz \tag{4.I.1}$$

For a beam element where the moment distribution along the element span $M(z)$ is linearly interpolated, i.e.,

$$M(z)=-M_0\left(1-\frac{z}{l}\right)+M_l\left(\frac{z}{l}\right) \tag{4.I.2}$$

where M_0 and M_l are the nodal moments obtained from pre-buckling analysis (Appendix 4H).Figure 4.I.1 shows the positive sign convention for end moments.

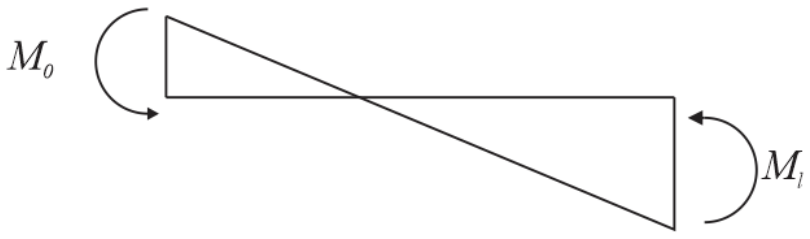

Figure 4.I.1 Sign convention for end moments

From Eq. (4.I.2), by substituting into Eq. (4.I.1), one obtains matrix $[B_4]$ as

$$[B_4] = \frac{1}{30l}\begin{bmatrix} 33M_0 - 3M_l & (27M_0 - 6M_l)l & -33M_0 + 3M_l & (6M_0 + 3M_l)l \\ 3M_0 l & (3M_0 - M_l)l^2 & -3M_0 l & M_l l^2 \\ -3M_0 + 33M_l & (3M_0 + 6M_l)l & 3M_0 - 33M_l & (-6M_0 + 27M_l)l \\ -3M(l)l & -M_0 l^2 & 3M_l l & (M_0 - 3M_l)l^2 \end{bmatrix}$$

(4.I.3)

List of Symbols

A	beam area;
A_i, A_i'	amplitudes of angle of twist functions in beam i;
A_f, A_w	areas for both flanges and web, respectively;
A_j, B_j	amplitudes of angle of twist functions;
a	distance between beam shear center and deck centerline;
B	point on cross-section contour;
B_1	sectorial origin;
$B(s)$	point at a distance s from the principal sectorial origin;
$[B_1], [B_2], [B_3], [B_4], [B_5]$	submatrices for elastic and geometric stiffness matrices;
C_w	warping constant;
$\langle D \rangle$	coefficient matrix;
E_b, E_w	modulus of elasticity of the flanges and web, respectively;
E_d	modulus of elasticity deck boards;
$[E_m(z)]$	diagonal matrix of exponential functions;
G_b, G_w	shear modulus of the flanges and web, respectively;
$[H]$	coefficient matrix;
h	distance of load point below deck centerline;
h_d	deck board thickness;
I_d	deck strong-axis moment of inertia;
I_x, I_y	moment of inertia about strong and weak axes, respectively;
J_b	beam Saint-Venant torsional constant;
J_f, J_w	Saint-Venant torsional constants for the flanges and web, respectively;
$[K_b]$	beam stiffness matrix;
$[K_d]$	deck stiffness matrix;

$[K_e]$ elastic stiffness matrix;

$[K_g]$ geometric stiffness matrix;

$[K_p]$ pre-buckling elastic stiffness matrix;

L_b, L_d beam and deck span, respectively;

$\langle L(z) \rangle$ Hermitian polynomials;

l element length;

l_n constant;

M_0, M_l strong-axis moments at element ends;

M_{cr} critical moment for uniform moments loading;

M_{e1}, M_{e2} deck board ends moment;

$M(z)$ reference strong-axis bending moment;

m number of elements per beam;

m_j constants in angle of twist functions;

$m_r(n)$ dimensionless critical moment;

N pole;

n integer in angles of twist functions;

n_1 ratio of shear moduli;

n_2 ratio of modulus of elasticity;

O origin;

$P(z)$ reference concentrated load;

P_0, P_l shear forces at element ends;

$\{Q\}$ energy equivalent load vector;

$q(z)$ reference transverse load;

$\{R\}$ vector of nodal reaction;

U internal strain energy;

U_{bi} internal strain energy in beam i;

U_d internal strain energy in deck boards;

U_d^* internal strain energy in one deck board;

U_L internal strain energy due to longitudinal strain;

U_{sv} internal strain energy due to Saint-Venant torsion;

u_i lateral displacement of beam i;

$(u_b)_i$ lateral displacements of beam nodes;

$\langle u_i \rangle$ generalized nodal lateral displacement vector;

V load potential energy;

V_{bi} load potential energy for external loads applied at beam i;

v_0, v_l vertical displacements at element ends;

$(v_b)_i, (v_d)_i$ vertical displacements of beam and deck nodes, respectively;

$v_p(z)$ pre-buckling vertical displacement;

$v(z)$ vertical displacement;

$\{v_p\}$ nodal displacement vector;

$w(z)$ average longitudinal displacement;

$\overline{w}(s,z)$ longitudinal displacement field;

$x(s)$ coordinate along *x* axis of a point at a distance *s* from the principal sectorial origin;

x, y, z Cartesian coordinates;

$y(s)$ coordinate along *y* axis of a point at a distance *s* from the principal sectorial origin;

z_0 distance from deck board to beam end-support along *z* axis.;

$\{\Delta\}$ element nodal displacement vector;

ε longitudinal strain;

θ_i angle of twist of beam i;

θ_0, θ_l angles of twist at element ends;

$\langle \theta_i \rangle$ generalized nodal angle of twist vector;

$(\theta_b)_i, (\theta_d)_i$ angle of twist of beam and deck nodes, respectively;

λ	load multiplier;
Π	total potential energy;
σ	longitudinal stress;
φ_0, φ_l	nodal rotations at element ends;
$\omega(s)$	sectorial coordinate.

References

[1] *ABAQUS 6.12-3* [Computer software]. Providence, RI, Dassault Systèmes Simulia.

[2] American Wood Council. (2015). "National design specification for wood construction." ANSI/AWC NDS-2015, Virginia, U.S.

[3] Apparao, T. V. S. R. (1968). "Problems in structural diaphragm bracing." *Report No. 331*, Dept. of Struct. Engrg., Cornell Univ., Ithaca, N.Y.

[4] Basaglia, C., Camotim, D., Gonçalves, R., and Graça, A. (2013). "GBT-based assessment of the buckling behaviour of cold-formed steel purlins restrained by sheeting." *Thin-Walled Struct.,* 72, 217-229.

[5] Bell., K., and Eggen., T. E. (2001). "Stability of timber beams and columns." *IABSE Symposium Report,* International Association for Bridge and Structural Engineering, 85(9), 30-36.

[6] Buchanan, A. (1986). "Combined bending and axial loading in lumber." *J. Struct. Eng.*, 10.1061/(ASCE)0733-9445(1986)112:12(2592), 2592-2609.

[7] Burow, J. R., Manbeck, H. B. and Janowiak, J. J. (2006). "Lateral stability of composite wood I-joists under concentrated-load bending." *Transactions of the ASABE,* 49(6), 1867-1880.

[8] Canadian Standard Association (CSA). (2014). "Engineering design in wood." *O86-14,* Mississauga, Ontario, Canada.

[9] Chu, X., Kettle, R., and Li, L. (2004). "Lateral-torsion buckling analysis of partial-laterally restrained thin-walled channel-section beams." *J. Constr. Steel Res.,* 60(8), 1159-1175

[10] Chu, X., Rickard, J., and Li, L. (2005). "Influence of lateral restraint on lateral-torsional buckling of cold-formed steel purlins." *Thin-Walled Struct.,* 43(5), 800-810.

[11] Du, Y. (2016). "Lateral torsional buckling of wooden beam-deck systems." M.A.Sc. thesis, Dept. of Civil Engineering, Uni. of Ottawa, Ontario, Canada.

[12] Errera, S. J., Pincus, G., and Fisher, G. P. (1967). "Columns and beams braced by diaphragms." *J. Struct. Div.,* 93(1), 295-318.

[13] Forest Products Laboratory (FPL). (2010). *Wood handbook-Wood as an engineering material*. Madison, U.S.

[14] Hindman, D. P., Harvey, H. B., and Janowiak, J. J. (2005a). "Measurement and

prediction of lateral torsional buckling loads of composite wood materials: Rectangular section." *Forest Products Journal,* 55(9), pp 42-47.

[15] Hindman, D. P., Harvey, H. B., and Janowiak, J. J. (2005b). "Measurement and prediction of lateral torsional buckling loads of composite wood materials: I-joist sections." *Forest Products Journal,* 55(10), 43-48.

[16] Hooley, R. F., and Madsen, B. (1964). "Lateral buckling of glued laminated beams." *J. Struct. Div.,* 90(ST3), pp. 201-218 .

[17] Jenkinson, P. M., and Zahn, J. J. (1972). "Lateral stability of beam and deck structure." *J. Struct. Div.,* 98(3), 599-609.

[18] Koka E. N. (1987). "Laterally loaded wood compression members finite element and reliability analysis." M.A.Sc. thesis, Uni. of British Columbia, Canada.

[19] Larue, B., Khelil, A., and Gueury, M. (2007). "Elastic flexural–torsional buckling of steel beams with rigid and continuous lateral restraints." *J. Constr. Steel Res.,* 63(5), 692-708.

[20] Li, L. (2004). "Lateral–torsional buckling of cold-formed zed-purlins partial-laterally restrained by metal sheeting." *Thin-Walled Struct.,* 42(7), 995-1011.

[21] Lucas, R., Al-Bermani, F., and Kitipomchai, S. (1997a). "Modelling of cold-formed purlin-sheeting systems—Part 1: Full model." *Thin-Walled Struct.,* 27(3), 223-243.

[22] Lucas, R., Al-Bermani, F., and Kitipornchai, S. (1997b). "Modelling of cold-formed purlin-sheeting systems—Part 2. Simplified model." *Thin-Walled Struct.,* 27(4), 263-286.

[23] Park, J., and Kang, Y. (2003). "Lateral buckling of beams with top bracing." *Struct.Eng.Mech.,* 16(5), 613-625.

[24] Park, J. S., Stallings, J. M., and Kang, Y. J. (2004). "Lateral–torsional buckling of prismatic beams with continuous top-flange bracing." *J. Constr. Steel Res.,* 60(2), 147-160.

[25] Peköz, T., and Soroushian, P. (1982). "Behaviour of C- and Z-purlins under wind uplift." *Proc., 6th Int. Specialty Conf. on Cold-Formed Steel Structures,* 409–429.

[26] Pincus, G., and Fisher, G. P. (1966). "Behavior of diaphragm-braced columns and beams." *J. Struct. Div.,* 92(2), 323-370.

[27] Roeder, C. W., and Assadi, M. (1982). "Lateral stability of I-beams with partial support." *J. Struct. Div.,* 108(8), 1768-1780.

[28] Song, X. and Lam, F. (2006). “Three dimensional stability analysis of wood beam-columns.” *In Proceedings of the 9th WCTE,* Portland, 1061-1067.

[29] Song, X. B., and Lam, F. (2009). “Stability analysis of laterally braced wood beam-columns subjected to biaxial eccentric loading.” *Comput. Struct.,* 87(17), 1058–1066.

[30] Song, X. B., and Lam, F. (2010). “Stability capacity and lateral bracing requirements of wood beam-columns.” *J. Struct. Eng.*, 10.1061/(ASCE)ST.1943-541X.0000095, 211-218.

[31] Steiger, R., and Fontana, M. (2005). "Bending moment and axial force interacting on solid timber beams." *Materials and structures*, 38(5), 507-513.

[32] Taylor, A. C., and Ojalvo, M. (1966). “Torsional restraint of lateral buckling.” *J. Struct. Div.,* 92(2), 115-130.

[33] Timoshenko, S., and Gere, J. (1961). *Theory of elastic stability*, 2nd ed. New York: McGraw-Hill.

[34] Trahair, N. S. (1979). “Elastic lateral buckling of continuously restrained beam columns.” *The profession of a civil engineer*, D. Campbell-Allen and E. H. Davis, eds., Sydney University Press, Sydney, 61–73.

[35] Trahair, N.S. (1993). *Flexural-torsional buckling of structures*. E & FN Spon, London.

[36] Vlasov, V. Z. (1961). *Thin-walled elastic beams*. 2nd. ed., Israel Program for Scientific Translations, Jerusalem.

[37] Xiao, Q. (2014). “Lateral torsional buckling of wood beams.” M.A.Sc. thesis, Dept. of Civil Engineering, Uni. of Ottawa, Ontario, Canada

[38] Ye, Z., Kettle, R. J., Li, L., and Schafer, B. W. (2002). “Buckling behavior of cold-formed zed-purlins partially restrained by steel sheeting.” *Thin-Walled Struct.,* 40(10), 853-864.

[39] Zahn, J. (1965). “Lateral stability of deep beams with shear-beam support.” U.S.D.A. Forest Service Research Paper FPL, 43.

[40] Zahn, J. (1972). "Shear stiffness of two-inch wood decks for roof systems." U.S.D.A. Forest Service Research Paper FPL ,155.

[41] Zahn, J. J. (1973). “Lateral stability of wood beam-and-deck systems.” *J. Struct. Div.,* 99(7), 1391-1408.

[42] Zahn, J. J. (1984). “Bracing requirements for lateral stability.” *J. Struct. Eng.,* 10.1061/(ASCE)0733-9445(1984)110:8(1786), 1786–1802.

[43] Zahn, J. (1986). “Design of wood members under combined load.” *J. Struct. Eng.*, 10.1061/(ASCE)0733-9445(1986)112:9(2109), 2109-2126.

[44] Zahn, J. (1988). “Combined−load stability criterion for wood beam−columns.” *J. Struct. Eng.*, 10.1061/(ASCE)0733-9445(1988)114:11(2612), 2612-2628.

CHAPTER 5: SWAY MODEL FOR THE LATERAL TORSIONAL BUCKLING ANALYSIS OF WOODEN TWIN-BEAM-DECK SYSTEMS

Abstract

The present study reports an investigation on the lateral torsional buckling of wooden twin beams braced by deck boards subjected to gravity or wind uplift loading. The restraining action of the deck boards is modelled as continuous partial lateral and twisting restraints provided at the top of both beams. A series of analytical and numerical solutions were developed for predicting the lateral torsional buckling capacity for twin-beam-deck systems under different loading and boundary conditions. A parametric study was then conducted to examine the effects of beam and deck span, load type, load height, lateral restraint height and stiffness and number of spans on the overall buckling capacity. The results show the restraining effects of deck boards have a significant influence on the lateral torsional buckling capacity of twin-beam-deck assemblies.

5.1 Introduction and Motivation

Modern timber floor and roof systems typically consist of a set of parallel deep beams braced at the top by tongue-and-groove wooden deck boards through nail connections. While deep beams provide efficient means of the material usage in bending, they are prone to lateral torsional buckling as a possible mode of failure. Deck boards can potentially improve the buckling capacity of such systems by partially restraining the twisting and relative lateral displacements between parallel beams. Current North American Standards (NDS 2015, CAN/CSA O86 2014) recognize the beneficial role of deck boards in suppressing the lateral torsional capacity of such systems when deck boards prevent the lateral displacement along the beam compression edge. However, no recommendations are provided for cases where (1) the tension edge is restrained, and (2) the deck boards are assumed to provide only partial lateral restraints. In the above context, the present study aims to develop analytical and numerical formulations capable of predicting the lateral torsional buckling capacity for wooden twin-beam-deck systems.

5.2 Literature Review

In general, lateral torsional buckling solutions for beam-deck systems can be categorized into sway models, whereby the beams are free to move laterally at deck level, and non-sway models where beams are restrained from lateral moments at the deck level. Consistent with the objective of the study, only sway models are reviewed in the paper. Firstly, studies on systems under gravity loads will be reviewed, followed by studies on systems under wind uplift. Next, studies focusing on the strength and stiffness requirements for continuous restraints are provided. Given that the relative lateral stiffness between twin beams heavily depends on the load-slip relationship for nailed wood connections, relevant key studies are then presented.

5.2.1 Beams with continuous elastic restraint under gravity loads

Vlasov (1961) formulated the general differential equations for a beam embedded in an elastic medium. The critical moment was determined for a beam braced by continuous elastic lateral and twisting restraints and subjected to uniform moment. Taylor and Ojalvo (1966) extended the work for doubly-symmetric I-section beams with continuous or discrete elastic twisting restraint under uniform and non-uniform moments. Pincus and Fisher (1966) developed a solution for twin beams braced by a shear diaphragm and subjected to uniform moments. The solution captured the shear and twisting actions of the deck boards. Other bracing scenarios were investigated by Errera et al. (1967). Beam-deck assemblies consisting of twin beams laterally braced at their compression flanges by the shear action of the deck were investigated by Apparao (1968) who developed a nonlinear load-deformation solution and a buckling eigen-value solution. Zahn (1965) formulated the governing equilibrium conditions for wooden rectangular beams laterally restrained by the shear action of deck boards and the validity of the solution was experimentally verified by Jenkinson and Zahn (1972). The shear stiffness of wooden deck boards needed as an input in the analytical models was studied by Zahn (1972) in another experimental study. A total potential energy formulation was also developed (Zahn 1973) for a beam within a floor system by accounting for the internal strain energy within the tributary decking strip of the beam. The formulation was then applied for simply-supported beams under uniform moments, concentrated loads, uniformly distributed loads, and cantilevers. Hancock and Trahair (1978) formulated a finite element based solution for continuously braced beam-columns. They characterized the deck as elastic restraints partially restraining

lateral displacement, twisting along beam longitudinal axis, weak-axis rotation and warping of the member. A closed-form solution was also developed for beam-columns by Trahair (1979). Assadi and Roeder (1985) investigated the stability of cantilevers with elastic lateral restraint at the top flange. Albert and Dawe (1990) developed a finite element solution for the buckling analysis of two-span continuous I-section beams whose top flanges are restrained by elastic lateral and twisting springs. For the purpose of capturing the interaction between the web and flanges, the flanges were modeled by one-dimensional beam elements while the web was modeled by plate elements. The inelastic behavior was captured by omitting yielded zones in the beam. Khelil and Larue (2008) developed an energy-based solution for simply-supported beams with continuous partial lateral restraint. The solution was able to predict the buckling capacity for uniform and non-uniform moment distributions. Chen and Li (2010) investigated the distortional buckling of purlins with continuous full lateral and partial twisting restraints under gravity load.

5.2.2 Beams with continuous elastic restraint under wind uplift

For steel purlin-sheeting assemblies, Pekoz and Soroushian (1982) developed a solution for critical uplift load by modelling the system as a beam on elastic foundation. Sokol (1996) modelled the restrained purlins as a single flange on elastic rotational foundation. Jiang and Davies (1997) studied the buckling behavior based on the Generalized Beam Theory (GBT). Lucas et al. (1997a) formulated a non-linear elasto-plastic finite element model with geometric nonlinearity. The model captured purlin-sheeting interaction and successfully modelled cross-sectional distortion and local buckling. In another study, Lucas et al. (1997b) developed a simplified model where the effects of sheeting were idealized as elastic springs. Ye et al. (2002) adopted the finite strip method to investigate the local, distortional and lateral torsional buckling of zed-purlins restrained by steel sheeting. The lateral torsional buckling capacity of channel purlins laterally braced by sheeting was investigated by Chu et al. (2004). Li (2004) and Chu et al. (2005) expanded the study for zed sections. Basaglia et al. (2013) developed a GBT solution for the local, distortional and lateral torsional buckling of channel and zed purlins restrained by sheeting and subjected to uplift loading. Apart from the studies of Pekoz and Soroushian (1982), Sokol (1996), Chu et al. (2004), Chu et al. (2005) and Li (2004), the above studies have focused on the local or distortional buckling of thin cold-formed sections. Table 5.1 summarizes various analytical and

numerical formulations for the stability of beams with continuous partial restraints.

Table 5.1 Comparative review of various formulations of the stability of beams braced by continuous partial restraints

	Methodology					Loading condition			Continuous restraint				End support				Cross-section			Others		
Source	Energy-based	Direct equilibrium	FEA	Finite strip	Generalized Beam Theory	Uniform moment	Gravity load	Wind uplift	Lateral	Shear	Twisting	Others	Simply-supported	Fix	Continuous	Cantilevers	I-section	Rectangular	C or Z section	Imperfection	Load position effect	Local or distortional buckling
Vlasov (1961)		✓				✓			✓		✓		✓				✓					
Zahn (1965)		✓				✓	✓			✓			✓			✓		✓				
Taylor and Ojalvo (1966)		✓				✓	✓				✓		✓				✓					
Pincus and Fisher (1966)	✓					✓				✓	✓		✓				✓					
Errera et al. (1967)	✓					✓				✓			✓	✓			✓					
Apparao (1968)		✓				✓				✓			✓				✓		✓	✓		
Zahn (1973)	✓					✓	✓			✓			✓			✓		✓				
Hancock and Trahair (1978)			✓			✓	✓					✓	✓			✓	✓				✓	
Trahair (1979)	✓	✓				✓						✓	✓				✓					
Pekoz and Soroushian (1982)	✓							✓	✓				✓						✓			
Assadi and Roeder (1985)	✓						✓		✓							✓	✓				✓	
Lawson and Nethercot (1985)	✓					✓	✓			✓			✓				✓				✓	
Albert and Dawe (1990)			✓			✓	✓		✓		✓		✓		✓		✓					✓
Sokol (1996)	✓						✓	✓	✓				✓		✓				✓			
Jiang and Davies (1997)					✓		✓	✓	✓		✓		✓						✓			✓
Ye et al. (2002)				✓		✓			✓		✓		✓						✓		✓	✓
Chu et al.(2004)	✓							✓	✓				✓	✓					✓		✓	
Li (2004)	✓							✓	✓		✓		✓	✓					✓		✓	
Chu et al.(2005)	✓							✓	✓				✓						✓		✓	
Khelil and Larue (2008)	✓					✓	✓	✓	✓				✓				✓				✓	
Chen and Li (2010)	✓						✓		✓		✓		✓						✓			✓
Basaglia et al. (2013)			✓		✓			✓	✓		✓		✓						✓			✓
Present study	✓		✓			✓	✓	✓	✓		✓		✓		✓		✓	✓			✓	

5.2.3 Strength and stiffness requirements for continuous restraints

Based on the models of Errera et al. (1967) and Apparao (1968), Nethercot and Trahair (1975) as well as Errera and Apparao (1976) proposed simplified equations for critical loads for beams continuously braced by a shear diaphragm under uniform moments. The stiffness requirement of the shear diaphragm was outlined to achieve desired moment resistance. The strength requirement was proposed for initially crooked beams. Starting from the models of Hancock and Trahair (1978) and Trahair (1979), Trahair and Nethercot (1984) added discrete restraint features to examine the effects of various types of continuous and discrete restraints on the buckling capacity of beam-columns. Lawson and Nethercot (1985) proposed a critical moment equation for beams braced by a shear diaphragm, which incorporates the effects of moment gradient and load height. The criteria to assess the adequacy of the diaphragm shear stiffness were developed. Helwig and Frank (1999) developed a finite-element model based on ANSYS for the stability of twin beams systems with metal sheeting acting as a shear diaphragm at the beams top flange. The authors confirmed the validity of the design equations proposed by Nethercot and Trahair (1975) for uniform moment and suggested new equations for transverse loads applied at different heights. Also proposed was the diaphragm shear stiffness required to achieve the design moment resistance. Helwig and Yura (2008a) proposed a moment gradient factor equations for beams with stocky webs and suggested the optimal diaphragm shear stiffness for beams with initial imperfections. In a later study, Helwig and Yura (2008b) quantified the forces in shear diaphragms and outlined a design procedure for the design of shear diaphragms.

5.2.4 Load-slip relationship for nailed wood connections

The load-slip relationship for nailed wood connection has been investigated analytically and experimentally. Early analytical work (e.g., Kuenzi 1951 and Noren 1962) was based on beam on linear elastic foundation analogy. Foschi (1974) improved the previous solutions by developing a new model based on a beam on non-linear foundation. The resulting equation was adopted by Hunt and Byrant (1990) and Erki (1991) in a finite element analysis context and by Heine and Dolan (2001) who developed a new load-slip model to incorporate forces due to the bending of the fasteners.

Based on the experimental studies, empirical mathematical models were developed

(e.g., Mclain 1975, Mack 1977, Morris and Gajjar 1981, Smith et al. 1988, Kermani and Goh 1999). Such models incorporated the effects of nail diameter and the member density. Pellicane (1991), SaRibeiro and Pellicane (1992) proposed new values for parameters in the Mclain's (1975) model. The mathematical model adopted for the nailed wood joints in the present study is based on the load-slip response equation of CAN/CSA O86 (2014) standard. The equation is based on the yield theory developed by Johansen (1949).

Compared with the analytical and numerical studies shown in Table 5.1, the present study focuses on wood material. In this respect, only Zahn (1965) and Zahn (1973) targeted wood beams. Also, the present study investigates stability problems where the decking detail provides continuous partial lateral and twisting restraints (in a manner similar to Vlasov 1961, Albert and Dawe 1990, Jiang and Davies 1997, Ye et al. 2002, Li 2004, Chen and Li 2010 and Basaglia et al. 2013). However, the Vlasov (1961) solution is limited to uniform moments and the remaining studies targeted either C or Z purlins. In contrast, the present study focuses on doubly-symmetric I-sections. Except for Li (2004), all other studies focused either on local or distortional buckling. In contrast, the present study investigates lateral torsional buckling.

5.3 Assumptions

The following assumptions have been adopted:

1. The deck boards are assumed to provide continuous relative partial lateral restraint by the combined lateral stiffness of nailed joints and deck boards (deck-joint assembly).
2. Partial twisting restraint is provided by the deck bending action.
3. Relative displacement between beams and deck boards at nailed joints is allowed.
4. The in-plane elastic shear restraint provided by the deck boards is negligible.
5. Throughout deformation, beam cross-sections remain rigid in their own plane, i.e., distortional effects are neglected.
6. Shear deformation effects within the beams are negligible.
7. Beam and deck materials are linearly elastic.
8. Pre-buckling deformation effects are neglected.

5.4 Formulation

5.4.1 Problem description and notation

The beam-deck system considered consists of two identical beams with

doubly-symmetric sections (either rectangular or I-shaped) connected to individual deck boards through nails. Figure 5.1 shows a cross-sectional view of the twin-beam-deck assembly. A left-hand coordinate system is used, with *z*-axis being along the longitudinal direction of the beam, and *x* and *y* axes taken in the plane of the cross-section. The positive sign convention adopted is consistent with that in Trahair (1993) where the angle of twist is clockwise. The twin beams are assumed to be subjected to a transverse load $q(z)$ applied at a distance h from the beam shear center. Under the external loads, the system undergoes vertical displacement $v_p(z)$ in going from Configuration 1 to 2, in which subscript p denotes the pre-buckling displacements. The applied loads are then assumed to increase by a factor λ to attain the threshold value $\lambda q(z)$ at the onset of buckling (Configuration 3). Under the load increase, pre-buckling deformations are assumed to linearly increase to $\lambda v_p(z)$. The system then undergoes lateral torsional buckling as manifested by lateral displacements $u_1(z), u_2(z)$ and angles of twist $\theta_1(z), \theta_2(z)$ (Configuration 4) where subscripts 1,2 respectively denote the field variables of the left and right beams. In Figure 5.1, points B and D are located at the deck underside and initially coincide with points A and C. At the onset of buckling, point A at the top of beam 1 is assumed to undergo a lateral displacement u_A that is different from that of point B at the deck underside. Also, point C located at the top of beam 2 undergoes a lateral displacement u_C which is distinct from that of point D, resulting in a relative displacement between the top of both beams. The magnitude of relative displacement depends on the shear stiffness of the nailed joints, the axial and flexural stiffness of the deck boards, including the effect of eccentricity between the deck board centerline and beam-deck interface.

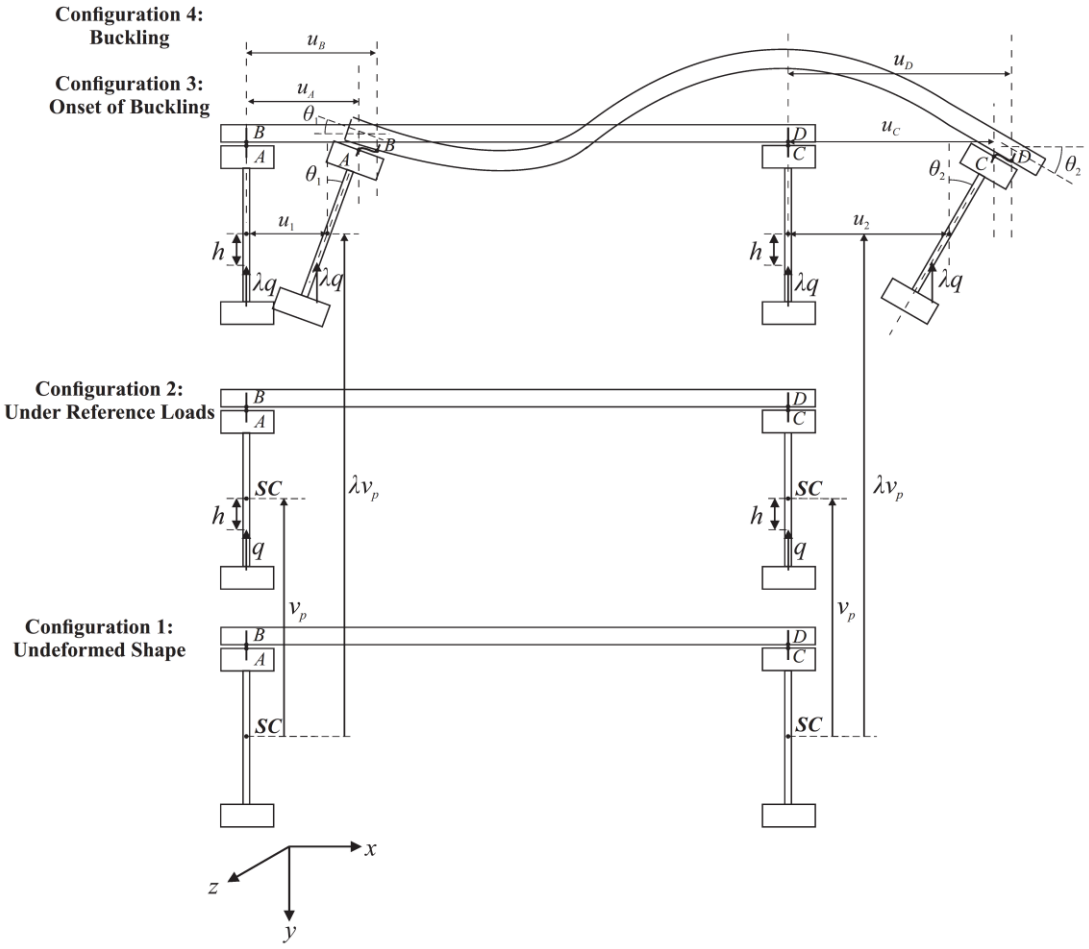

Figure 5.1 Different stages of deformation

5.4.2 Total potential energy

The total potential energy Π of the twin-beam-deck system is

$$\Pi = U + V \tag{5.1}$$

in which U is the internal strain energy and V is the load potential energy. In Eq. (5.1), the internal strain energy has four contributions $U = U_{b1} + U_{b2} + U_t + U_l$, where U_{bi} $(i = 1, 2)$ is the internal strain energy stored in beam i, U_t is the internal strain energy for the partial twisting restraint of the deck bending action, and U_l is the internal strain energy for the relative partial lateral restraint of the deck-joint assembly. The load potential energy V consists of two components, i.e., $V = V_{b1} + V_{b2}$, one for each beam. The individual energy terms are given below.

5.4.2.1 Internal strain energy for the twin beams

The internal strain energy stored in beam i due to weak-axis bending, Saint-Venant torsion, and warping torsion takes the form (Trahair 1993)

$$U_{bi} = \frac{1}{2}\int_0^{L_b} E_b I_y u_i''^2 dz + \frac{1}{2}\int_0^{L_b} G_b J_b \theta_i'^2 dz + \frac{1}{2}\int_0^{L_b} E_b C_w \theta_i''^2 dz, \qquad (i = 1,2) \tag{5.2}$$

where E_b is the beam modulus of elasticity, I_y is the moment of inertia about weak-axis, G_b is the shear modulus, J_b is the Saint-Venant torsional constant, C_w is the warping constant and L_b is the beam span, and all primes denote differentiation with respect to coordinate z taken along the beam longitudinal axis. For I-section members where the web and flanges have different materials, the transformed section properties have been provided in Appendix 5A.

5.4.2.2 Load potential energy

The load potential energy for external loads applied at beam i is

$$V_{bi} = \lambda\left(\int_0^{L_b} M\theta_i u_i'' dz + \frac{1}{2}\int_0^{L_b} qh\theta_i^2 dz\right), \qquad (i = 1,2) \tag{5.3}$$

where M is the strong-axis moment induced by reference transverse load q (taken positive when acting downwards), and one recalls that λ is an unknown load multiplier to be obtained from the buckling analysis and h is the distance between the loading point and beam shear center (taken positive when the loading point is below beam shear center). The first term in Eq. (5.3) is the destabilizing term due to strong-axis flexure while the second term accounts for the load potential energy gain due to the load height effect relative to the beam shear center.

5.4.2.3 Internal strain energy for the partial twisting restraint

For a given deck board at a distance z_0 from the beam end support, the end moments M_{e1} and M_{e2} can be expressed in terms of the angles of twist $\theta_1(z_0)$ and $\theta_2(z_0)$ as

$$\begin{Bmatrix} M_{e1}(z_0) \\ M_{e2}(z_0) \end{Bmatrix} = \frac{2E_d I_d}{L_d}\begin{bmatrix} 2 & 1 \\ 1 & 2 \end{bmatrix}\begin{Bmatrix} \theta_1(z_0) \\ \theta_2(z_0) \end{Bmatrix} \tag{5.4}$$

where E_d is the deck modulus of elasticity, I_d is the moment of inertia about the deck strong-axis and L_d is the span of deck board. The internal strain energy stored in this deck board is

$$U_t^* = \frac{1}{2}M_{e1}(z)\theta_1(z_0) + \frac{1}{2}M_{e2}(z)\theta_2(z_0) \tag{5.5}$$

From Eq. (5.4), by substituting into Eq. (5.5), one obtains the internal strain energy stored in this deck board

$$U_t^* = \frac{E_d I_d}{L_d}\left\langle \theta_1(z_0) \quad \theta_2(z_0)\right\rangle \begin{bmatrix} 2 & 1 \\ 1 & 2 \end{bmatrix} \begin{Bmatrix} \theta_1(z_0) \\ \theta_2(z_0) \end{Bmatrix} \tag{5.6}$$

The internal strain energy U_t for the whole deck is simply the summation of energy from each deck board, which can be approximately written in an integration form as

$$U_t = \sum U_t^* \approx \frac{E_d h_d^3}{12 L_d} \int_0^{L_b} \left\langle \theta_1(z) \quad \theta_2(z)\right\rangle \begin{bmatrix} 2 & 1 \\ 1 & 2 \end{bmatrix} \begin{Bmatrix} \theta_1(z) \\ \theta_2(z) \end{Bmatrix} dz \tag{5.7}$$

where h_d is the deck board thickness.

5.4.2.4 Internal strain energy for the relative partial lateral restraint

For the deck board at a distance z_0 from beam end support, the lateral displacements of points A and C at the beams top (Figure 5.1) are expressed in terms of the lateral displacement u_i and angle of twist θ_i as

$$u_A(z_0) = u_1(z_0) + \frac{h_b}{2}\theta_1(z_0) \tag{5.8}$$

$$u_C(z_0) = u_2(z_0) + \frac{h_b}{2}\theta_2(z_0) \tag{5.9}$$

where h_b is the beam depth. Assuming an idealized elastic behavior, the lateral force F in the nailed joint is proportional to the relative displacement $u_c - u_A$. The constant of proportionality k depends on the shear stiffness of the nailed joints as well as the deck axial and flexural stiffness and takes the form (Appendix 5B)

$$k = \frac{\bar{n} E_d b h_d k_n}{2 E_d b h_d + 4 \bar{n} L_d k_n} \tag{5.10}$$

where $\bar{n}$ is the number of nails at each joint, b is deck board width, and k_n is the shear stiffness of a single-nail joint. The internal strain energy stored is

$$U_l^* = \frac{k}{2}(u_C - u_A)^2 = \frac{k}{2}\left\{u_2(z_0) - u_1(z_0) + \frac{h_b}{2}\left[\theta_2(z_0) - \theta_1(z_0)\right]\right\}^2 \tag{5.11}$$

For the whole decking, the internal strain energy for the relative partial lateral restraint of the deck-joint assembly is the summation of the energy contributions from all deck boards, which can be approximated in an integral form as

$$U_l = \sum U_l^* \approx \frac{\bar{k}}{2}\int_0^{L_b}\left[u_2 - u_1 + \frac{h_b}{2}(\theta_2 - \theta_1)\right]^2 dz \tag{5.12}$$

where the relative lateral stiffness per unit deck width $\bar{k} = k/b$ has been defined.

In summary, from Eqs. (5.2),(5.3),(5.7), and (5.12), by substituting into Eq. (5.1), one obtains the total potential energy of the twin-beam-deck assembly

$$\begin{aligned}\Pi = &\frac{1}{2}\int_0^{L_b} E_b I_y u_1''^2 dz + \frac{1}{2}\int_0^{L_b} G_b J_b \theta_1'^2 dz + \frac{1}{2}\int_0^{L_b} E_b C_w \theta_1''^2 dz + \lambda \int_0^{L_b} M\theta_1 u_1'' dz + \frac{\lambda}{2}\int_0^{L_b} qh\theta_1^2 dz \\ &+ \frac{1}{2}\int_0^{L_b} E_b I_y u_2''^2 dz + \frac{1}{2}\int_0^{L_b} G_b J_b \theta_2'^2 dz + \frac{1}{2}\int_0^{L_b} E_b C_w \theta_2''^2 dz + \lambda \int_0^{L_b} M\theta_2 u_2'' dz + \frac{\lambda}{2}\int_0^{L_b} qh\theta_2^2 dz \\ &+ \frac{E_d h_d^3}{6L_d}\int_0^{L_b} \left(\theta_1^2 + \theta_1\theta_2 + \theta_2^2\right) dz + \frac{\bar{k}}{2}\int_0^{L_b} \left[u_2 - u_1 + \frac{h_b}{2}\left(\theta_2 - \theta_1\right)\right]^2 dz\end{aligned} \tag{5.13}$$

5.4.3 Conditions of neutral stability and boundary conditions

The total potential energy is a functional of lateral displacements u_i, angles of twist θ_i and their derivatives. The equilibrium configuration is obtained by setting the first variation to zero, i.e., $\delta\Pi = 0$. By performing integration by parts (Appendix 5C), the following equilibrium equations are recovered

$$\begin{aligned}&E_b C_w \theta_1^{IV} - G_b J_b \theta_1'' + \lambda\left(M u_1'' + qh\theta_1\right) + \frac{E_d h_d^3}{6L_d}\left(2\theta_1 + \theta_2\right) + \frac{\bar{k}h_b}{2}\left[u_1 - u_2 + \frac{h_b}{2}\left(\theta_1 - \theta_2\right)\right] = 0 \\ &E_b I_y u_1^{IV} + \lambda M\theta_1'' + \frac{\bar{k}}{2}\left[2u_1 - 2u_2 + h_b\left(\theta_1 - \theta_2\right)\right] = 0 \\ &E_b C_w \theta_2^{IV} - G_b J_b \theta_2'' + \lambda\left(M u_2'' + qh\theta_2\right) + \frac{E_d h_d^3}{6L_d}\left(\theta_1 + 2\theta_2\right) - \frac{\bar{k}h_b}{2}\left[u_1 - u_2 + \frac{h_b}{2}\left(\theta_1 - \theta_2\right)\right] = 0 \\ &E_b I_y u_2^{IV} + \lambda M\theta_2'' - \frac{\bar{k}}{2}\left[2u_1 - 2u_2 + h_b\left(\theta_1 - \theta_2\right)\right] = 0\end{aligned} \tag{5.14}$$

The corresponding boundary conditions are

$$\left.\begin{array}{ll}\left[\left(E_b I_y u_1''' + \lambda M\theta_1'\right)\delta u_1\right]_0^{L_b} = 0 & \left[\left(E_b I_y u_2''' + \lambda M\theta_2'\right)\delta u_2\right]_0^{L_b} = 0 \\ \left[\left(E_b I_y u_1'' + \lambda M\theta_1\right)\delta u_1'\right]_0^{L_b} = 0 & \left[\left(E_b I_y u_2'' + \lambda M\theta_2\right)\delta u_2'\right]_0^{L_b} = 0 \\ \left[\left(G_b J_b \theta_1' - E_b C_w \theta_1'''\right)\delta\theta_1\right]_0^{L_b} = 0 & \left[\left(G_b J_b \theta_2' - E_b C_w \theta_2'''\right)\delta\theta_2\right]_0^{L_b} = 0 \\ \left[E_b C_w \theta_1''\delta\theta_1'\right]_0^{L_b} = 0 & \left[E_b C_w \theta_2''\delta\theta_2'\right]_0^{L_b} = 0\end{array}\right\} \text{at } z = 0,\ l \tag{5.15}$$

5.5 Solutions for Twin-beam-deck Systems

5.5.1 Simply-supported beams under uniform moments

For laterally and torsionally simply-supported twin beams, the boundary conditions in Eq. (5.15) lead to

$$\begin{aligned}
&u_1(0)=u_1(L_b)=u_1''(0)=u_1''(L_b)=0\\
&\theta_1(0)=\theta_1(L_b)=\theta_1''(0)=\theta_1''(L_b)=0\\
&u_2(0)=u_2(L_b)=u_2''(0)=u_2''(L_b)=0\\
&\theta_2(0)=\theta_2(L_b)=\theta_2''(0)=\theta_2''(L_b)=0
\end{aligned} \tag{5.16}$$

The displacement fields are assumed as sinusoidal functions, i.e., $u_i = A_i \sin\left(n\pi z/L_b\right)$ and $\theta_i = B_i \sin\left(n\pi z/L_b\right)$ $(i=1,2)$ $(n=1,2,3,\cdots$, which satisfy all the boundary conditions in Eq. (5.16). By substituting the assumed displacement fields into Eq, (5.14), one recover four algebraic equations. The determinant of the resulting matrix of coefficients is set to zero to recover the critical moment λM from

$$\begin{vmatrix}
\frac{\bar{k}h_b}{2}-\lambda M l_n^{\,2} & \psi_n+\frac{\bar{k}h_b^{\,2}}{4} & -\frac{\bar{k}h_b}{2} & \frac{E_d h_d^{\,3}}{6L_d}-\frac{\bar{k}h_b^{\,2}}{4}\\
E_b I_y l_n^{\,4}+\bar{k} & -\lambda M l_n^{\,2}+\frac{\bar{k}h_b}{2} & -\bar{k} & -\frac{\bar{k}h_b}{2}\\
-\frac{\bar{k}h_b}{2} & \frac{E_d h_d^{\,3}}{6L_d}-\frac{\bar{k}h_b^{\,2}}{4} & \frac{\bar{k}h_b}{2}-\lambda M l_n^{\,2} & \psi_n+\frac{\bar{k}h_b^{\,2}}{4}\\
-\bar{k} & -\frac{\bar{k}h_b}{2} & E_b I_y l_n^{\,4}+\bar{k} & -\lambda M l_n^{\,2}+\frac{\bar{k}h_b}{2}
\end{vmatrix}=0 \tag{5.17}$$

where the parameters $l_n = n\pi/L_b$ and $\psi_n = E_b C_w l_n^{\,4} + G_b J_b l_n^{\,2} + E_d h_d^{\,3}/3L_d$ have been defined.

Special case:

For the special case where the relative lateral stiffness of the deck-joint assembly is omitted, i.e., $\bar{k}=0$, Eq. (5.17) leads to the following simplified roots

$$\begin{aligned}
(\lambda M)_{1n} &= \pm\sqrt{E_b I_y E_b C_w\left(\frac{n\pi}{L_b}\right)^4 + E_b I_y G_b J_b\left(\frac{n\pi}{L_b}\right)^2 + \frac{E_b I_y E_d h_d^{\,3}}{6L_d}}\\
(\lambda M)_{2n} &= \pm\sqrt{E_b I_y E_b C_w\left(\frac{n\pi}{L_b}\right)^4 + E_b I_y G_b J_b\left(\frac{n\pi}{L_b}\right)^2 + \frac{E_b I_y E_d h_d^{\,3}}{2L_d}}
\end{aligned} \tag{5.18}$$

The smallest value is obtained by setting $n=1$ in Eq. (5.18), leading to the critical moment $M_{cr}=\left(\lambda M\right)_{1n}$. This coincides with Vlasov (1961). Also, the critical moment expression reverts to the classical solution (e.g., Timoshenko and Gere 1961) when the partial twisting restraint by the deck bending action is omitted, i.e., $\left(E_b I_y E_d h_d^{\,3}/6L_d\right)\to 0$.

5.5.2 Simply-supported beams under non-uniform moments

Assuming the displacement fields to be sinusoidal， i.e., $u_i=A_i'\sin\left(l_n z\right)$ and $\theta_i=B_i'\sin\left(l_n z\right)$ $\left(n=1,2,3,\cdots\right.$ and substituting into Eq. (5.13), one obtains

$$\begin{aligned}\Pi=&\frac{1}{2}\int_0^{L_b}E_b I_y A_1'^2 l_n^{\,4}\sin^2\left(l_n z\right)dz+\frac{1}{2}\int_0^{L_b}G_b J_b B_1'^2 l_n^{\,2}\cos^2\left(l_n z\right)dz+\frac{1}{2}\int_0^{L_b}E_b C_w B_1'^2 l_n^{\,4}\sin^2\left(l_n z\right)dz\\&-\int_0^{L_b}\lambda M A_1' B_1' l_n^{\,2}\sin^2\left(l_n z\right)dz+\frac{1}{2}\int_0^{L_b}\lambda q h B_1'^2\sin^2\left(l_n z\right)dz+\frac{1}{2}\int_0^{L_b}E_b I_y A_2'^2 l_n^{\,4}\sin^2\left(l_n z\right)dz\\&+\frac{1}{2}\int_0^{L_b}G_b J_b B_2'^2 l_n^{\,2}\cos^2\left(l_n z\right)dz+\frac{1}{2}\int_0^{L_b}E_b C_w B_2'^2 l_n^{\,4}\sin^2\left(l_n z\right)dz-\int_0^{L_b}\lambda M A_2' B_2' l_n^{\,2}\sin^2\left(l_n z\right)dz\\&+\frac{1}{2}\int_0^{L_b}\lambda q h B_2'^2\sin^2\left(l_n z\right)dz+\frac{E_d h_d^{\,3}}{6L_d}\int_0^{L_b}\left(B_1'^2+B_1'B_2'+B_2'^2\right)\sin^2\left(l_n z\right)dz\\&+\frac{\bar{k}}{2}\int_0^{L_b}\left[\left(A_2'-A_1'\right)\sin\left(l_n z\right)+\frac{h_b}{2}\left(B_2'-B_1'\right)\sin\left(l_n z\right)\right]^2 dz\end{aligned}\tag{5.19}$$

For a given moment distribution, the stationarity conditions of Eq. (5.19) are evoked and the determinant of the resulting matrix of coefficients is set to zero to recover approximate expressions for the critical load multiplier. The above procedure is applied to two loading types: (1) Uniformly distributed loads (UDL), and (2) mid-span concentrated loads. The details are provided in Appendix 5D.

5.5.3 Finite element formulation

The Hermitian polynomials are adopted to relate the lateral displacement fields u_i and rotation fields θ_i $\left(i=1,2\right)$ to the generalized nodal displacements, i.e.

$$\begin{aligned}u_i\left(z\right)&=\left\langle L\left(z\right)\right\rangle_{1\times 4}^{T}\left\{u_i\right\}_{4\times 1}\\\theta_i\left(z\right)&=\left\langle L\left(z\right)\right\rangle_{1\times 4}^{T}\left\{\theta_i\right\}_{4\times 1}\end{aligned}\tag{5.20}$$

where

$\langle L(z)\rangle_{1\times4}^{T} = \left\langle \left(1-3z^2/l^2+2z^3/l^3\right) \quad \left(z-2z^2/l+z^3/l^2\right) \quad \left(3z^2/l^2-2z^3/l^3\right) \quad \left(z^3/l^2-z^2/l\right) \right\rangle$ is the vector of Hermitian interpolation functions and l is the element length, $\langle u_i\rangle_{1\times4}^{T} = \left\langle u_0 \quad u_0' \quad u_l \quad u_l' \right\rangle_i$ is the generalized nodal lateral displacement vector and $\langle \theta_i\rangle_{1\times4}^{T} = \left\langle \theta_0 \quad \theta_0' \quad \theta_l \quad \theta_l' \right\rangle_i$ is the generalized nodal angle of twist vector, where subscripts 0 and l denote nodal points of the element. From Eq. (5.20), by substituting into Eq. (5.13), one obtains

$$\Pi = \frac{1}{2}\left\langle \langle u_1\rangle_{1\times4}^{T} \quad \langle u_2\rangle_{1\times4}^{T} \quad \langle \theta_1\rangle_{1\times4}^{T} \quad \langle \theta_2\rangle_{1\times4}^{T} \right\rangle \left[[K_e] - \lambda [K_g] \right]_{16\times16} \begin{Bmatrix} \{u_1\}_{4\times1} \\ \{u_2\}_{4\times1} \\ \{\theta_1\}_{4\times1} \\ \{\theta_2\}_{4\times1} \end{Bmatrix} \tag{5.21}$$

where the elastic stiffness matrix $[K_e]$ has three contributions, $[K_e] = [K_b] + [K_t] + [K_l]$. Matrix $[K_b]$ is the beam stiffness matrix, $[K_t]$ is the stiffness matrix for partial twisting restraint, and $[K_l]$ is the stiffness matrix for the relative partial lateral restraint. The beam stiffness matrix $[K_b]$ is

$$[K_b] = \begin{bmatrix} E_b I_y [B_1] & [0] & [0] & [0] \\ [0] & E_b I_y [B_1] & [0] & [0] \\ [0] & [0] & E_b C_w [B_1] + G_b J_b [B_2] & [0] \\ [0] & [0] & [0] & E_b C_w [B_1] + G_b J_b [B_2] \end{bmatrix}_{16\times16}$$

and the stiffness matrix for the partial twisting restraint $[K_t]$ is

$$[K_t] = \frac{E_d h_d^{\,3}}{6L_d} \begin{bmatrix} [0] & [0] & [0] & [0] \\ [0] & [0] & [0] & [0] \\ [0] & [0] & 2[B_3] & [B_3] \\ [0] & [0] & [B_3]^T & 2[B_3] \end{bmatrix}_{16\times16}$$

and the stiffness matrix for the relative partial lateral restraint $[K_l]$ is

$$[K_l] = \frac{\bar{k}}{4} \begin{bmatrix} 4[B_3] & -4[B_3] & 2h_b[B_3]^T & -2h_b[B_3]^T \\ -4[B_3]^T & 4[B_3] & -2h_b[B_3]^T & 2h_b[B_3]^T \\ 2h_b[B_3] & -2h_b[B_3] & h_b^{\,2}[B_3] & -h_b^{\,2}[B_3] \\ -2h_b[B_3] & 2h_b[B_3] & -h_b^{\,2}[B_3]^T & h_b^{\,2}[B_3] \end{bmatrix}_{16\times16}$$

The geometric stiffness matrix $\left[K_g\right]$ takes the form

$$\left[K_g\right]=\begin{bmatrix} [0] & [0] & -[B_4]^T & [0] \\ [0] & [0] & [0] & -[B_4]^T \\ -[B_4] & [0] & -h[B_5] & [0] \\ [0] & -[B_4] & [0] & -h[B_5] \end{bmatrix}_{16\times16}$$

and submatrices $[B_1],[B_2],[B_3],[B_4],[B_5]$ have been defined in Appendix 5E. From Eq. (5.21), by evoking the stationarity of the total potential energy, i.e., $\delta\Pi=0$, one obtains

$$\left(\left[K_e\right]_{16\times16}-\lambda\left[K_g\right]_{16\times16}\right)\begin{Bmatrix} \{u_1\}_{4\times1} \\ \{u_2\}_{4\times1} \\ \{\theta_1\}_{4\times1} \\ \{\theta_2\}_{4\times1} \end{Bmatrix}=\{0\}_{16\times1} \tag{5.22}$$

5.6 Results

A wooden twin-beam-deck assembly with commonly used material and practical dimensions was chosen as a reference case. The reference case was used to assess the validity of the results based on the present closed-form, energy-based and FEA solutions through comparisons to the results predicted by the ABAQUS FEA software. The verified model was then used to conduct a parametric study by varying one parameter at a time from the reference case and observing the critical moments and buckling mode shapes. For the verification study, the transverse loads were applied at the beam shear center. For the parametric study, unless specified otherwise, the transverse loads were applied at the deck centerline.

The reference wooden beam-deck assembly consists of a simply-supported twin beams connected by deck boards through nail connections. The reference beam and deck span are 6 m and 2 m, respectively. The beams are assumed to be glu-laminated Spruce-Lodgepole Pine-Jack Pine 20f-EX with 570 mm depth and 80 mm width. The modulus of elasticity and shear modulus are assumed to be 10,300 MPa and 474 MPa, respectively. The nominal bending moment resistance based on material failure is 270 kNm. The deck boards are assumed to be Spruce-Pine-Fir No. 2 grade and are 38 mm thick with a modulus of elasticity of 10,000 MPa. All the material properties mentioned above are based on CAN/CSA Standard O86 (2014) and FPL (2010). Two 3.76 mm

nails are assumed to be installed at each beam-deck intersection. In addition to the reference case, twelve other cases were considered by varying load types, beam and deck span, load height, relative lateral restraint height and stiffness, number of spans and whether the partial lateral or twisting restraint was included in the analysis. Table 5.2 provides a summary of all the parametric runs conducted.

Table 5.2 Summary of parametric runs

Case No.	Closed-form or energy-based solution	Present FEA	ABAQUS	Load type	Beam span (m)	Deck span (m)	Relative lateral stiffness per unit deck width (kN/m/m)	Load Position	Height of lateral restraint	No. of Spans	Partial relative lateral or twisting restraint included	Figure or table link
Reference	✓	✓	✓	UM	6	2	/	/	BT	1	Y	Figure 5.3(a,b)
1	✓	✓	✓	UDL	6	2	/	BSC	BT	1	Y	Figure 5.3(c,d)
2	✓	✓	✓	CL	6	2	/	BSC	BT	1	Y	Figure 5.3(e,f)
3	✓	✓		UDL	2-10	2	/	DC	BT	1	Y	Figure 5.3g
4	✓	✓		UDL	6	1-5	/	DC	BT	1	Y	Figure 5.3h
5		✓		UDL	2,6	2	1-100000	BSC	BT	1	Y	Figure 5.4a
6		✓		UDL	6	2	/	DC	DC-BSC	1	Y	Figure 5.4b
7		✓		UDL	2-10	2	/	DC	BT	1	Y/N	Figure 5.4(c,d)
8		✓		UDL	4,6,8	2	/	DC/BSC/BB	BT	1	Y	Table 5.3
9		✓		CL	6	1,3,5	/	DC/BSC/BB	BT	1	Y	Table 5.4
10		✓		UDL	4-10	2	/	DC	BT	2	Y	Figure 5.5a
11		✓		CL	4-10	2	/	DC	BT	2	Y	Figure 5.5b
12		✓		UDL	4-10	2	/	DC	BT	1/2	Y	Table 5.5

Note:
UM=uniform moments, UDL=uniformly distributed loads, CL= mid-span concentrated loads,
DC=deck centerline, BSC=beam shear center, BB=beam bottom, BT= beam top,
Y=yes, N=no.

5.6.1 Details of ABAQUS model

The finite-element program ABAQUS 6.12-3 was used to conduct an eigenvalue buckling analysis of the twin-beam-deck assembly. The two-node B31OS element was used to model the twin beams. Each node has seven degrees of freedom (i.e., three translations, three rotations, and one warping deformation). The element accounts for shear deformation only due to bending but ignores shear deformation induced by warping. Two types of elements were chosen to capture the twisting restraint of the

deck and the relative lateral restraint of the deck-joint assembly. The B31 element was used to model the flexural stiffness of the deck boards. The B31 element has two nodes with six degrees of freedom per node (i.e., three translations and three rotations). The two-node SPRING2 spring element was employed to simulate the partial relative lateral restraining action between the top of both beams for the deck-joint assembly.

Figure 5.2 shows the twin-beam-deck model developed, with B31OS elements depicted at the centroidal axes of the twin beams, B31 elements at the deck board centerlines, and SPRING2 elements spanning between the top of the twin beams. The number of B31OS elements in each beam was chosen to be consistent with the number of deck boards. Each deck node (lying on line 2 or 5 in Figure 5.2) was tied to the corresponding centroidal node (on line 1 or 4). Also, each spring node (on line 3 or 6) was tied to the corresponding centroidal node (on line 1 or 4). Both rigid links were defined using the BEAM type multi-point constraint (*MPC) feature in ABAQUS.

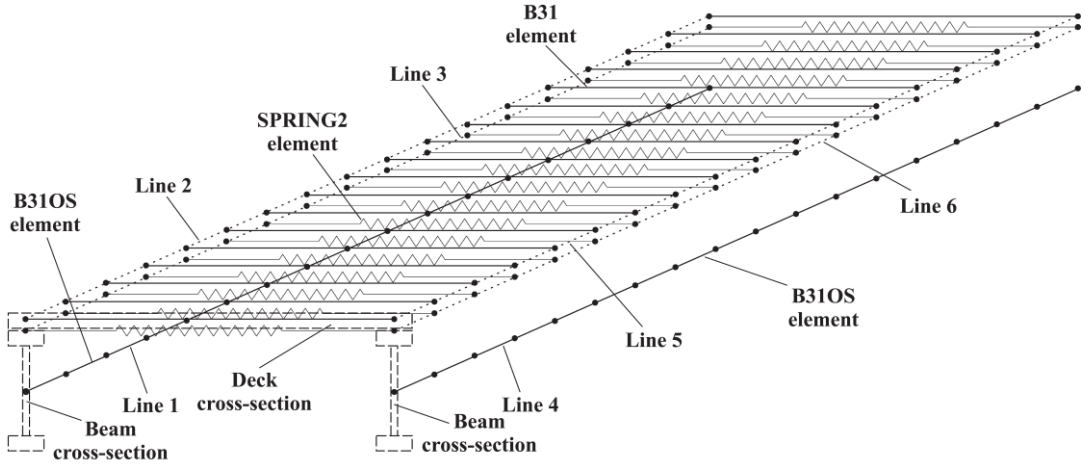

Figure 5.2 ABAQUS twin-beam-deck model

5.6.2 Mesh convergence study

A mesh convergence study was performed for the present FEA solution and ABAQUS for the cases of uniform moments (Figure 5.3a,b), UDL (Figure 5.3c,d), and mid-span concentrated loads (Figure 5.3e,f). For a twin-beam-deck system, the relative lateral stiffness per unit deck width $\bar{k}$ is a function of deck width b, which indicates different mesh choices in the present FEA model could possibly affect the critical moment. Detailed discussions will be provided in Appendix 5F. For systems with transverse loads applied at the beam shear center, it is observed that the critical positive moments (tension at the bottom) and negative moments are identical. Further

discussions will also be provided in Section 5.6.5. Thus, only the magnitudes of the moments are presented. Among all three load types investigated, the present FEA results converge from above and no more than ten beam elements are needed to attain convergence. Similar observations can be made for the ABAQUS model for the cases of UDL and mid-span loads. For uniform moments, however, 30 elements per beam are needed for ABAQUS to converge. In order to insure full convergence, 30 elements per beam were taken for all subsequent runs in the present FEA and ABAQUS model (In present FEA, the computational time required for 30 elements per beam is relatively short and 30 elements per beam renders better representation of buckling mode shapes). In both solutions, a single element was enough to accurately represent the flexural action of the deck.

5.6.3 Verification of results

For uniform moments (Figure 5.3a), the critical moments determined by the present closed-form and FEA solutions yield the same value of 193 kNm, compared with a slightly lower value of 192 kNm predicted from ABAQUS. This is attributed to the fact that the ABAQUS B31OS elements incorporate shear deformation effects due to flexure and thus provides a more flexible representation of the system. The mode shapes predicted by all three solutions are in close agreement (Figure 5.3b). For UDL (Figure 5.3c), the approximate energy-based formulation predicts a critical moment of 222 kNm, a slightly higher value than 212.1 kNm obtained from the present FEA and 211.8 kNm from ABAQUS. Unlike the case of uniform moments where the assumed sinusoidal displacement fields accurately match those based on the present FEA and ABAQUS, Figure 5.3d depicts a difference in mode shapes between the energy-based solution and the other two solutions, resulting in a stiffer representation of the system, and leading to a critical moment that is 4.46% higher than that based on the present FEA solution. For mid-span concentrated loading, the larger difference in the twisting angle distribution (Figure 5.3f) results in a larger buckling capacity overestimation (Figure 5.3e). The above comparisons show very good agreement between the present FEA model and ABAQUS. Although, the approximate energy-based solution overestimates the buckling capacity, the modelling and computational effort involved is significantly lower than that of both FEA solutions. The validity of the approximate solution is further examined by varying the beam and deck span in Figure 5.3(g,h) where the results are compared against the present FEA. In Figure 5.3g, the beam span varies

from 2 m to 10 m while the deck span is kept at 2 m. The approximate solution for upward and downward UDL predicts critical moments that are larger by 8% or less than those predicted by the present FEA. Also, in Figure 5.3h where the deck span varies from 1 m to 5 m and the beam span is kept at 6 m, the results show the approximate solution predicts critical moments close to those based on the present FEA.

5.6.4 Effects of beam and deck span

The effect of beam and deck span are illustrated in Figure 5.3(g,h). When the beam span increases from 2m to 10m (Figure 5.3g), the buckling capacity for upward UDL as predicted by the present FEA decreases from 412 kNm to 204 kNm. In contrast, for downward UDL, the capacity is lower than that based on upward loading and the critical moment declines slightly from 219 kNm to 198 kNm. Further discussion will be provided under Section 5.6.8. For both upward and downward UDL, as the deck span increases from 1 m to 5 m, Figure 5.3h shows a consistent decline in buckling capacity. The critical moment corresponding to the case of a 5m deck span is roughly half of the capacity of the case of the 1m deck span.

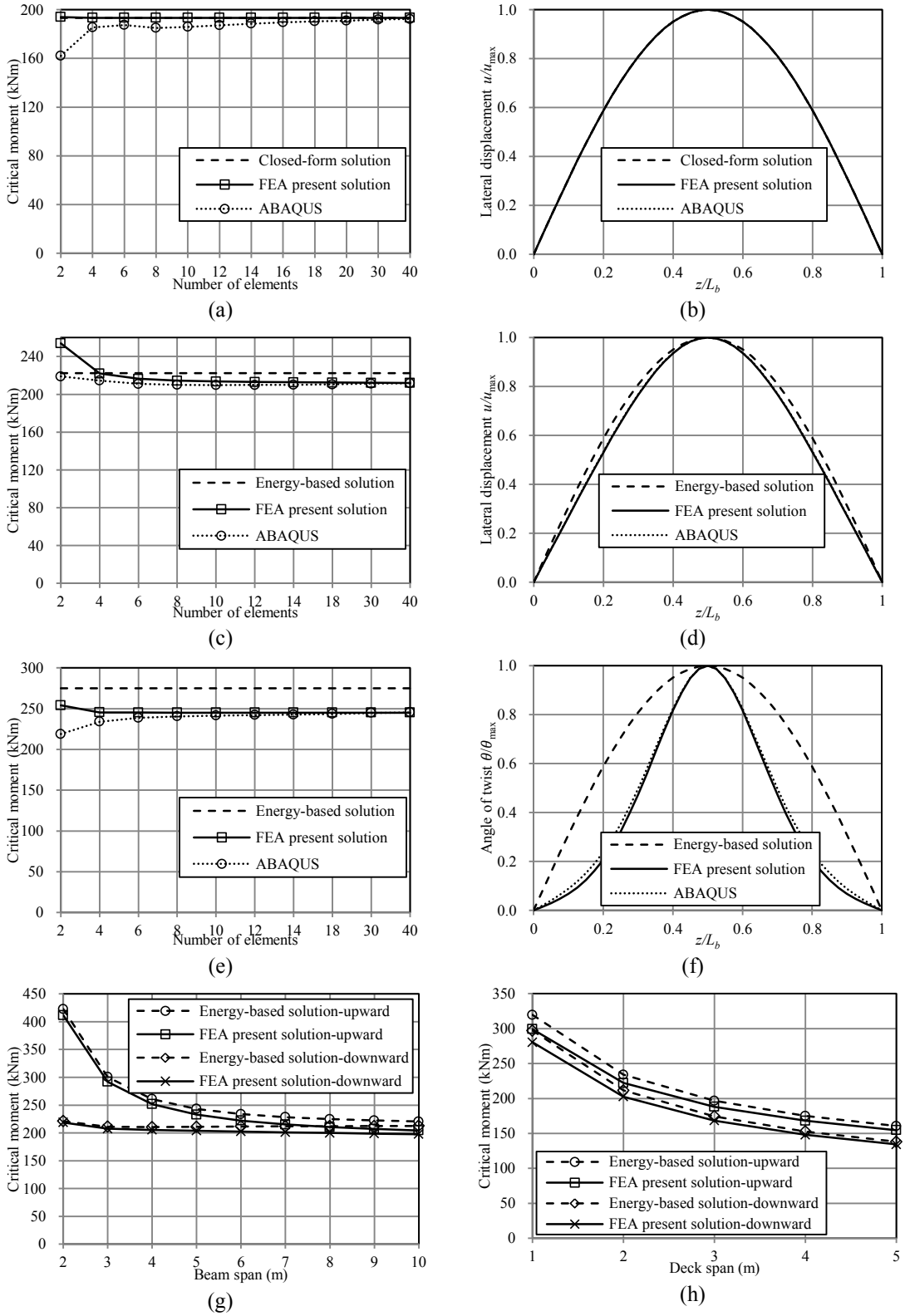

Figure 5.3 (a) Convergence study for uniform moments, (b) mode shapes for uniform moments, (c) convergence study for UDL, (d) mode shapes for UDL, (e) convergence study for mid-span concentrated loads, (f) mode shapes for mid-span concentrated loads, (g) critical moments for UDL with varying beam span, (h) critical moments for UDL with varying deck span

5.6.5 Effect of the relative lateral stiffness of the deck-joint assembly

Figure 5.4a shows the critical moments as a function of the relative lateral stiffness per unit deck width $\bar{k}$ for twin beams subjected to UDL acting at the height of beam shear center. Two beam spans were investigated, i.e., 2 m and 6 m. For the 2 m span, the critical moments for downward loading increase with $\bar{k}$ up to 100 kN/m/m, after which the critical moments remain constant at 301 kNm. In contrast, the critical moments for upward loading remain constant at 250 kNm irrespective of the magnitude of $\bar{k}$. For the 6 m span, the critical moments for upward and downward UDL increase as $\bar{k}$ increases. The increase in critical moment for downward loading is faster than that of upward loading, resulting in a higher buckling capacity for a certain stiffness range. The critical moments for upward and downward loading are found equal with a magnitude of 212 kNm when $\bar{k}$ exceeds the threshold value of 45.3 kN/m/m. For the reference deck-joint assembly, $\bar{k}$ corresponding to a single nail per joint is 5572 kN/m/m (Appendix 5B), while that based on two nails per joint is 9974 kN/m/m. Both values are depicted by the vertical lines on Figure 5.4a. For the problems examined, both stiffness values far exceed the threshold stiffness value, resulting in identical critical moment magnitude for upward and downward loading. Further investigation on beam spans of 4m and longer suggests similar conclusions. Such results were omitted from Figure 5.4a, to avoid clutter. The present example suggests that a beam-deck connection with a single nail provides enough lateral stiffness to develop their peak critical moments.

5.6.6 Effect of lateral restraint height

For the reference twin-beam-deck assembly subjected to UDL, the relative lateral restraint of the deck-joint assembly is hypothetically moved from the beam shear center to the deck centerline and the corresponding moments are presented in Figure 5.4b. Two categories of restraint stiffness were considered: below and above the threshold value. Considered was the relative lateral stiffness per unit deck width $\bar{k}$ of 10 kN/m/m, a value below the threshold stiffness. For upward loading, the critical moments are observed to decrease from 205 kNm to 185 kNm as the restraint moves from the shear center to the deck centerline. In contrast, for downward loading, the critical moments are observed to increase from 168 kNm to 189 kNm. The results suggest that the restraint height has a moderate effect on the critical moments for $\bar{k}$

below the threshold value. For a relative lateral stiffness above the threshold stiffness, the critical moments corresponding to upward and downward loading remain constant at 222 kNm and 203 kNm, respectively.

Insight on the above observations can be provided by examining the associated mode shapes. For a relative lateral stiffness below the threshold value, the modes are observed to be symmetric (i.e., $u_1 = -u_2$ and $\theta_1 = -\theta_2$). Thus, the last term in Eq. (5.13) is non-zero and the internal strain energy for the deck-joint assembly is influenced by the restraint height. In contrast, when the relative lateral stiffness is beyond the threshold value, the modes become anti-symmetric (i.e., $u_1 = u_2$ and $\theta_1 = \theta_2$), causing the last term of Eq. (13) to vanish, thus eliminating the dependence of the solution on the restraint height.

5.6.7 Effects of partial relative lateral and twisting restraints

The critical moments for the reference twin-beam-deck assembly subjected to UDL applied at the deck centerline are examined for various restraint scenarios: (1) partial relative lateral and twisting restraints included, (2) partial twisting restraint with no relative partial lateral restraint, (3) relative partial lateral restraint with no partial twisting restraint, and (4) no restraints. For downward loading (Figure 5.4c), the contribution of the partial twisting restraint and relative partial lateral restraint is illustrated by the gap between the upper solid line and the dotted line. The contribution of the restraint grows as the span increases from 2 m to 6 m, after which the restraint contributes a steady 40% of the total capacity. Interestingly, the results corresponding to twin-beams with relative partial lateral restraint alone (no twisting restraint) are observed to coincide with those of no restraints. The presence of relative lateral restraint between identical beams identically loaded provides no lateral torsional buckling restraining action to both beams. Identical conclusions can be drawn for the case of upward loading (Figure 5.4d).

5.6.8 Effect of load position

Three load positions are considered: (1) Deck centerline, (2) beam shear center and (3) beam bottom. The critical moments are examined for beam spans of 4, 6, and 8m and deck spans of 1, 3, and 5 m and results are presented in Table 5.3 and Table 5.4 respectively. For downward loading, because of the destabilizing effect induced by deck centerline loading, the buckling capacities are observed to be lower than those

based on beam shear center loading. The percentage decreases are 10.1%, 4.25% and 2.44% for 4, 6 and 8 m, respectively. In contrast, loading at the beam bottom is found to be associated with a stabilizing effect which increases the buckling capacity. The percentage increases are 10.5%, 4.72% and 2.44% for beam spans of 4, 6 and 8m, respectively. For upward loading, an opposite trend is observed where deck centerline loading is found to correspond to the highest critical moments. The results in Table 5.3 suggest that the load position effect is more pronounced in short span beams. In contrast, the results in Table 5.4 suggest that the load position effect is more significant in long span decks.

For loads applied at deck centerline, the load position effect causes the critical moments due to upward loading to be higher than those based on downward loading. For loading applied to the bottom of the beams, an opposite trend is observed.

5.6.9 Effect of beam span on two-span continuous twin-beam-deck systems

Figure 5.5(a,b) show the buckling capacity of a two-span continuous twin-beam-deck system with varying beam span under UDL and mid-span concentrated loads applied to both spans. For downward loading, the critical moments at mid-span remain nearly constant at 200 kNm and are found to be insensitive of the span. In contrast, for upward loading, critical moments are found to decrease as the span increases from 4 to 10m. This trend is consistent with the observations from single-span beams. Table 5.5 provides a comparison of the critical moments for single-span and two-span twin-beam-deck systems with a UDL applied at the deck centerline. For upward and downward loading, the results suggest that the critical moments for two-span twin-beam-deck assemblies are slightly higher than those based on single-span assemblies of the same span.

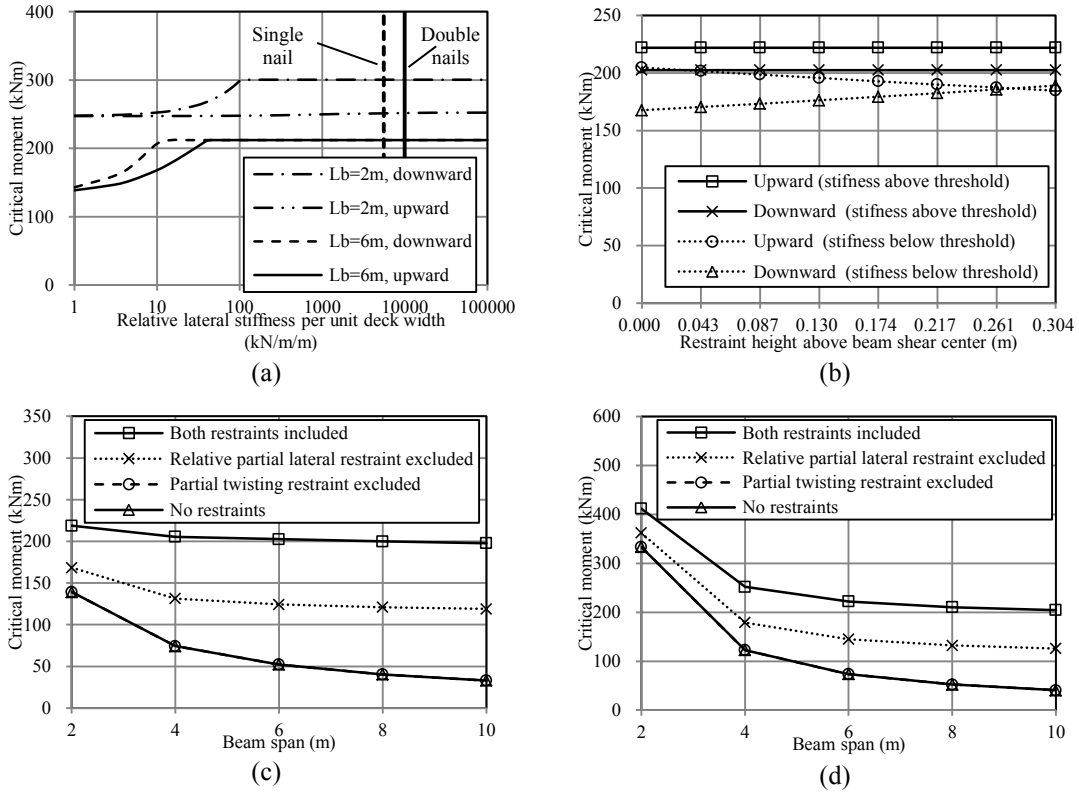

Figure 5.4 (a) Buckling capacity for varying relative lateral stiffness per unit deck width, (b) effect of relative lateral restraint height; Buckling capacity as influenced by inclusion/exclusion of partial relative lateral and twisting restraints under (c) downward UDL with varying beam span, (d) upward UDL with varying beam span

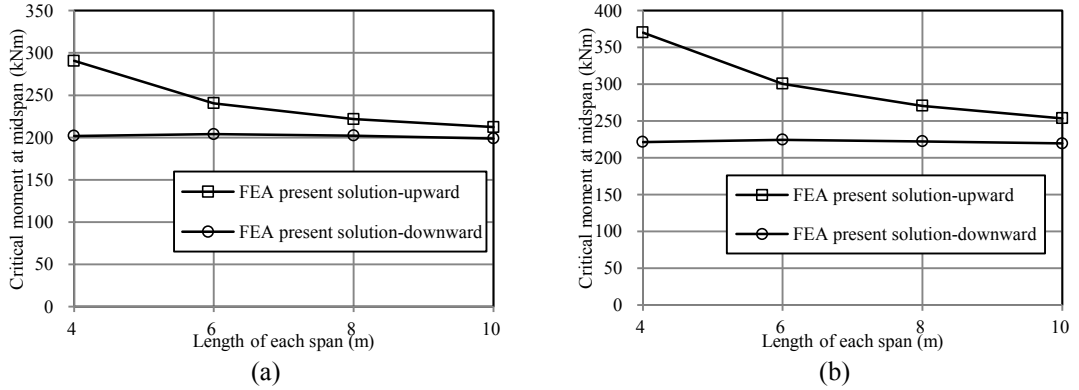

Figure 5.5 Buckling capacity for a two-span continuous twin-beam-deck system with varying span under (a) UDL, (b) mid-span concentrated loads

Table 5.3 Load position effect for different beam spans

Beam span (m)	Load position	Downward UDL		Upward UDL	
		Critical moment (kNm)	Difference	Critical moment (kNm)	Difference
4	Deck centerline	205	-10.1%	252	10.5%
	Beam shear center	228	/	228	/
	Beam bottom	250	9.65%	176	-22.8%
6	Deck centerline	203	-4.25%	222	4.72%
	Beam shear center	212	/	212	/
	Beam bottom	222	4.72%	203	-4.25%
8	Deck centerline	200	-2.44%	210	2.44%
	Beam shear center	205	/	205	/
	Beam bottom	210	2.44%	200	-2.44%

Table 5.4 Load position effect for different deck spans

Deck span (m)	Load position	Downward UDL		Upward UDL	
		Critical moment (kNm)	Difference	Critical moment (kNm)	Difference
1	Deck centerline	280	-3.21%	299	3.31%
	Beam shear center	290	/	290	/
	Beam bottom	299	3.10%	281	-3.01%
3	Deck centerline	168	-5.46%	188	5.73%
	Beam shear center	178	/	178	/
	Beam bottom	188	5.37%	169	-5.12%
5	Deck centerline	134	-6.84%	155	7.29%
	Beam shear center	144	/	144	/
	Beam bottom	154	6.82%	135	-6.42%

Table 5.5 Comparison of critical moments between single-span and two-span twin beams

Beam span/ length of each span (m)	Critical moment for downward UDL (kNm)			Critical moment for upward UDL (kNm)		
	Single-span system	Two-span system	Ratio	Single-span system	Two-span system	Ratio
4	205	202	0.985	252	291	1.12
6	203	204	1.01	222	240	1.08
8	200	202	1.01	210	222	1.06
10	198	199	1.01	204	212	1.04

5.7 Conclusions

A family of solutions was developed for predicting the lateral torsional buckling capacity of twin beams continuously braced by deck boards. The solutions are applicable to general loading and boundary conditions while capturing the continuous relative partial lateral restraint provided by the stiffness of the deck-joint assembly and the partial twisting restraint provided by the deck bending stiffness. The results based on the models developed are observed to be in close agreement with those based on ABAQUS and involve a minimal computational effort.

For wooden twin-beam-deck systems with practical dimensions and material properties, the following observations were made:

1. Both upward and downward loading can induce lateral torsional buckling. For loads applied at deck centerline, the critical moments based on upward loading are higher than based on downward loading. The opposite is observed for cases where loads applied at the beam bottom. For medium and long span beams loaded at the shear center, the critical moments for upward and downward loading are found identical for beam-deck assemblies where the relative lateral stiffness of the deck-joint assembly exceeds the threshold value.
2. The combined continuous partial relative lateral and twisting restraints significantly increase the lateral torsional buckling capacity. However, the presence of relative partial lateral restraint alone provides no buckling capacity increase.
3. As the beam span increases, the buckling capacity for upward loading decreases while that based on downward loading remains essentially constant.
4. As the deck span increases, the buckling capacity for both upward and downward loading was found to decrease significantly.
5. The load position greatly influences the buckling capacity for short span beams or long span deck. For upward loading, the buckling capacity was found to decrease as the point of application of the load moves downwards. An opposite trend is observed for downward loading.
6. The height of relative lateral restraint has no effect on the buckling capacity when the relative lateral stiffness of the deck-joint assembly exceeds the threshold stiffness value.
7. For two-span twin-beam-deck systems, the trend between the beam span and buckling capacity is similar to that of single span systems. The buckling capacity for

two-span systems is slightly higher than that of a single-span system with the same span.

Appendix 5A Transformed Section Properties for Composed I-section Beams

For a composite I-section beam with both flanges having different material from the web, the transformed sections are to take the form

$$\begin{aligned} J_b &= J_f + n_1 J_w \\ I_y &= I_{yy,f} + n_2 I_{yy,w} \\ C_w &= I_{\omega\omega,f} + n_2 I_{\omega\omega,w} \end{aligned} \tag{5.A.1}$$

in which J_f and J_w are the Saint-Venant torsional constants for both flanges and the web, respectively, $n_1 = G_w / G_b$ is the ratio of shear modulus, G_w for the web to that of the flange, $n_2 = E_w / E_b$ is the ratio of modulus of elasticity, E_w of the web to that of the flange, and the following sectional properties have been defined

$$\begin{aligned} I_{yy,f} &= \int_{A_f} x^2 dA_f, I_{yy,w} = \int_{A_w} x^2 dA_w, \\ I_{\omega\omega,f} &= \int_{A_f} \omega^2 dA_f, I_{\omega\omega,w} = \int_{A_w} \omega^2 dA_w \end{aligned} \tag{5.A.2}$$

where A_f is the area of both flanges, A_w is the area of the web, and ω is the sectorial coordinate based on a fixed radius taken from the shear center to the sectorial origin.

Appendix 5B Relative Lateral Stiffness of the Deck-joint Assembly

This appendix shows the details of quantifying the relative lateral stiffness k for a deck board nailed at each end (deck-joint assembly). The stiffness k can be conceived to be that of three springs in tandem (i.e., two springs, each representing the shear stiffness k_j of the joint at the beam-deck interface, and another spring representing the deck axial stiffness k_d). By adding the flexibility of the three components, one has $1/k = 1/k_j + 1/k_d + 1/k_j$. Solving for overall stiffness k, one obtains

$$k = \frac{k_d k_j}{2k_d + k_j} \tag{5.B.1}$$

Assuming $\bar{n}$ nails are installed at each joint and the shear stiffness for a single-nail joint is k_n, the shear stiffness at the joint is $k_j = \bar{n}k_n$. The single-nail joint stiffness k_n is based on the load-slip relationship recommended in CAN/CSA O86-14. The shear deformation of the single-nail joint Δ_n is

$$\Delta_n = 0.5 d_F K_m \left(\frac{F}{F_u} \right)^{1.7} \tag{5.B.2}$$

where d_F is the nail diameter in mm, K_m is the service creep factor accounting for load duration and moisture level, and F_u is the lateral strength resistance as governed by the smallest capacities amongst different failure modes. In the present study, the value $K_m = 1$ was used. Eq. (5.B.2) is based on the work of Johansen (1949) and is applicable when the lateral load meets the condition $F \le (1/3) F_u$. The shear stiffness k_n is taken as the initial stiffness (i.e., gradient that joins the origin and 10% of lateral strength resistance F_u) as predicted by Eq. (5.B.2).

The model for quantifying the deck axial stiffness at the height of beam-deck interface is schematically depicted in Figure 5.B.1. The deck board is assumed to be subject to a pair of eccentric loads F acting at the beam-deck interface. The deck board lateral deformation Δ has two components, an axial deformation Δ_1, and another deformation Δ_2 associated with transverse bending, i.e.,

$$\Delta = \Delta_1 + \Delta_2 = \frac{F L_d}{E_d b h_d} + \frac{M_d M_0 L_d}{E_d I_d} \tag{5.B.3}$$

where M_d is the bending moment induce by eccentric lateral loads F and is expressed as $M_d = Fh_d/2$, and M_0 is the moment for unit lateral loads. From the expressions for M_d and M_0, by substituting into Eq. (5.B.3), one obtains

$$\Delta = \frac{FL_d}{E_d b h_d} + \frac{Fh_d{}^2 L_d}{4E_d I_d} = \frac{4FL_d}{E_d b h_d} \tag{5.B.4}$$

and the axial stiffness of the deck board at the height of beam-deck interface is $k_d = E_d b h_d / 4L_d$.

From the expression of k_d, by substituting into Eq. (5.B.1), one obtains the relative lateral stiffness

$$k = \frac{\bar{n} E_d b h_d k_n}{2E_d b h_d + 4\bar{n} L_d k_n} \tag{5.B.5}$$

For a deck board that is 38 mm thick, 200 mm wide and 2 m long with a modulus of elasticity of 10,000 MPa, the relative lateral stiffness corresponding to a single 3.76 mm nail at each joint is $k = 1114$ kN/m ($\bar{k} = k/b = 5572$ kN/m/m) while that based on two nails at each joint is $k = 1995$ kN/m ($\bar{k} = 9974$ kN/m/m).

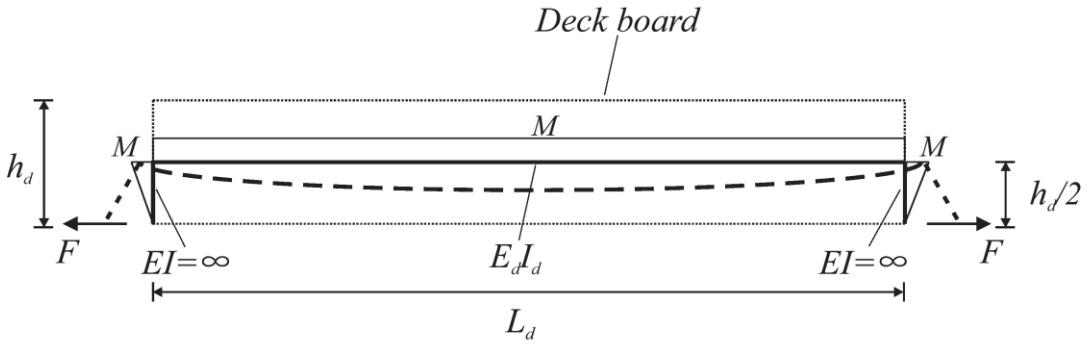

Figure 5.B.1 Cross-sectional elevation of a deck board with axial deformation due to eccentric lateral loading *F* acting at the deck underside

Appendix 5C Derivation of Equilibrium Equations and Boundary Conditions

Starting from the total potential energy expression in Eq. (5.13), this appendix shows the details of deriving the conditions of equilibrium (neutral) stability and the associated boundary conditions. The variation of the total potential energy is

$$\begin{aligned}\delta\Pi = &\int_0^{L_b} E_b I_y u_1'' \delta u_1'' dz + \lambda \int_0^{L_b} M\theta_1 \delta u_1'' dz + \lambda \int_0^{L_b} M u_1'' \delta\theta_1 dz + \frac{E_d h_d^3}{6L_d} \int_0^{L_b} (2\theta_1 + \theta_2)\delta\theta_1 dz \\ &+ \int_0^{L_b} G_b J_b \theta_1' \delta\theta_1' dz + \int_0^{L_b} E_b C_w \theta_1'' \delta\theta_1'' dz + \lambda \int_0^{L_b} qh\theta_1 \delta\theta_1 dz + \int_0^{L_b} E_b I_y u_2'' \delta u_2'' dz + \lambda \int_0^{L_b} M\theta_2 \delta u_2'' dz \\ &+ \lambda \int_0^{L_b} M u_2'' \delta\theta_2 dz + \frac{E_d h_d^3}{6L_d} \int_0^{L_b} (\theta_1 + 2\theta_2)\delta\theta_2 dz + \int_0^{L_b} G_b J_b \theta_2' \delta\theta_2' dz + \int_0^{L_b} E_b C_w \theta_2'' \delta\theta_2'' dz \\ &+ \lambda \int_0^{L_b} qh\theta_2 \delta\theta_2 dz + \frac{\bar{k}}{2}\left\{ \int_0^{L_b} \left[2u_1 - 2u_2 + h_b(\theta_1 - \theta_2)\right]\delta u_1 dz - \int_0^{L_b} \left[2u_1 - 2u_2 + h_b(\theta_1 - \theta_2)\right]\delta u_2 dz \right. \\ &\left. + h_b \int_0^{L_b} \left[u_1 - u_2 + \frac{h_b}{2}(\theta_1 - \theta_2)\right]\delta\theta_1 dz - h_b \int_0^{L_b} \left[u_1 - u_2 + \frac{h_b}{2}(\theta_1 - \theta_2)\right]\delta\theta_2 dz \right\} \\ &= 0\end{aligned} \tag{5.C.1}$$

From Eq. (5.C.1), through integration by parts, one obtains

$$\begin{aligned}&\int_0^{L_b} E_b I_y u_1'' \delta u_1'' dz = \left[E_b I_y u_1'' \delta u_1'\right]_0^{L_b} - \left[\left(E_b I_y u_1''\right)' \delta u_1\right]_0^{L_b} + \int_0^{L_b} \left(E_b I_y u_1''\right)'' \delta u_1 dz \\ &\int_0^{L_b} G_b J_b \theta_1' \delta\theta_1' dz = \left[G_b J_b \theta_1' \delta\theta_1\right]_0^{L_b} - \int_0^{L_b} \left(G_b J_b \theta_1'\right)' \delta\theta_1 dz \\ &\int_0^{L_b} E_b C_w \theta_1'' \delta\theta_1'' dz = \left[E_b C_w \theta_1'' \delta\theta_1'\right]_0^{L_b} - \left[\left(E_b C_w \theta_1''\right)' \delta\theta_1\right]_0^{L_b} + \int_0^{L_b} \left(E_b C_w \theta_1''\right)'' \delta\theta_1 dz \\ &\int_0^{L_b} M\theta_1 \delta u_1'' dz = \left[M\theta_1 \delta u_1'\right]_0^{L_b} - \left[\left(M\theta_1\right)' \delta u_1\right]_0^{L_b} + \int_0^{L_b} \left(M\theta_1\right)'' \delta u_1 dz\end{aligned} \tag{5.C.2}$$

$$\int_0^{L_b} E_b I_y u_2'' \delta u_2'' dz = \left[E_b I_y u_2'' \delta u_2' \right]_0^{L_b} - \left[\left(E_b I_y u_2'' \right)' \delta u_2 \right]_0^{L_b} + \int_0^{L_b} \left(E_b I_y u_2'' \right)'' \delta u_2 dz$$

$$\int_0^{L_b} G_b J_b \theta_2' \delta \theta_2' dz = \left[G_b J_b \theta_2' \delta \theta_2 \right]_0^{L_b} - \int_0^{L_b} \left(G_b J_b \theta_2' \right)' \delta \theta_2 dz \tag{5.C.3}$$

$$\int_0^{L_b} E_b C_w \theta_2'' \delta \theta_2'' dz = \left[E_b C_w \theta_2'' \delta \theta_2' \right]_0^{L_b} - \left[\left(E_b C_w \theta_2'' \right)' \delta \theta_2 \right]_0^{L_b} + \int_0^{L_b} \left(E_b C_w \theta_2'' \right)'' \delta \theta_2 dz$$

$$\int_0^{L_b} M \theta_2 \delta u_2'' dz = \left[M \theta_2 \delta u_2' \right]_0^{L_b} - \left[\left(M \theta_2 \right)' \delta u_2 \right]_0^{L_b} + \int_0^{L_b} \left(M \theta_2 \right)'' \delta u_2 dz$$

From Eqs. (5.C.2),(5.C.3), by substituting into Eq. (5.C.1), one recovers the equilibrium equations

$$E_b C_w \theta_1^{IV} - G_b J_b \theta_1'' + \lambda \left(M u_1'' + q h \theta_1 \right) + \frac{E_d h_d^3}{6 L_d} \left(2\theta_1 + \theta_2 \right) + \frac{\bar{k} h_b}{2} \left[u_1 - u_2 + \frac{h_b}{2} \left(\theta_1 - \theta_2 \right) \right] = 0$$

$$E_b I_y u_1^{IV} + \lambda M \theta_1'' + \frac{\bar{k}}{2} \left[2u_1 - 2u_2 + h_b \left(\theta_1 - \theta_2 \right) \right] = 0$$

$$E_b C_w \theta_2^{IV} - G_b J_b \theta_2'' + \lambda \left(M u_2'' + q h \theta_2 \right) + \frac{E_d h_d^3}{6 L_d} \left(\theta_1 + 2\theta_2 \right) - \frac{\bar{k} h_b}{2} \left[u_1 - u_2 + \frac{h_b}{2} \left(\theta_1 - \theta_2 \right) \right] = 0$$

$$E_b I_y u_2^{IV} + \lambda M \theta_2'' - \frac{\bar{k}}{2} \left[2u_1 - 2u_2 + h_b \left(\theta_1 - \theta_2 \right) \right] = 0 \tag{5.C.4}$$

and the boundary conditions are

$$\left.\begin{array}{ll} \left[\left(E_b I_y u_1''' + \lambda M \theta_1' \right) \delta u_1 \right]_0^{L_b} = 0 & \left[\left(E_b I_y u_2''' + \lambda M \theta_2' \right) \delta u_2 \right]_0^{L_b} = 0 \\ \left[\left(E_b I_y u_1'' + \lambda M \theta_1 \right) \delta u_1' \right]_0^{L_b} = 0 & \left[\left(E_b I_y u_2'' + \lambda M \theta_2 \right) \delta u_2' \right]_0^{L_b} = 0 \\ \left[\left(G_b J_b \theta_1' - E_b C_w \theta_1''' \right) \delta \theta_1 \right]_0^{L_b} = 0 & \left[\left(G_b J_b \theta_2' - E_b C_w \theta_2''' \right) \delta \theta_2 \right]_0^{L_b} = 0 \\ \left[E_b C_w \theta_1'' \delta \theta_1' \right]_0^{L_b} = 0 & \left[E_b C_w \theta_2'' \delta \theta_2' \right]_0^{L_b} = 0 \end{array}\right\} \text{at } z = 0,\ l \tag{5.C.5}$$

Appendix 5D Derivation of the Critical Load for Simply-supported Beams under Non-uniform Moments

This appendix shows the derivation of critical load for UDL and mid-span concentrated loads applied to twin beams.

Case 1: Uniformly distributed load

For reference UDL q, the strong-axis moment distribution is $M = q\left(L_b z - z^2\right)/2$. From Eq. (5.19), by substituting M and applying the principle of stationary potential energy $\partial\pi/\partial A_1' = \partial\pi/\partial A_2' = \partial\pi/\partial B_1' = \partial\pi/\partial B_2' = 0$, one obtains

$$\begin{aligned}
\delta\Pi = {} & \delta A_1'\left\{E_b I_y A_1' l_n^{\,4} - \frac{\lambda q B_1'\left(n^2\pi^2+3\right)}{12} + \frac{\bar{k}}{2}\left[2\left(A_1'-A_2'\right)+h_b\left(B_1'-B_2'\right)\right]\right\} \\
& + \delta B_1'\left\{E_b C_w B_1' l_n^{\,4} + G_b J_b B_1' l_n^{\,2} - \frac{\lambda q A_1'\left(n^2\pi^2+3\right)}{12} + \lambda q h B_1' + \frac{E_d h_d^{\,3}}{6L_d}\left(2B_1'+B_2'\right)\right. \\
& \left. + \frac{\bar{k}}{2}\left[h_b\left(A_1'-A_2'\right) + \frac{h_b^{\,2}\left(B_1'-B_2'\right)}{2}\right]\right\} \\
& + \delta A_2'\left\{E_b I_y A_2' l_n^{\,4} - \frac{\lambda q B_2'\left(n^2\pi^2+3\right)}{12} + \frac{\bar{k}}{2}\left[2\left(A_2'-A_1'\right)+h_b\left(B_2'-B_1'\right)\right]\right\} \\
& + \delta B_2'\left\{E_b C_w B_2' l_n^{\,4} + G_b J_b B_2' l_n^{\,2} - \frac{\lambda q A_2'\left(n^2\pi^2+3\right)}{12} + \lambda q h B_2' + \frac{E_d h_d^{\,3}}{6L_d}\left(2B_2'+B_1'\right)\right. \\
& \left. + \frac{\bar{k}}{2}\left[h_b\left(A_2'-A_1'\right) + \frac{h_b^{\,2}\left(B_2'-B_1'\right)}{2}\right]\right\} \\
= {} & 0
\end{aligned} \tag{5.D.1}$$

which leads to

$$\begin{bmatrix}
E_b I_y l_n^{\,4} + \bar{k} & \alpha_n & -\bar{k} & -\frac{\bar{k}h_b}{2} \\
\alpha_n & \psi_n + \frac{\bar{k}h_b^{\,2}}{4} + \lambda q h & -\frac{\bar{k}h_b}{2} & \frac{E_d h_d^{\,3}}{6L_d} - \frac{\bar{k}h_b^{\,2}}{4} \\
-\bar{k} & -\frac{\bar{k}h_b}{2} & E_b I_y l_n^{\,4} + \bar{k} & \alpha_n \\
-\frac{\bar{k}h_b}{2} & \frac{E_d h_d^{\,3}}{6L_d} - \frac{\bar{k}h_b^{\,2}}{4} & \alpha_n & \psi_n + \frac{\bar{k}h_b^{\,2}}{4} + \lambda q h
\end{bmatrix}
\begin{Bmatrix} A_1' \\ B_1' \\ A_2' \\ B_2' \end{Bmatrix}_n
= \begin{Bmatrix} 0 \\ 0 \\ 0 \\ 0 \end{Bmatrix} \tag{5.D.2}$$

where $\alpha_n = -\lambda q\left(n^2\pi^2+3\right)/12 + \bar{k}h_b/2$ and $\psi_n = E_b C_w l_n^{\,4} + G_b J_b l_n^{\,2} + E_d h_d^{\,3}/3L_d$ has been previously defined.

Case 2: Mid-span concentrated loads

For the reference mid-span concentrated loads P, the strong-axis moment distribution is $M = 1/2Pz \quad (0 \le z < L_b/2)$ and $M = P(L_b - z)/2 \quad (L_b/2 \le z < L_b)$. From Eq. (5.19), by Substituting M and applying the principle of stationary potential energy, one obtains

$$\begin{aligned}
\delta\Pi = {} & \delta A_1' \left\{ E_b I_y A_1' l_n^{\,4} - \frac{\lambda P B_1' \left(4 + n^2\pi^2\right)}{8L_b} + \frac{\bar{k}}{2}\left[2\left(A_1' - A_2'\right) + h_b\left(B_1' - B_2'\right)\right] \right\} \\
& + \delta B_1' \left\{ E_b C_w B_1' l_n^{\,4} + G_b J_b B_1' l_n^{\,2} - \frac{\lambda P A_1' \left(4 + n^2\pi^2\right)}{8L_b} + \frac{2\lambda P h B_1'}{L_b} \right. \\
& \left. + \frac{E_d h_d^{\,3}}{6L_d}\left(2B_1' + B_2'\right) + \frac{\bar{k}}{2b}\left[h_b\left(A_1' - A_2'\right) + \frac{h_b^{\,2}\left(B_1' - B_2'\right)}{2} \right] \right\} \\
& \delta A_2' \left\{ E_b I_y A_2' l_n^{\,4} - \frac{\lambda P B_2' \left(4 + n^2\pi^2\right)}{8L_b} + \frac{\bar{k}}{2b}\left[2\left(A_2' - A_1'\right) + h_b\left(B_2' - B_1'\right)\right] \right\} \\
& + \delta B_2' \left\{ E_b C_w B_2' l_n^{\,4} + G_b J_b B_2' l_n^{\,2} - \frac{\lambda P A_2' \left(4 + n^2\pi^2\right)}{8L_b} + \frac{2\lambda P h B_2'}{L_b} \right. \\
& \left. + \frac{E_d h_d^{\,3}}{6L_d}\left(2B_2' + B_1'\right) + \frac{\bar{k}}{2b}\left[h_b\left(A_2' - A_1'\right) + \frac{h_b^{\,2}\left(B_2' - B_1'\right)}{2} \right] \right\} \\
= {} & 0
\end{aligned} \tag{5.D.3}$$

which leads to

$$\begin{bmatrix}
E_b I_y l_n^{\,4} + \bar{k} & \beta_n & -\bar{k} & -\frac{\bar{k} h_b}{2} \\
\beta_n & \psi_n + \frac{2\lambda P h}{L_b} + \frac{\bar{k} h_b^{\,2}}{4} & -\frac{\bar{k} h_b}{2} & \frac{E_d h_d^{\,3}}{6L_d} - \frac{\bar{k} h_b^{\,2}}{4} \\
-\bar{k} & -\frac{\bar{k} h_b}{2} & E_b I_y l_n^{\,4} + \bar{k} & \beta_n \\
-\frac{\bar{k} h_b}{2} & \frac{E_d h_d^{\,3}}{6L_d} - \frac{\bar{k} h_b^{\,2}}{4} & \beta_n & \psi_n + \frac{2\lambda P h}{L_b} + \frac{\bar{k} h_b^{\,2}}{4}
\end{bmatrix}
\begin{Bmatrix} A_1' \\ B_1' \\ A_2' \\ B_2' \end{Bmatrix}_n
= \begin{Bmatrix} 0 \\ 0 \\ 0 \\ 0 \end{Bmatrix} \tag{5.D.4}$$

where $\beta_n = -\lambda P\left(4 + n^2\pi^2\right)/8L_b + \bar{k} h_b/2$ and $\psi_n = E_b C_w l_n^{\,4} + G_b J_b l_n^{\,2} + E_d h_d^{\,3}/3L_d$ has been previously defined. .

For non-trivial solution in Eqs. (5.D.2),(5.D.4), the determinant should vanish, resulting in four roots in each case. Among the roots obtained in each case, the lowest positive value is the critical downward load and the highest negative value is the critical upward load.

Appendix 5E Expressions for Submatrices in Elastic and Geometric Stiffness Matrices

This appendix provides the expressions for submatrices $[B_1]$, $[B_2]$, $[B_3]$, $[B_4]$, $[B_5]$ introduced after Eq. (5.21)

$$[B_1]=\int_0^l \{L''(z)\}_{4\times1}\langle L''(z)\rangle_{1\times4}^T dz=\frac{1}{l^3}\begin{bmatrix}12 & 6l & -12 & 6l\\ 6l & 4l^2 & -6L & 2l^2\\ -12 & -6l & 12 & -6l\\ 6l & 2l^2 & -6l & 4l^2\end{bmatrix},$$

$$[B_2]=\int_0^l \{L'(z)\}_{4\times1}\langle L'(z)\rangle_{1\times4}^T dz=\frac{1}{30l}\begin{bmatrix}36 & 3l & -36 & 3l\\ 3l & 4l^2 & -3l & -l^2\\ -36 & -3l & 36 & -3l\\ 3l & -l^2 & -3l & 4l^2\end{bmatrix},$$

$$[B_3]=\int_0^l \{L(z)\}_{4\times1}\langle L(z)\rangle_{1\times4}^T dz=\frac{l}{420}\begin{bmatrix}156 & 22l & 54 & -13l\\ 22l & 4l^2 & 13l & -3l^2\\ 54 & 13l & 156 & -22l\\ -13l & -3l^2 & -22l & 4l^2\end{bmatrix},$$

$$[B_4]=\int_0^l M(z)\{L(z)\}_{4\times1}\langle L''(z)\rangle_{1\times4}^T dz,\quad [B_5]=\int_0^l q(z)\{L(z)\}_{4\times1}\langle L(z)\rangle_{1\times4}^T dz \tag{5.E.1}$$

For a beam element where the moment distribution along the element span $M(z)$ is linearly interpolated, i.e.,

$$M(z)=-M_0\left(1-\frac{z}{l}\right)+M_l\left(\frac{z}{l}\right) \tag{5.E.2}$$

where M_0 and M_l are the nodal moments obtained from the pre-buckling analysis. Figure 5.E.1 shows the positive sign convention for end moments.

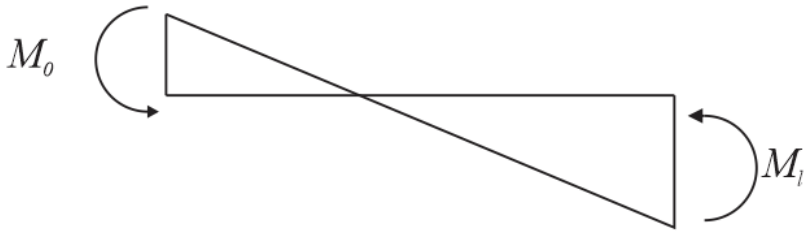

Figure 5.E.1 Sign convention for end moments

From Eq. (5.E.2), by substituting into Eq. (5.E.1), one obtains matrix $[B_4]$ as

$$[B_4] = \frac{1}{30l}\left[\begin{array}{c|c|c|c} 33M_0 - 3M_l & (27M_0 - 6M_l)l & -33M_0 + 3M_l & (6M_0 + 3M_l)l \\ \hline 3M_0 l & (3M_0 - M_l)l^2 & -3M_0 l & M_l l^2 \\ \hline -3M_0 + 33M_l & (3M_0 + 6M_l)l & 3M_0 - 33M_l & (-6M_0 + 27M_l)l \\ \hline -3M(l)l & -M_0 l^2 & 3M_l l & (M_0 - 3M_l)l^2 \end{array}\right]$$

(5.E.3)

Appendix 5F Relationship between the Number of Beam Elements and the Relative Lateral Stiffness per Unit Deck Width

The relative lateral stiffness per unit deck width $\overline{k}$ is a function of deck width b which is determined by the beam span and the number of elements used in the finite element analysis. For the reference twin-beam-deck system, the $\overline{k}$ values corresponding to various meshes are shown in Table 5.F.1. The table shows that $\overline{k}$ is sensitive to the number of elements per beam, which suggests that a different mesh could possibly yield a different critical moment. However, as suggested in Figure 5.4a, the critical moment remains at a constant value when the stiffness is beyond 45 kN/m/m. Since $\overline{k}$ for various meshes far exceeds the threshold value of 45 kN/m/m, the critical moment is not sensitive to model discretization.

Table 5.F.1 Relative lateral stiffness per unit deck width for various model discretizations

Number of elements per beam	Relative lateral stiffness per unit deck width (kN/m/m)
5	1.05×10^3
10	3.87×10^3
15	5.57×10^3
20	7.15×10^3
25	8.61×10^3
30	9.97×10^3
35	11.2×10^3
40	12.4×10^3

List of Symbols

A, B, C, D	nodes located at beams upside or deck underside;
A_i, A_i'	amplitudes of lateral displacement functions;
B_i, B_i'	amplitudes of the angle of twist functions;
$[B_1], [B_2], [B_3], [B_4], [B_5]$	submatrices of the elastic and geometric stiffness matrices;
b	deck board width;
C_w	warping constant;
d_F	nail diameter;
E_b, E_d	modulus of elasticity of beam and deck, respectively;
F	lateral load at the beam-deck intersection;
F_u	lateral strength resistance;
G_b	shear modulus of the beam;
h	distance between loading point and beam shear center;
h_b, h_d	depth of beam and deck, respectively;
I_d	moment of inertia of a deck board in the strong-axis;
I_y	moment of inertia about beam weak-axis;
J_b	beam Saint-Venant torsional constant;
K_m	service creep factor accounting for load duration and moisture level;
$[K_b]$	beam stiffness matrix;
$[K_e]$	elastic stiffness matrix;
$[K_g]$	geometric stiffness matrix;
$[K_l]$	stiffness matrix for the relative lateral restraint;
$[K_t]$	stiffness matrix for the twisting restraint;
k	relative lateral stiffness;
$\bar{k}$	relative lateral stiffness per unit deck width;
k_d	axial stiffness of deck board at the height of beam top;

k_j shear stiffness at the beam-deck joint;

k_n shear stiffness of a single-nail joint;

L_b, L_d beam and deck span, respectively;

$\langle L(z) \rangle^T$ Hermitian polynomials;

l element length;

l_n constant;

M reference strong-axis moment;

M_0 deck strong-axis moment under unit eccentric lateral loads;

M_{cr} critical moment

M_d deck strong-axis moment under eccentric lateral loads;

M_{e1}, M_{e2} deck board end moments;

n integer;

$\overline{n}$ number of nails at each joint;

P reference concentrated load;

$q(z)$ reference transverse load;

U internal strain energy;

U_{bi} internal strain energy in beam i;

U_l internal strain energy for the relative partial lateral restraint;

U_t internal strain energy for the partial twisting restraint;

U_l^* internal strain energy for the relative partial lateral restraint in one deck board;

U_t^* internal strain energy for the partial twisting restraint in one deck board;

u_A, u_C lateral displacements for nodes A and C, respectively;

u_i lateral displacement of beam i;

$\langle u_i \rangle$ generalized nodal lateral displacement vector;

V load potential energy;

V_{bi} load potential energy for beam i;

$v_p(z)$	prebuckling vertical displacement;
x, y, z	Cartesian coordinates;
z_0	distance from a given deck board to beam end-support;
Δ	deck lateral deformation;
Δ_1	deck axial deformation;
Δ_2	deck axial deformation due to transverse bending;
Δ_n	joint deformation of a single-nail joint;
θ_i	angle of twist of beam i;
$\langle \theta_i \rangle$	generalized nodal angel of twist vector;
λ	load multiplication factor;
Π	total potential energy.

References

[1] *ABAQUS 6.12-3* [Computer software]. Providence, RI, Dassault Systèmes Simulia.

[2] Albert, C., and Dawe, J. (1990). "Buckling of continuous steel girders with flange restraint." *Can. J. Civ. Eng.,* 17(2), 121-128.

[3] American Wood Council. (2015). "National Design Specification for Wood Construction." *ANSI/AWC NDS-2015,* Virginia, U.S.

[4] Apparao, T. V. S. R. (1968). "Problems in structural diaphragm bracing." *Report No. 331*, *Dept. of Struct. Engrg.,* Cornell Univ., Ithaca, N.Y.

[5] Assadi, M., and Roeder, C. W. (1985). "Stability of continuously restrained cantilevers." *J. Eng. Mech.,* 111(12), 1440-1456.

[6] Basaglia, C., Camotim, D., Gonçalves, R., and Graça, A. (2013). "GBT-based assessment of the buckling behaviour of cold-formed steel purlins restrained by sheeting." *Thin-Walled Struct.,* 72, 217-229.

[7] Canadian Standard Association (CSA). (2014). "Engineering design in wood." *O86-14,* Mississauga, Ontario, Canada.

[8] Chen, J. K., and Li L. Y. (2010). "Distortional buckling of cold-formed steel sections subjected to uniformly distributed transverse loading." *Int. J. Struct. Stab. Dy.,* 10(5), 1017–1030.

[9] Chu, X., Kettle, R., and Li, L. (2004). "Lateral-torsion buckling analysis of partial-laterally restrained thin-walled channel-section beams." *J. Constr. Steel Res.,* 60(8), 1159-1175.

[10] Chu, X., Rickard, J., and Li, L. (2005). "Influence of lateral restraint on lateral-torsional buckling of cold-formed steel purlins." *Thin-Walled Struct.,* 43(5), 800-810.

[11] Erki, M. (1991). "Modelling the load-slip behaviour of timber joints with mechanical fasteners." *Can. J. Civ. Eng.,* 18(4), 607-616.

[12] Errera, S. J., Pincus, G., and Fisher, G. P. (1967). "Columns and beams braced by diaphragms." *J. Struct. Div.,* 93(1), 295-318.

[13] Errera, S. J., and Apparao, T. (1976). "Design of I-shaped beams with diaphragm bracing. " *J. Struct. Div.*, 102(4), 769–781.

[14] Forest Products Laboratory (FPL). (2010). *Wood Handbook-Wood as an Engineering Material*. Madison, U.S.

[15] Foschi, R. O. (1974). "Load-slip characteristics of nails." *Wood Sci,* 7(1), 69-76.

[16] Hancock, G. J., and Trahair, N. S. (1978). "Finite element analysis of the lateral buckling of continuously restrained beam-columns." *Civ. Engrg. Trans*., Institution of Engineers, Australia, CE20, 120-127.

[17] Heine, C. P., and Dolan, J. D. (2001). "A new model to predict the load-slip relationship of bolted connections in timber." *Wood Fiber Sci.,* 33(4), 534-549.

[18] Helwig, T. A., and Frank, K. H. (1999). "Stiffness requirements for diaphragm bracing of beams." *J. Struct. Eng.,* 125(11), 1249-1256.

[19] Helwig, T. A., and Yura, J. A. (2008a). "Shear diaphragm bracing of beams. I: Stiffness and strength behavior." *J. Struct. Eng.,* 134(3), 348-356.

[20] Helwig, T. A., and Yura, J. A. (2008b). "Shear diaphragm bracing of beams. II: Design requirements." *J. Struct. Eng.,* 134(3), 357-363.

[21] Hunt, R. D., and Bryant, A. H. (1990). "Laterally loaded nail joints in wood." *J. Struct. Eng.,* 116(1), 111-124.

[22] Jenkinson, P. M., and Zahn, J. J. (1972). "Lateral stability of beam and deck structure." *J. Struct. Div.,* 98(3), 599-609.

[23] Jiang, C., and Davies J. M. (1997). "Design of thin-walled purlins for distortional buckling." *Thin-Walled Struct.,* 29(1–4), 189–202.

[24] Johansen, K. W. (1949). "Theory of timber connections." *Publ. Int. Assoc. Bridge Struct. Eng.,* 9, 249–262.

[25] Kermani, A., and Goh, H. (1999). "Load-Slip characteristics of multi-nailed timber joints." *Proc. Inst. Civ. Eng., Struct. Build.,* 134(1), 31-43.

[26] Khelil, A., and Larue, B. (2008). "Simple solutions for the flexural-torsional buckling of laterally restrained I-beams." *Eng. Struct.,* 30(10), 2923-2934.

[27] Kuenzi, E. W. (1951). "Theoretical design of a nailed or bolted joint under lateral load." *Rep. Forest Products Lab., No. D1951,* Forest Products Lab., Madison, Wis.

[28] Lawson, R., and Nethercot, D. (1985). "Lateral stability of I-beams restrained by profiled sheeting." *The Struct. Engr*., London, 63B(1), 3–13.

[29] Li, L. (2004). "Lateral–torsional buckling of cold-formed zed-purlins partial-laterally restrained by metal sheeting." *Thin-Walled Struct.,* 42(7), 995-1011.

[30] Lucas, R., Al-Bermani, F., and Kitipomchai, S. (1997a). "Modelling of cold-formed purlin-sheeting systems—Part 1: Full model." *Thin-Walled Struct.,* 27(3), 223-243.

[31] Lucas, R., Al-Bermani, F., and Kitipornchai, S. (1997b). "Modelling of cold-formed purlin-sheeting systems—Part 2. Simplified model." *Thin-Walled Struct.,* 27(4), 263-286.

[32] Mack, J. (1977). "The load-displacement curve for nailed joints." *J. Inst. Wood Sci.,* 7(6), 34–36.

[33] McLain, T. E. (1975). "Curvilinear load-slip relations in laterally loaded nailed joints." M.A.Sc. thesis, Colorado State Uni., Colorado, U.S.

[34] Morris, E., and Gajjar, S. (1981). "Load-displacement relationship for nailed joints with solid timber and plywood members." *J. Inst. Wood Sci.,* 9(2), 62-64.

[35] Nethercot, D. A., and Trahair, N. S. (1975). "Design of diaphragm-braced I-beams." *J. Struct. Div.,* 101(10), 2045-2061.

[36] Noren, B. (1962). "Nailed joints: A contribution to the theoretical analysis of yield and strength." *Proc. First Int. Symp. on Joints in Timber Engrg.,* 66-76.

[37] Peköz, T., and Soroushian, P. (1982). "Behaviour of C- and Z-purlins under wind uplift." *Proc., 6th Int. Specialty Conf. on Cold-Formed Steel Structures,* 409–429.

[38] Pellicane, P. (1991). "Mechanical behavior of nailed joints with various side member materials." *J. Test. Eval.,* 19(2), 97-106.

[39] Pincus, G., and Fisher, G. P. (1966). "Behavior of diaphragm-braced columns and beams." *J. Struct. Div.,* 92(2), 323-370.

[40] Sà Ribeiro, R. A., and Pellicane, P. J. (1992). "Modeling load-slip behavior of nailed joints." *J. Mater. Civ. Eng.,* 4(4), 385-398.

[41] Smith, I., Whale, L. R., Anderson, C., Hilson, B. O., and Rodd, P. D. (1988). "Design properties of laterally loaded nailed or bolted wood joints." *Can. J. Civ. Eng.,* 15(4), 633-643.

[42] Sokol L. (1996). "Stability of cold formed purlins braced by steel sheeting. " *Thin-Walled Struct.,* 25(4),247–268.

[43] Taylor, A. C., and Ojalvo, M. (1966). "Torsional restraint of lateral buckling." *J. Struct. Div.,* 92(2), 115-130.

[44] Timoshenko, S.P., and Gere, J. M. (1961). *Theory of elastic stability*, 2nd ed. New York: McGraw-Hill.

[45] Trahair, N. S. (1979). "Elastic lateral buckling of continuously restrained beam columns." *The profession of a civil engineer*, D. Campbell-Allen and E. H. Davis, eds., Sydney University Press, Sydney, Australia, 61–73.

[46] Trahair, N. S., and Nethercot, D. A. (1984). “Bracing requirements in thin-walled structures.” Chapter 3, *Developments in thin-walled structures,* J. Rhodes and A. C. Walker, eds., Vol. 2, Elsevier Applied Science Publishers, London, 93–130.

[47] Trahair, N.S. (1993). *Flexural-Torsional Buckling of Structures*. E & FN Spon, London.

[48] Vlasov, V. Z. (1961). *Thin-walled elastic beams*. 2nd. ed., Israel Program for Scientific Translations, Jerusalem.

[49] Ye, Z., Kettle, R. J., Li, L., and Schafer, B. W. (2002). "Buckling behavior of cold-formed zed-purlins partially restrained by steel sheeting." *Thin-Walled Struct.,* 40(10), 853-864.

[50] Zahn, J. (1965). "Lateral stability of deep beams with shear-beam support." *U.S.D.A. Forest Service Research Paper FPL 43.*

[51] Zahn, J. (1972). "Shear stiffness of two-inch wood decks for roof systems." *U.S.D.A. Forest Service Research Paper FPL 155.*

[52] Zahn, J. J. (1973). "Lateral stability of wood beam-and-deck systems." *J. Struct. Div.,* 99(7), 1391-1408.

CHAPTER 6:SUMMARY AND CONCLUSIONS

6.1 Summary

1. A comparative study between the two ABAQUS models was conducted to investigate the behavior differences between the non-sway and sway models.
2. Two sets of models were then developed for the lateral torsional buckling analysis of wooden twin-beam-deck assemblies. In the first model, the deck is assumed to provide full lateral restraint to the twin beams so as to prevent sway. Under this assumption, the lateral displacement at the section shear center was expressed in terms of the angle of twist. In the second model, the beams are allowed to sway laterally and the two displacement fields were assumed to be independent.
3. Within each set of models, the total potential energy was expressed and the stationarity conditions were evoked to formulate a series of analytical and numerical solutions. In the non-sway models, the following solutions were developed: (1) A closed-form solution for simply-supported beams under uniform moments, (2) an analytical solution for beams with arbitrary boundary conditions and subjected to uniform moments, (3) an energy-based approximate solution for simply-supported beams under non-uniform moments, and (4) a finite element solution capable of solving general boundary and loading conditions. In the sway model, solutions developed include: (1) A closed-form solution for simply-supported beams under uniform moments, (2) an energy-based approximate solution for simply-supported beams under non-uniform moments, and (3) a finite element solution. All solutions were compared against ABAQUS models for verification.
4. The solutions verified were then used to conduct parametric studies where the effects of beam and deck span, load type and height, lateral and twisting restraints, lateral restraint height and stiffness and continuous beams on the lateral torsional buckling capacity were assessed.

6.2 Conclusions

For wooden twin-beam-deck systems with practical dimensions and material properties, the following conclusions were made:

1. Only net uplift loads are found to induce lateral torsional buckling of non-sway twin-beam-deck assemblies while both gravity and wind uplift loads are associated with the lateral torsional buckling of the sway model.
2. The continuous bracing action of deck boards providing either partial or rigid lateral restraint as well as partial twisting restraint on either the compression or tension side of the beams is found to significantly increase the lateral torsional buckling capacity of twin-beam-deck assemblies.
3. For the case of wind uplift, the non-sway model consistently predicts higher critical moments than those based on the sway model. Large differences in capacities are observed for twin-beam-deck systems with long beam span or short deck span.
4. Compared with laterally and torsionally unrestrained beams, the buckling capacity increases in both models is largely attributed to the deck bending action. In the sway model, the presence of relative partial lateral restraint alone provides no buckling capacity increase for equally loaded beams.
5. For twin-beam-deck systems under uplift, the non-sway model shows no clear trend between the buckling capacity and beam span while the sway model suggests a downward trend. For the case of gravity loads, the buckling capacity predicted by the sway model remains essentially constant irrespective of the beam span.
6. As the deck span is increased, both models predict a significant decline in buckling resistance.
7. The load position greatly influences the buckling capacity for systems involving *short span* beams or *long span* decks. The load position effect is also observed to be more substantial in the non-sway model. Due to the load position effect, the buckling capacity under wind uplift acting at the beam top can be higher than that based on gravity loads acting at the same location.
8. In the non-sway model, the lateral restraint height is observed to have a significant impact on the buckling capacity. In the sway model, the lateral restraint height has no effect on the buckling capacity when the relative stiffness exceeds the threshold stiffness.

9. For the sway model, the lateral stiffness of the deck-joint assembly with two nails at each joint is shown to provide enough lateral stiffness to develop the maximal lateral torsional buckling capacity.
10. The buckling capacity for twin-beam-deck systems with continuous beams is slightly higher than that of a single-span system with the same span.

6.3 Recommendations for Future Research

Possible extensions of the present study are:

1. Developing analytical and numerical models that incorporate the effects of shear deformation and cross-section distortion of wooden beams.
2. Developing models which incorporate the effects of beam initial imperfections.
3. Developing more detailed shell-based or 3D finite element models.
4. Conducting full scale lateral torsional buckling test of beam-deck assemblies.

Appendix A MATLAB PROGRAMME FOR THE NON-SWAY MODEL

Input Data

All the parameters required for the twin-beam-deck assemblies are inputted in a Microsoft Excel spreadsheet with separate worksheets recording data relate to node coordinates, element, cross-section, material properties, load information and boundary conditions. A sample input for a twin-beam-deck assembly with 6 m beam span and 2 m deck span under UDL applied at deck centerline is shown below.

Node info:

Number of beam nodes	14	
Node number	*x*-coordinate (m)	*z*-coordinate (m)
1	0.0	0.0
2	0.0	1.0
3	0.0	2.0
4	0.0	3.0
5	0.0	4.0
6	0.0	5.0
7	0.0	6.0
8	2.0	0.0
9	2.0	1.0
10	2.0	2.0
11	2.0	3.0
12	2.0	4.0
13	2.0	5.0
14	2.0	6.0

Element info:

Number of beam elements	12	
Number of deck elements	6	
Beam element number	Material type	Cross-section type
1	1	1
2	1	1
3	1	1
4	1	1
5	1	1
6	1	1
7	1	1
8	1	1
9	1	1
10	1	1
11	1	1
12	1	1

Deck element number	Material type	Cross-section type	Deck connectivity			
			1st joint	2nd joint	3rd joint	4th joint
1	1	1	1	2	8	9
2	1	1	2	3	9	10
3	1	1	3	4	10	11
4	1	1	4	5	11	12
5	1	1	5	6	12	13
6	1	1	6	7	13	14

Cross-section info:

Number of section types	1									
Section type	I_{wyy} (m^4)	I_{www} (m^4)	J_w (m^4)	I_{wxx} (m^4)	I_{fyy} (m^4)	I_{fww} (m^4)	J_f (m^4)	I_{fxx} (m^4)	a (m)	h_d (m)
1	0	0	0	0	2.4E-05	6.6E-07	8.9E-05	1.2E-03	0.304	0.038

Material info:

Number of material types	1				
Material type	E_w (Pa)	G_w (Pa)	E_f (Pa)	G_f (Pa)	E_d (Pa)
1	0	0	1.03E+10	4.74E+08	1.00E+10

Load info:

Beam number	Number of UDL	Starting point (m)	Ending point (m)	Magnitude (N/m)	Load height (m)
1	1	0	6	1	0
2	1	0	6	1	0

Boundary conditions:

Number of pre-buckling boundary con.	4
Number of buckling boundary con.	4

Pre-buckling boundary con.	DOFs restrained
1	1
2	13
3	15
4	27

Buckling boundary conditions	DOFs restrained
1	1
2	21
3	23
4	43

Programme Developed in Matlab

```
% 1. READ NODE INFO
[nm,nn]=readnodecoordinate();
```

```
% Subroutine
function[nm,nn]=readnodecoordinate()
% Extract node info from Excel
[num]=xlsread('input','Nodes');
nn=num(1,2); % Number of nodes forming twin beams:
% Build node matrix “nm” to store the coordinate info
for i=1:nn
nm(i,1)=num(3+i,1); % Node number stored in the first column of matrix “nm”
nm(i,2)=num(3+i,2); % First coordinate stored in the second column of matrix “nm”
nm(i,3)=num(3+i,3); % Second coordinate stored in the third column of matrix “nm”
end
```

```
% 2. READ BEAM MATERIAL INFO
bmm=readbeammaterial();
```

```
% Subroutine
function[bmm]=readbeammaterial()
% Extract beam material properties from Excel
[num]=xlsread('input','Materials');
tn=num(1,2); % Number of material types
% Build beam material matrix “bmm” for storing material info for each material type
for i=1:tn
bmm(1,i)=num(3+i,2);   % Store the modulus of elasticity of the web
bmm(2,i)=num(3+i,3);   % Store the shear modulus of the web
bmm(3,i)=num(3+i,4);   % Store the modulus of elasticity of the flanges
bmm(4,i)=num(3+i,5);   % Store the shear modulus of the flanges
end
```

```
% 3. READ DECK MATERIAL INFO
dmm=readdeckmaterial();
```

```
% Subroutine
function[dmm]=readdeckmaterial()
% Extract deck material properties from Excel
[num]=xlsread('input','Materials');
tn=num(1,2); % Number of deck material types:
% Build deck material matrix “dmm” for storing material info for every material type
```

```
for i=1:tn
dmm(1,i)=num(3+i,6);   % Store the modulus of elasticity
end
```

% 4. READ BEAM CROSS-SECTION PROPERTIES

```
bcm=readbeamcs();
```

```
% Subroutine
function[bcm]=readbeamcs()
% Extract beam cross-section info from Excel
[num]=xlsread('input','Cross-section');
cn=num(1,2);   % Number of cross-section types:
% Build beam cross-section matrix "bcm" for info related to every cross-section type
for i=1:cn
bcm(1,i)=num(3+i,2); % Store I_wyy
bcm(2,i)=num(3+i,3); % Store I_wωω
bcm(3,i)=num(3+i,4); % Store J_w
bcm(4,i)=num(3+i,5); % Store I_wxx
bcm(5,i)=num(3+i,6); % Store I_fyy
bcm(6,i)=num(3+i,7); % Store I_fωω
bcm(7,i)=num(3+i,8); % Store J_f
bcm(8,i)=num(3+i,9); % Store I_fxx
bcm(9,i)=num(3+i,10); % Store the distance between beam shear center and deck center
end
```

% 5. READ DECK CROSS-SECTION INFO

```
dcm=readdeckcs();
```

```
% Subroutine
function[dcm]=readdeckcs()
% Extract deck cross-section info from Excel
[num]=xlsread('input','Cross-section');
cn=num(1,2); % Number of cross-section types
% Build deck cross-section matrix "dcm" storing section info for every cross-section type
for i=1:cn
dcm(1,i)=num(3+i,11); % Store deck thickness
end
```

% 6 READ BEAM ELEMENT DATA

```
% 6.1 Count the number of beam elements in each beam
[nm2,en]=callbeamelnumber(nm,nn);
```

```
% Subroutine
function[nm2,en]=callbeamelnumber(nm,nn)
% Extract the first coordinate of beam nodes from node matrix “nm”
nm1=nm(:,2);
% Create a virtual point following the end of matrix “nm1”
nm2=[nm1;-1];
% Count the number of elements in each beam
en=0;
for i=1:nn
if nm2(i,1)==nm2(i+1,1)
en=en+1;
else
en=en;
end
end
```

```
% 6.2 Call beam element connectivity matrix
[bel]=callbeamconnect(en,nm2);
```

```
% Subroutine
function[bel]=callbeamconnect(en,nm2)
aa=0;
for i=1:en
if nm2(i+aa)==nm2(i+aa+1)
bel{i}=[i+aa,i+aa+1];
else
aa=aa+1;
bel{i}=[i+aa,i+aa+1];
end
end
```

```
% 6.3 CALL BEAM ELEMENT MATERIAL AND CROSS-SECTION PROPERTIES
[belm,belc]=cbeamelmcs(en,bmm,bcm);
```

```
% Subroutine
function[belm,belc]=cbeamelmcs(en,bmm,bcm)
% Extract beam element info from Excel
[num]=xlsread('input','Element');
% Form beam element matrix “bemc” (containing info regarding element number, material
```

```
type and cross-section type)
for i=1:en
bemc(i,1)=num(3+i,1);   % Store beam element number
bemc(i,2)=num(3+i,2);   % Store beam element material type
bemc(i,3)=num(3+i,3);   % Store beam element cross-section type
end
% Store the element material type in vector “belm” and cross-section type in vector “belc”
for i=1:en
bmt=bemc(i,2);     % Beam material type vector
bct=bemc(i,3); % Beam cross-section type vector
belm{i}=bmm(:,bmt);   % Beam material type for element i
belc{i}=bcm(:,bct); % Beam cross-section type for element i
end


% 7 READ DECK ELEMENT DATA
% 7.1 Read deck connectivity vector
[del,dn]=rdeckconnect();
-----------------------------------------------------------------------------------------------------------
% Subroutine
function[del,dn]=rdeckconnect()
% Extract deck element info from Excel
[num]=xlsread('input','Element');
dn=num(2,2); % Number of deck elements
% Form deck connectivity vector “del” for deck element i
for i=1:dn
del{i}(1,1)=num(3+i,8);    % Node number for first point
del{i}(1,2)=num(3+i,9);    % Node number for second point
del{i}(1,3)=num(3+i,10);   % Node number for third point
del{i}(1,4)=num(3+i,11);   % Node number for forth point
end

% 7.2 Read deck element material and cross-section properties
[delm,delc]=rdeckmcs(dn,dmm,dcm);
-----------------------------------------------------------------------------------------------------------
% Subroutine
function[delm,delc]=rdeckmcs(dn,dmm,dcm)
% Extract deck element info from Excel
[num]=xlsread('input','Element');
% Form deck element matrix (containing info relate to element number, material and
cross-section types)
for i=1:dn
```

```
demc(i,1)=num(3+i,5);   % Store deck element number
demc(i,2)=num(3+i,6);   % Store deck element material type
demc(i,3)=num(3+i,7);   % Store deck element cross-section type
end
% Form deck element material vector “delm” and cross-section vector “delc” for element i
for i=1:dn
dmt=demc(i,2);      % Deck material type vector
dct=demc(i,3);      % Deck cross-section type vector
delm{i}=dmm(:,dmt);
     delc{i}=dcm(:,dct);
end
```

% 8. CALL TRANSFORMED MATERIAL AND CROSS-SECTION PROPERTIES

```
[Eb,Gb,J,Ib,C,a]=ctransmcs(belm,belc,en);
```

```
% Subroutine
function[Eb,Gb,J,Ib,C,a]=ctransmcs(belm,belc,en)
% Store material and cross-section properties for beam element i
for i=1:en
Ew{i}=belm{i}(1,1);         % Modulus of elasticity of the web
Gw{i}=belm{i}(2,1);          % Shear modulus of the web
Ef{i}=belm{i}(3,1);          % Modulus of elasticity of the flanges
Gf{i}=belm{i}(4,1);          % Shear modulus of the flanges
n1{i}=Gw{i}/Gf{i};          % Ratio for shear modulus
n2{i}=Ew{i}/Ef{i};          % Ratio for modulus of elasticity
Eb{i}=Ef{i};          % Set the transformed modulus of elasticity to be that of the flanges
Gb{i}=Gf{i};       % Set the transformed shear modulus to be that of the flanges
Jw{i}=belc{i}(3,1);            % Saint-Venant torsional constant for the web
Iwyy{i}=belc{i}(1,1);         % Moment of inertia of the web aboutweak-axis
Iwww{i}=belc{i}(2,1);        % Warping constant of the web
Jf{i}=belc{i}(7,1);       % Saint-Venant torsional constant for the flanges
Ifyy{i}=belc{i}(5,1);          % moment of inertia of the flanges about weak-axis
Ifww{i}=belc{i}(6,1);       % warping constant of the flanges
a{i}=belc{i}(9,1);              % distance between beam shear center and deck centerline
J{i}=Jf{i}+n1{i}*Jw{i};    % Transformed Saint-Venant torsional constant
Ib{i}=Ifyy{i}+n2{i}*Iwyy{i}; % Transformed moment of inertia about beam weak-axis
Cw{i}=Ifww{i}+n2{i}*Iwww{i}; % Transformed warping constant
C{i}=Ib{i}*a{i}^2+Cw{i};         % Transformed constant C
End
```

% 9. PRE-BUCKLING ANALYSIS

% 9.1 Call the number of beams and the number of nodes in each beam

```
% 9.1.1 Call coordinates for beam node
[bncoordxp,bncoordyp]=cxycoorp(nn,nm);
-----------------------------------------------------------------------------------------------------------------
% Subroutine
function[bncoordxp,bncoordyp]=cxycoorp(nn,nm)
% Build beam node coordinate vectors
for i=1:nn
bncoordxp(nm(i,1),1)=nm(i,2);   % Beam x coordinate vector
bncoordyp(nm(i,1),1)=nm(i,3);   % Beam y coordinate vector
end

%9.1.2 Call the number of nodes in each beam
nnb=cnodenumberbeamip(bn,nn,nm2);
-----------------------------------------------------------------------------------------------------------------
% Subroutine
function[nnb]=cnodenumberbeamip(bn,nn,nm2)
% nnb{i+1} stores the number of nodes in beam i
qqq=1;
for i=2:bn+1
    nnb{i}=1;
    for j=qqq:nn
        if nm2(j,1)~=nm2(j+1,1)
            qqq=j+1;
            break
        else
            nnb{i}=nnb{i}+1;
        end
    end
end

% 9.2 Call pre-buckling elastic stiffness matrix and load vector
%9.2.1 Read the number of UDL applied to each beam
-----------------------------------------------------------------------------------------------------------------
% Extract load info from EXCEL
[num]=xlsread('input','Loading');
% Read the number of UDL applied to element i
for i=1:bn
    udln{i}=num(3,i);
end

%9.2.2 Read UDL magnitude and starting, ending coordinates
-----------------------------------------------------------------------------------------------------------------
```

```
for i=1:bn
for j=1:udln{i}
udl{i}{j}=num(6+j*3,i); % Magnitude of the j^th UDL applied to beam i
    udlcoor{i}{j}(1,1)=num(4+j*3,i);% Starting coordinate of the j^th UDL applied to beam i
udlcoor{i}{j}(1,2)=num(5+j*3,i); % Ending coordinate of the j^th UDL applied to beam i
    end
end
```

%9.2.3 Store UDL info

```
%9.2.3.1 Call the starting and ending coordinates of element i
j=0;
for i=1:en
if bncoordxp(i+j,1)==bncoordxp(i+j+1,1)
                eny{i}(1,1)=bncoordyp(i+j,1); % Starting coordinate of element i
eny{i}(1,2)=bncoordyp(i+j+1,1); % Ending coordinate of element i
    else
                eny{i}(1,1)=bncoordyp(i+j+1,1);
          eny{i}(1,2)=bncoordyp(i+j+2,1);
          j=j+1;
    end
end
%9.2.3.2 Call the beam number for element k
for k=1:en
    kk=0;
    for i=1:bn
        qq=nnb{i+1}-1;
        kk=qq+kk;
        if k<=kk
                            p{k}=i;       % Beam number for element k
        break
    end
    end
end
%9.2.3.3 Call the number of UDL applied to element i, and the starting and ending point of
UDL in each element, the magnitude of UDL
for i=1:en
    elb{i}=nm(bel{i}(1,2),3)-nm(bel{i}(1,1),3);      % Length of element i
end
for k=1:en
nudl{k}=0;
        for j=1:udln{p{k}}
```

```
if eny{k}(1,1)>=udlcoor{p{k}}{j}(1,1) &&
eny{k}(1,2)<= udlcoor{p{k}}{j}(1,2)
        % Number of UDL applied to element i
                nudl{k}=nudl{k}+1;
% Starting and ending points of the j^th udl applied to element i,
coord{k}{nudl{k}}(1,1)=0;                    coord{k}{nudl{k}}(1,2)=elb{k};
                u{k}{nudl{k}}=udl{p{k}}{j};
            elseif eny{k}(1,1)<udlcoor{p{k}}{j}(1,1)&&
                  eny{k}(1,2)<udlcoor{p{k}}{j}(1,2) &&
eny{k}(1,2)>udlcoor{p{k}}{j}(1,1)
                nudl{k}=nudl{k}+1;
                coord{k}{nudl{k}}(1,1)=udlcoor{p{k}}{j}(1,1)-eny{k}(1,1);
                coord{k}{nudl{k}}(1,2)=elb{k};
                u{k}{nudl{k}}=udl{p{k}}{j};
             elseif eny{k}(1,1)>udlcoor{p{k}}{j}(1,1) &&
eny{k}(1,2)>udlcoor{p{k}}{j}(1,2) &&
                eny{k}(1,1)<udlcoor{p{k}}{j}(1,2)
                nudl{k}=nudl{k}+1;
                coord{k}{nudl{k}}(1,1)=0;
                coord{k}{nudl{k}}(1,2)=udlcoor{p{k}}{j}(1,2)-eny{k}(1,1);
                u{k}{nudl{k}}=udl{p{k}}{j};
            elseif eny{k}(1,1)<=udlcoor{p{k}}{j}(1,1) &&
                  eny{k}(1,2)>=udlcoor{p{k}}{j}(1,2)
                     nudl{k}=nudl{k}+1;
                coord{k}{nudl{k}}(1,1)=udlcoor{p{k}}{j}(1,1)-eny{k}(1,1);
                coord{k}{nudl{k}}(1,2)=udlcoor{p{k}}{j}(1,2)-eny{k}(1,1);
                u{k}{nudl{k}}=udl{p{k}}{j};
          else
              nudl{k}=nudl{k}+0;
          end
      end
end
```

%9.2.4 Store concentrated load info

```
%9.2.4.1 Read the number of concentrated loads applied to beam element i
for i=1:bn
    cln{i}=num(4,i);
end
%9.2.4.2 Read concentrated load magnitude and the loading point
for i=1:bn
for j=1:cln{i}
```

```
cl{i}{j}=num(6+j*2,8+i); % Magnitude of the j^th concentrated load in beam i
clcoor{i}{j}(1,1)=num(5+j*2,8+i); % Loading point of the j^th concentrated load in beam i
    end
end
%9.2.4.3 Call the number of concentrated loads, the loading points, the load magnitude
for i=1:en
    elb{i}=nm(bel{i}(1,2),3)-nm(bel{i}(1,1),3); % Length of each beam element
end
for k=1:en
ncl{k}=0;
        for j=1:cln{p{k}}
            if eny{k}(1,1)<=clcoor{p{k}}{j}(1,1)&& eny{k}(1,2)>clcoor{p{k}}{j}(1,1)
                ncl{k}=ncl{k}+1;
                ccoord{k}{ncl{k}}(1,1)=clcoor{p{k}}{j}(1,1)-eny{k}(1,1);
                P{k}{ncl{k}}=cl{p{k}}{j};
            end
        end
end
```

%9.2.5 Call beam element pre-buckling stiffness matrix

```
%9.2.5.1 Call beam element pre-buckling local stiffness matrix
for i=1:en
elb{i}=nm(bel{i}(1,2),3)-nm(bel{i}(1,1),3);
% Beam element pre-buckling local stiffness matrix
    Kp{i}=Eb{i}*Ibx{i}/elb{i}^3*[12 6*elb{i} -12 6*elb{i};
          6*elb{i} 4*elb{i}^2 -6*elb{i} 2*elb{i}^2;
          -12 -6*elb{i} 12 -6*elb{i};
          6*elb{i} 2*elb{i}^2 -6*elb{i} 4*elb{i}^2];
end
%9.2.5.2 Call beam element prebuckling global stiffness matrix
%9.2.5.2.1 Call beam element global degree of freedoms (DoF)
for i=1:en
dbel{i}=[1+2*(bel{i}(1,1)-1),2+2*(bel{i}(1,1)-1),1+2*(bel{i}(1,2)-1),2+2*(bel{i}(1,2)-1)];
end
%9.2.5.2.2 Call beam element pre-buckling global stiffness matrix
Kpg=vpa(zeros(2*nn,2*nn));
for h=1:en
    for i=1:4
        for j=1:4
            Kpg(dbel{h}(1,i),dbel{h}(1,j))=Kp{h}(i,j)+Kpg(dbel{h}(1,i),dbel{h}(1,j));
        end
```

```
    end
end
```

%9.2.6 Call global load vector

```
%9.2.6.1 Call local load vector
syms x
%9.2.6.1.1 Local load vector for the reference UDL applied along the span of the beams
for i=1:en
    q{i}=0;
end
% Build local load vector for the reference UDL
for i=1:en
        L1{i}=1-3*x^2/elb{i}^2+2*x^3/elb{i}^3;
        L2{i}=x-2*x^2/elb{i}+x^3/elb{i}^2;
        L3{i}=3*x^2/elb{i}^2-2*x^3/elb{i}^3;
        L4{i}=x^3/elb{i}^2-x^2/elb{i};
        Ql{i}(1,1)=q{i}*int(L1{i},0,elb{i});
        Ql{i}(2,1)=q{i}*int(L2{i},0,elb{i});
        Ql{i}(3,1)=q{i}*int(L3{i},0,elb{i});
        Ql{i}(4,1)=q{i}*int(L4{i},0,elb{i});
end
%9.2.6.1.2 Build load vector for other UDL
%9.2.6.1.2.1 Count beam elements with at least one UDL applied
eel=0;
for i=1:en
if nudl{i}~=0
eel=eel+1; % Number of beam elements with at least one UDL applied
aa(eel,1)=i; % Vector storing the elements that are loaded
    end
end
%9.2.6.1.2.2 Build local load vector for these UDL
for i=1:en
    Qla{i}(1,1)=0;
    Qla{i}(2,1)=0;
    Qla{i}(3,1)=0;
    Qla{i}(4,1)=0;
end
for i=1:eel
    k=aa(i,1);
    for j=1:nudl{k}
        uu=u{k}{j};
```

```
        y1=coord{k}{j}(1,1);
        y2=coord{k}{j}(1,2);
        Qll{k}(1,1)=uu*int(L1{k},y1,y2);
        Qll{k}(2,1)=uu*int(L2{k},y1,y2);
        Qll{k}(3,1)=uu*int(L3{k},y1,y2);
        Qll{k}(4,1)=uu*int(L4{k},y1,y2);
Qla{k}(1,1)=Qla{k}(1,1)+Qll{k}(1,1);          Qla{k}(2,1)=Qla{k}(2,1)+Qll{k}(2,1);
        Qla{k}(3,1)=Qla{k}(3,1)+Qll{k}(3,1);
        Qla{k}(4,1)=Qla{k}(4,1)+Qll{k}(4,1);
    end
end
for i=1:en
   Qlf{i}(1,1)=Ql{i}(1,1)+Qla{i}(1,1);
   Qlf{i}(2,1)=Ql{i}(2,1)+Qla{i}(2,1);
   Qlf{i}(3,1)=Ql{i}(3,1)+Qla{i}(3,1);
   Qlf{i}(4,1)=Ql{i}(4,1)+Qla{i}(4,1);
end
%9.2.6.1.3 Build load vector for concentrated loads
%9.2.6.1.3.1 Count beam elements with at least one concentrated load applied
eel=0;
for i=1:en
if ncl{i}~=0
eel=eel+1; % Number of beam elements with at least one concentrated load applied
aa(eel,1)=i; % Vector storing the elements that are loaded
    end
end
for i=1:en
    Qla{i}(1,1)=0;
    Qla{i}(2,1)=0;
    Qla{i}(3,1)=0;
    Qla{i}(4,1)=0;
end
%9.2.6.1.3.2 Build local load vector for concentrated loads
for i=1:eel
    k=aa(i,1);
    for j=1:ncl{k}
        pp=P{k}{j};
        x=ccoord{k}{j}(1,1);
        L11{k}=1-3*x^2/elb{k}^2+2*x^3/elb{k}^3;
        L22{k}=x-2*x^2/elb{k}+x^3/elb{k}^2;
        L33{k}=3*x^2/elb{k}^2-2*x^3/elb{k}^3;
        L44{k}=x^3/elb{k}^2-x^2/elb{k};
```

```
        Qll{k}(1,1)=pp*L11{k};
        Qll{k}(2,1)=pp*L22{k};
        Qll{k}(3,1)=pp*L33{k};
        Qll{k}(4,1)=pp*L44{k};                    Qla{k}(1,1)=Qla{k}(1,1)+Qll{k}(1,1);
        Qla{k}(2,1)=Qla{k}(2,1)+Qll{k}(2,1);
        Qla{k}(3,1)=Qla{k}(3,1)+Qll{k}(3,1);
        Qla{k}(4,1)=Qla{k}(4,1)+Qll{k}(4,1);
    end
end
for i=1:en
   Qlf{i}(1,1)=Qlf{i}(1,1)+Qla{i}(1,1);
   Qlf{i}(2,1)=Qlf{i}(2,1)+Qla{i}(2,1);
   Qlf{i}(3,1)=Qlf{i}(3,1)+Qla{i}(3,1);
   Qlf{i}(4,1)=Qlf{i}(4,1)+Qla{i}(4,1);
end
%9.2.6.1.2 Build global load vector
Qg=vpa(zeros(2*nn,1));
for h=1:en
    for i=1:4
        Qg(dbel{h}(1,i),1)=Qlf{h}(i,1)+Qg(dbel{h}(1,i),1);
    end
end

%9.3 Enforce boundary conditions
[Kpge,Qge]=callboundaryconp(Kpg,Qg);
-------------------------------------------------------------------------------------------------------------
%Subroutine
function[Kpge,Qge]=callboundaryconp(Kpg,Qg)
% Extract boundary condition info from EXCEL
[num]=xlsread('input','Boundary condition');
bcn=num(1,2);   % Number of boundary conditions
for i=1:bcn
    dof(i,1)=num(3+i,2);   % Vector storing the DoF restrained
end
% Enforce boundary conditions
for i=1:bcn
Kpg(dof(i,1),:)=0;
Kpg(:,dof(i,1))=0;
Kpg(dof(i,1),dof(i,1))=1;
Qg(dof(i,1),:)=0;
end
Kpge=Kpg;
```

```
Qge=Qg;

%9.4 Recover moment in each beam node
[F]=callnodalforcep(Kpge,Qge,en,Kp,Qlf,bn,nnb);
-----------------------------------------------------------------------------------------------------------------
%Subroutine
function[F]=callnodalforcep(Kpge,Qge,en,Kp,Qlf,bn,nnb)
% Seperate Kpges,Qges for element i from Kpge and Qge
aa=0;
for i=1:bn
    aa=aa+nnb{i};
    Kpges{i}=Kpge(1+aa*2:aa*2+2*nnb{i+1},1+aa*2:aa*2+2*nnb{i+1});
    Qges{i}=Qge(1+aa*2:aa*2+2*nnb{i+1},1);
end
% Call global nodal displacement vector for each beam
for i=1:bn
    Vn{i}=inv(Kpges{i})*Qges{i};
end
% Call local force vector for each element
for i=1:bn
for j=1:nnb{i+1}-1
    % Separate displacement vector for the j^th element of beam i
        Vns{i}{j}=Vn{i}(1+2*(j-1):4+2*(j-1),1);
    end
end
for i=1:bn
    nnb{i+1}=nnb{i+1}-1;
end
aa=0;
for i=1:bn
    aa=aa+nnb{i};
    for j=1:nnb{i+1}
            h=aa+j;
            Vnsa{h}=Vns{i}{j};
    end
end
for i=1:en
    F{i}=Kp{i}*Vnsa{i}-Qlf{i};
end
for i=1:en
    M{i}{1}=-F{i}(2,1);
    M{i}{2}=-F{i}(4,1);
```

```
end
```

% 10. CALL LOCAL BEAM ELEMENT STIFFNESS MATRIX

```
[kkk]=xlsread('input','Loading');
Lh=kkk(24,1); % Load height relative to deck centerline
for i=1:en
elb{i}=nm(bel{i}(1,2),3)-nm(bel{i}(1,1),3); % Length of beam element i
% Submatrix B1
    B1{i}=1/elb{i}^3*[12 6*elb{i} -12 6*elb{i};
          6*elb{i} 4*elb{i}^2 -6*elb{i} 2*elb{i}^2;
          -12 -6*elb{i} 12 -6*elb{i};
          6*elb{i} 2*elb{i}^2 -6*elb{i} 4*elb{i}^2];
% Submatrix B2
    B2{i}=1/(30*elb{i})*[36 3*elb{i} -36 3*elb{i};
             3*elb{i} 4*elb{i}^2 -3*elb{i} -elb{i}^2;
             -36 -3*elb{i} 36 -3*elb{i};
             3*elb{i} -elb{i}^2 -3*elb{i} 4*elb{i}^2];
% Submatrix B3
    B3{i}=elb{i}/420*[156 22*elb{i} 54 -13*elb{i};
          22*elb{i} 4*elb{i}^2 13*elb{i} -3*elb{i}^2;
          54 13*elb{i} 156 -22*elb{i};
          -13*elb{i} -3*elb{i}^2 -22*elb{i} 4*elb{i}^2];
% Submatrix B4
B4{i}=[(11*M{i}{1}-M{i}{2})/(10*elb{i}), 9*M{i}{1}/10-M{i}{2}/5,
-(11*M{i}{1}-M{i}{2})/(10*elb{i}) M{i}{1}/5+M{i}{2}/10;
    M{i}{1}/10 elb{i}*(3*M{i}{1}-M{i}{2})/30 -M{i}{1}/10 elb{i}*M{i}{2}/30;
-(M{i}{1}-11*M{i}{2})/(10*elb{i}) M{i}{1}/10+M{i}{2}/5
 (M{i}{1}-11*M{i}{2})/(10*elb{i}) -M{i}{1}/5+9*M{i}{2}/10;
-M{i}{2}/10 -M{i}{1}*elb{i}/30 M{i}{2}/10 elb{i}*(M{i}{1}-3*M{i}{2})/30];
Ke{i}=Eb{i}*C{i}*B1{i}+Gb{i}*J{i}*B2{i}; % Build local beam stiffness matrix
Kg{i}=2*a{i}*B4{i}-Lh*B3{i}; % Build local geometric stiffness matrix
end
```

% 11. CALL LOCAL DECK ELEMENT STIFFNESS MATRIX

```
Kd=clocadeckmatrix(dn,del,nm2,nm,delm,delc,B3);
```

```
%Subroutine
function[Kd]=clocadeckmatrix(dn,del,nm2,nm,delm,delc,B3)
for i=1:dn
```

```
Ld{i}=nm2(del{i}(1,3),1)-nm2(del{i}(1,1),1); % Length of each deck element
b{i}=nm(del{i}(1,2),3)-nm(del{i}(1,1),3);     % Width of each deck element
    Kd1{i}=4*delm{i}*(b{i}*delc{i}^3/12)/(Ld{i}*b{i})*B3{i};
    Kd2{i}=2*delm{i}*(b{i}*delc{i}^3/12)/(Ld{i}*b{i})*B3{i};
% Local deck element stiffness matrix
    Kd{i}=[Kd1{i} Kd2{i};
           Kd2{i} Kd1{i}];
end
```

% 12. CALL GLOBAL STIFFNESS MATRICES

% 12.1 Call global beam stiffness matrix

```
%12.1.1 Call global beam element DoF
for i=1:en
dbel{i}=[1+2*(bel{i}(1,1)-1),2+2*(bel{i}(1,1)-1),1+2*(bel{i}(1,2)-1),2+2*(bel{i}(1,2)-1)];
end
%12.1.2 Call global beam elastic stiffness matrix
KE=vpa(zeros(2*nn,2*nn));
for h=1:en
    for i=1:4
        for j=1:4
            KE(dbel{h}(1,i),dbel{h}(1,j))=Ke{h}(i,j)+KE(dbel{h}(1,i),dbel{h}(1,j));
        end
    end
end
```

% 12.2 Call global geometric stiffness matrix

```
KG=vpa(zeros(2*nn,2*nn));
for h=1:en
    for i=1:4
        for j=1:4
KG(dbel{h}(1,i),dbel{h}(1,j))=Kg{h}(i,j)+KG(dbel{h}(1,i),dbel{h}(1,j));
        end
    end
end
```

% 12.3 Call global deck stiffness matrix

```
% 12.3.1 Call global deck element DoF
for i=1:dn
```

```
ddel{i}=[1+2*(del{i}(1,1)-1),2+2*(del{i}(1,1)-1),1+2*(del{i}(1,2)-1),2+2*(del{i}(1,2)-1),1+
2*(del{i}(1,3)-1),2+2*(del{i}(1,3)-1),1+2*(del{i}(1,4)-1),2+2*(del{i}(1,4)-1)];
end
% 12.3.2 Call global deck stiffness matrix
K2=zeros(2*nn,2*nn);
for h=1:dn
    for i=1:8
        for j=1:8
            K2(ddel{h}(1,i),ddel{h}(1,j))=Kd{h}(i,j)+K2(ddel{h}(1,i),ddel{h}(1,j));
        end
    end
end
```

% 13. Enforce boundary conditions

```
[num]=xlsread('input','Boundary condition');
bcn=num(1,2);   % Number of boundary conditions
for i=1:bcn
dof(i,1)=num(3+i,2);   % DoF that are restrained
end
K=double(KE+K2);         % Global elastic stiffness matrix
for i=1:bcn
K(dof(i,1),:)=0;
K(:,dof(i,1))=0;
K(dof(i,1),dof(i,1))=1;
KG(dof(i,1),:)=0;
KG(:,dof(i,1))=0;
End
K=double(K);
KG=double(KG);
```

% 14. RECOVER THE CRITICAL LOAD

```
 [V,D]=eig(K,KG)
% D is the matrix containing eigen value and V is the matrix containing eigen vector
```

Sample Output

Case Number 1 (Chapter 4)

Critical moment= 253 kNm

Buckling amplitude of angle of twist for beam 1

z coordinate (m)	Amplitude
0.0	0.00
1.0	-0.65
2.0	-0.77
3.0	0.00
4.0	-0.77
5.0	-0.65
6.0	0.00

Appendix B MATLAB PROGRAMME FOR THE SWAY MODEL

Sample Input

The sample example illustrated below is aimed for a twin-beam-deck assembly with 6 m beam span and 2 m deck span under mid-span concentrated loads.

System info:

NJ	NMat Beam	NSec Beam	NEl Beam	NMat Deck	NSec Deck	NEl Deck	NSupV	NSupLT
14	1	1	12	1	1	6	4	4

Note: definitions of the parameters are shown in the programme part.

Node info:

Node number	*x*-coordinate (m)	*z*-coordinate (m)
1	0.0	0.0
2	0.0	1.0
3	0.0	2.0
4	0.0	3.0
5	0.0	4.0
6	0.0	5.0
7	0.0	6.0
8	2.0	0.0
9	2.0	1.0
10	2.0	2.0
11	2.0	3.0
12	2.0	4.0
13	2.0	5.0
14	2.0	6.0

Element info:

Beam element number	Material type	Cross-section type
1	1	1
2	1	1
3	1	1
4	1	1
5	1	1
6	1	1
7	1	1
8	1	1
9	1	1
10	1	1
11	1	1
12	1	1

Deck element number	Material type	Cross-section type	Connectivity			
			1st joint	2nd joint	3rd joint	4th joint
1	1	1	1	2	8	9
2	1	1	2	3	9	10
3	1	1	3	4	10	11
4	1	1	4	5	11	12
5	1	1	5	6	12	13
6	1	1	6	7	13	14

Cross-section info:

Section type	I_{wyy} (m^4)	I_{www} (m^4)	J_w (m^4)	I_{wxx} (m^4)	I_{fyy} (m^4)	I_{fww} (m^4)	J_f (m^4)	I_{fxx} (m^4)	h_d (m)	b (m)	h (m)
1	0	0	0	0	2.4E-05	6.6E-07	8.9E-05	1.2E-03	0.038	0.6	0.57

Material info:

Material type	Ew (Pa)	Gw (Pa)	Ef (Pa)	Gf (Pa)	Ed (Pa)	k (N/m)
1	0	0	1.0E+10	4.7E+08	1.00E+10	2.0 E+06

Load info:

Beam element number	UDL live	UDL dead	Cl live	ClLive loading point	Cl2	Cl2 loading point	Cl3	Cl3 loading point	Mlive	Mlive loading point	M2	M2 loading point
1	0	0	0	0	0	0	0	0	0	0	0	0
2	0	0	0	0	0	0	0	0	0	0	0	0
3	0	0	**1**	**1**	0	0	0	0	0	0	0	0
4	0	0	0	0	0	0	0	0	0	0	0	0
5	0	0	0	0	0	0	0	0	0	0	0	0
6	0	0	0	0	0	0	0	0	0	0	0	0
7	0	0	0	0	0	0	0	0	0	0	0	0
8	0	0	0	0	0	0	0	0	0	0	0	0
9	0	0	**1**	**1**	0	0	0	0	0	0	0	0
10	0	0	0	0	0	0	0	0	0	0	0	0
11	0	0	0	0	0	0	0	0	0	0	0	0
12	0	0	0	0	0	0	0	0	0	0	0	0

Boundary conditions:

Pre-buckling	Node number	Vetical dis.	Rotation
1	1	1	0
2	7	1	0
3	8	1	0
4	14	1	0

Buckling boundary con.	Node number	Lateral dis.	First derivative	Angle of twist	First derivative
1	1	1	0	1	0
2	7	1	0	1	0
3	8	1	0	1	0
4	14	1	0	1	0

Programme Developed in Matlab

```
%1. READ INFO OF THE TWIN-BEAM-DECK ASSEMBLY
%1.1 Read system info
[NJ,NMatBeam,NSecBeam,NElBeam,NMatDeck,NSecDeck,NElDeck,NSupV,NSup
LT]=ReadSystemInfo();
-----------------------------------------------------------------------------------------------------------
% Subroutine
function[NJ,NMatBeam,NSecBeam,NElBeam,NMatDeck,NSecDeck,NElDeck,NSupV,NSup
LT]=ReadSystemInfo()
% Extract system info from Excel
[num]=xlsread('input2','System info');
NJ=num(1,1);                % Number of joints
NMatBeam=num(1,2);          % Number of beam material types
NSecBeam=num(1,3);          % Number of cross-section types
NElBeam=num(1,4);           % Number of beam elements in twin beams
NMatDeck=num(1,5);          % Number of deck material types
NSecDeck=num(1,6);          % Number of deck cross-section types
NElDeck=num(1,7);           % Number of deck elements
NSupV=num(1,8);             % Number of vertical supports
NSupLT=num(1,9);            % Number of lateral and torsional supports


%1.2 Read node info
[Coord]=ReadNodeCoordinate(NJ);
-----------------------------------------------------------------------------------------------------------
% Subroutine
function[Coord]=ReadNodeCoordinate(NJ)
% Extract node info from Excel
[num]=xlsread('input2','Nodes');
nn=num(1,2);                % Node number
% Build node coordinate matrix
for i=1:NJ
Coord(i,1)=num(i,2);    % First coordinate of node i
Coord(i,2)=num(i,3);    % Second coordinate of node i
end


%1.3 Read beam material info
[MatBeam]=ReadBeamMaterialInfo(NMatBeam);
-----------------------------------------------------------------------------------------------------------
% Subroutine
function[MatBeam]=ReadBeamMaterialInfo(NMatBeam)
```

```
% Extract beam material info from Excel
 [num]=xlsread('input2','Materials');
% Build beam material info matrix
for i=1:NMatBeam
MatBeam(i,1)=num(i,2);          % Modulus of elasticity of the web
MatBeam(i,2)=num(i,3);          % Shear modulus of the web
MatBeam(i,3)=num(i,4);          % Modulus of elasticity of the flanges
MatBeam(i,4)=num(i,5);          % Shear modulus of the flanges
end
```

%1.4 Read beam cross-section info

[SecBeam]=ReadBeamSectionInfo(NSecBeam);

```
% Subroutine
function[SecBeam]=ReadBeamSectionInfo(NSecBeam)
% Extract beam section info from Excel
[num]=xlsread('input2','Cross-section');
% Build beam section info matrix
for i=1:NSecBeam
SecBeam(i,1)=num(i,2);          % Moment of inertia of the web about its weak-axis
SecBeam(i,2)=num(i,3);          % Warping constant of the web
SecBeam(i,3)=num(i,4);          % Saint-Venant torsional constant for the web
SecBeam(i,4)=num(i,5);          % Moment of inertia of the web about its strong-axis
SecBeam(i,5)=num(i,6);          % Moment of inertia of the flanges about its weak-axis
SecBeam(i,6)=num(i,7);          % Warping constant of the flanges
SecBeam(i,7)=num(i,8);          % Saint-Venant torsional constant for the flanges
SecBeam(i,8)=num(i,9);          % Moment of inertia of the flanges about its strong-axis
end
```

%1.5 Read beam element info

[ElBeam]=ReadBeamElementInfo(NElBeam);

```
% Subroutine
function[ElBeam]=ReadBeamElementInfo(NElBeam)
% Extract beam element info from Excel
[num]=xlsread('input2','Element');
% Build beam element info matrix
for i=1:NElBeam
    ElBeam(i,1)=num(i,2);           % Element material type
    ElBeam(i,2)=num(i,3);           % Element cross-section type
```

```
    ElBeam(i,3)=num(i,4);              % First node of the element
    ElBeam(i,4)=num(i,5);              % Second node of the element
end
```

%1.6 Read deck material info

```
[MatDeck]=ReadDeckMaterialInfo(NMatDeck);
-----------------------------------------------------------------------------------------------------------
% Subroutine
function[MatDeck]=ReadDeckMaterialInfo(NMatDeck)
% Extract deck material info from Excel
[num]=xlsread('input2','Materials');
% Build deck material info matrix
for i=1:NMatDeck
    MatDeck(i,1)=num(i,6);       % Modulus of elasticity of the deck
    MatDeck(i,2)=num(i,7);       % Lateral stiffness of the deck-joint assembly
end
```

%1.7 Read deck cross-section info

```
[SecDeck]=ReadDeckSectionInfo(NSecDeck);
-----------------------------------------------------------------------------------------------------------
% Subroutine
function[SecDeck]=ReadDeckSectionInfo(NSecDeck)
% Extract deck section info from Excel
[num]=xlsread('input2','Cross-section');
% Build deck section info matrix
for i=1:NSecDeck
    SecDeck(i,1)=num(i,10);            % Deck board thickness
    SecDeck(i,2)=num(i,11);            % Deck board width
    SecDeck(i,3)=num(i,12);            % Beam height (an indicator of lateral restraint height)
end
```

%1.8 Read deck element info

```
[ElDeck]=ReadDeckElementInfo(NElDeck);
-----------------------------------------------------------------------------------------------------------
% Subroutine
function[ElDeck]=ReadDeckElementInfo(NElDeck)
% Extract deck element info from Excel
[num]=xlsread('input2','Element');
% Build deck element info matrix
```

```
for i=1:NElDeck
    ElDeck(i,1)=num(i,8);              % Element material type
    ElDeck(i,2)=num(i,9);              % Element section type
    ElDeck(i,3)=num(i,10);       % First node of the element
    ElDeck(i,4)=num(i,11);       % Second node of the element
    ElDeck(i,5)=num(i,12);       % Third node of the element
    ElDeck(i,6)=num(i,13);       % Fourth node of the element
end
```

%1.9 Read support info

[SupCodePre,SupCodeBuckling]=ReadBoundaryCon(NSupV,NSupLT);

```
% Subroutine
function[SupCodePre,SupCodeBuckling]=ReadBoundaryCon(NSupV,NSupLT)
% Extract support info from Excel
[num]=xlsread('input2','Boundary condition');
% Build vertical support matrix
for i=1:NSupV
    SupCodePre(i,1)=num(i,2);        % Node number
    SupCodePre(i,2)=num(i,3);        % Vertical movement (1=Yes, 0=No)
    SupCodePre(i,3)=num(i,4);        % Rotation
end
% Build lateral and twisting support matrix
for i=1:NSupLT
    SupCodeBuckling(i,1)=num(i,7); % Node number
    SupCodeBuckling(i,2)=num(i,8); % Lateral displacement
    SupCodeBuckling(i,3)=num(i,9);       % First derivative of lateral displacement
SupCodeBuckling(i,4)=num(i,10);     % Twist angle
    SupCodeBuckling(i,5)=num(i,11);      % First derivative of twist angle
end
```

%1.10 Read loading info

[ElForce]=ReadLoadingInfo(NElBeam);

```
% Subroutine
function[ElForce]=ReadLoadingInfo(NElBeam)
% Extract loading info from Excel
[num]=xlsread('input2','Loading');
% Build loading info matrix
for i=1:NElBeam
```

```
    ElForce(i,1)=num(i,2);          % UDL live load
    ElForce(i,2)=num(i,3);          % UDL dead load
    ElForce(i,3)=num(i,4);          % Concentrated load live
    ElForce(i,4)=num(i,5);          % Loading point of live concentrated load
    ElForce(i,5)=num(i,6);          % Concentrated load dead
    ElForce(i,6)=num(i,7);          % Loading point of dead concentrated load
    ElForce(i,7)=num(i,8);          % Concentrated load dead
ElForce(i,8)=num(i,9);          % Loading point of dead concentrated load
ElForce(i,9)=num(i,10);         % End moment live
    ElForce(i,10)=num(i,11);        % Live end moment loading point
    ElForce(i,11)=num(i,12);        % End moment dead
    ElForce(i,12)=num(i,13);        % Dead end moment loading point
end


%2. PRE-BUCKLING ANALYSIS
%2.1 Build structural pre-buckling elastic stiffness matrix and energy vector
%2.1.1 Create variables and matrices
-------------------------------------------------------------------------------------------------------
nn=0;                           % Used for counting number
aa=0;                           % Used for counting number
% Create pre-buckling elastic stiffness matrix (entries will be added subsequently)
KSPre=vpa(zeros(2*NJ,2*NJ));
% Create energy equivalent load vector for all the live loads (entries will be added
subsequently)
QSPreLive=zeros(2*NJ,1);
% Create energy equivalent load vector for all the dead loads (entries will be added
subsequently)
QSPreDead=zeros(2*NJ,1);

for i=1:NElBeam
%2.1.2 Call relevant info
-------------------------------------------------------------------------------------------------------
    % Call basic material and cross-section info
MT=ElBeam(i,1);             % Material type for element i
SecT=ElBeam(i,2);           % Cross-section type for element i
Ew=MatBeam(MT,1);  % Modulus of elasticity of the web
Ef=MatBeam(MT,3);           % Modulus of elasticity of the flanges
Iwxx=SecBeam(SecT,4);       % Moment of inertia of the web about strong-axis
Ifxx=SecBeam(SecT,8);       % Moment of inertia of the flanges about strong-axis
% Call transformed material and cross-section info
E=Ef;                       % Transformed modulus of elasticity
```

```
n2=Ew/Ef;                   % Ratio of the modulus of elasticity
Ixx=Ifxx+n2*Iwxx;           % Transformed beam moment of inertia about strong-axis
% Call the length for element i
    if Coord(i+nn,1)==Coord(i+1+nn,1)
            Lb=Coord(i+1+nn,2)-Coord(i+nn,2);
    else
            nn=nn+1;
            Lb=Coord(i+1+nn,2)-Coord(i+nn,2);
    end
    % Call element pre-buckling connectivity vector
    if Coord(i+aa,1)==Coord(i+1+aa,1)
            bel=[i+aa,i+aa+1];
    else
            aa=aa+1;
            bel=[i+aa,i+aa+1];
end
% Build beam element pre-buckling connectivity vector
BeamElConPre=[1+2*(bel(1,1)-1),2+2*(bel(1,1)-1),1+2*(bel(1,2)-1),2+2*(bel(1,2)-1)];

%2.1.3 Call stiffness matrix for element i
-------------------------------------------------------------------------------------------------------------
KElPre=E*Ixx/Lb^3*[12 6*Lb -12 6*Lb;
            6*Lb 4*Lb^2 -6*Lb 2*Lb^2;
            -12 -6*Lb 12 -6*Lb;
            6*Lb 2*Lb^2 -6*Lb 4*Lb^2];

%2.1.4 Calculate Fixed End reactions for live load in element i
-------------------------------------------------------------------------------------------------------------
    syms x
    %2.1.4.1 Store all the load info from loading info matrix
     UDLLive=ElForce(i,1);          % UDL live load
UDLDead=ElForce(i,2);           % UDL dead load
ClLive=ElForce(i,3);            % Concentrated load live
CoordClLive=ElForce(i,4);       % Loading point of live concentrated load
Cl2=ElForce(i,5);               % Concentrated load dead
CoordCl2=ElForce(i,6);          % Loading point of dead concentrated load
Cl3=ElForce(i,7);               % Concentrated load dead
CoordCl3=ElForce(i,8);          % Loading point of dead concentrated load
MLive=ElForce(i,9);             % End moment live
CoordMLive=ElForce(i,10);       % Live end moment loading point
M2=ElForce(i,11);               % End moment dead
CoordM2=ElForce(i,12);          % Dead end moment loading point
```

```
%2.1.4.2 Build energy equivalent load vector for live load
%2.1.4.2.1Build vector of Hermitian interpolation
    L1=1-3*x^2/Lb^2+2*x^3/Lb^3;
    L2=x-2*x^2/Lb+x^3/Lb^2;
    L3=3*x^2/Lb^2-2*x^3/Lb^3;
L4=x^3/Lb^2-x^2/Lb;
%2.1.4.2.2 Build energy equivalent load vector for UDL
    QElPreLive(1,1)=UDLLive*int(L1,0,Lb);
    QElPreLive(2,1)=UDLLive*int(L2,0,Lb);
    QElPreLive(3,1)=UDLLive*int(L3,0,Lb);
QElPreLive(4,1)=UDLLive*int(L4,0,Lb);
%2.1.4.2.3 Build energy equivalent load vector for concentrated loads
% Input loading point
    if CoordClLive==0
        x=0;                % distance from the first point of the element
    else if CoordClLive==1
        x=Lb;                    % distance from the first point of the element
        end
    end
    L11=eval(L1);
    L22=eval(L2);
    L33=eval(L3);
    L44=eval(L4);
    QElPreLive(1,1)=ClLive*L11+QElPreLive(1,1);
    QElPreLive(2,1)=ClLive*L22+QElPreLive(2,1);
    QElPreLive(3,1)=ClLive*L33+QElPreLive(3,1);
QElPreLive(4,1)=ClLive*L44+QElPreLive(4,1);

%2.1.5 Calculate Fixed End reactions for dead load in element i
-------------------------------------------------------------------------------------------------------------
%2.1.5.1 Build energy equivalent load vector for UDL
QElPreDead(1,1)=UDLDead*int(L1,0,Lb);
QElPreDead(2,1)=UDLDead*int(L2,0,Lb);
QElPreDead(3,1)=UDLDead*int(L3,0,Lb);
QElPreDead(4,1)=UDLDead*int(L4,0,Lb);
%2.1.5.2 Build energy equivalent load vector for concentrated load
% Input loading point for the first concentrated load (dead)
if CoordCl2==0
        x=0;                % distance from the first point of the element
else if CoordCl2==1
        x=Lb;               % distance from the first point of the element
        end
```

```
end
L11=eval(L1);
L22=eval(L2);
L33=eval(L3);
L44=eval(L4);
QElPreDead(1,1)=Cl2*L11+QElPreDead(1,1);
QElPreDead(2,1)=Cl2*L22+QElPreDead(2,1);
QElPreDead(3,1)=Cl2*L33+QElPreDead(3,1);
QElPreDead(4,1)=Cl2*L44+QElPreDead(4,1);
% Input loading point for the second concentrated load (dead)
if CoordCl3==0
        x=0;
else if CoordCl3==1
        x=Lb;
        end
end
L11=eval(L1);
L22=eval(L2);
L33=eval(L3);
L44=eval(L4);
QElPreDead(1,1)=Cl3*L11+QElPreDead(1,1);
QElPreDead(2,1)=Cl3*L22+QElPreDead(2,1);
QElPreDead(3,1)=Cl3*L33+QElPreDead(3,1);
QElPreDead(4,1)=Cl3*L44+QElPreDead(4,1);
clear x

%2.1.6 Build beam global elastic stiffness matrix
-----------------------------------------------------------------------------------------------------------
for i=1:4
        for j=1:4
KSPre(BeamElConPre(1,i),BeamElConPre(1,j))=KElPre(i,j)+KSPre(BeamElConPre(1,i),Bea
mElConPre(1,j));
        end
end

%2.1.7 Build global energy equivalent load vector for live loads
-----------------------------------------------------------------------------------------------------------
    for j=1:4
QSPreLive(BeamElConPre(1,j),1)=QElPreLive(j,1)+QSPreLive(BeamElConPre(1,j),1);
    end
QSPreLive(2*bel(1,(CoordMLive+1)),1)=MLive+QSPreLive(2*bel(1,(CoordMLive+1)),1);
```

```
%2.1.8 Build global energy equivalent load vector for dead loads
-----------------------------------------------------------------------------------------------------------
for j=1:4
QSPreDead(BeamElConPre(1,j),1)=QElPreDead(j,1)+QSPreDead(BeamElConPre(1,j),1);
end
QSPreDead(2*bel(1,(CoordM2+1)),1)=M2+QSPreDead(2*bel(1,(CoordM2+1)),1);
end

%2.2 Enforce pre-buckling support conditions
[KSPre,QSPreLive,QSPreDead]=CallEnforcingBoundaryConPre(NSupV,SupCodePre
,KSPre,QSPreLive,QSPreDead);
-----------------------------------------------------------------------------------------------------------
Subroutine
function[KSPre,QSPreLive,QSPreDead]=CallEnforcingBoundaryConPre(NSupV,SupCodePr
e,KSPre,QSPreLive,QSPreDead)
nn=0;                   % nn is the number of degree of freedoms (DoF) restrained
% Count the number of DoF restrained and store the relevant info into a vector
for i=1:NSupV
    for j=2:3
        if SupCodePre(i,j)==1
            nn=nn+1;                        .
            dof(nn,1)=1+2*(SupCodePre(i,1)-1)+j-2; % Vector storing the DoF restrained
        end
    end
end
% Enforce boundary conditions
for h=1:nn
    KSPre(dof(h,1),:)=0;
    KSPre(:,dof(h,1))=0;
    KSPre(dof(h,1),dof(h,1))=1;
    QSPreLive(dof(h,1),:)=0;
    QSPreDead(dof(h,1),:)=0;
end

%2.3 Solve for pre-buckling displacements
[VSPreLive,VSPreDead]=CallStructureNodalDisplacementVector(KSPre,QSPreLive,
QSPreDead);
-----------------------------------------------------------------------------------------------------------
Subroutine
function[VSPreLive,VSPreDead]=CallStructureNodalDisplacementVector(KSPre,QSPreLive,
QSPreDead)
VSPreLive=inv(KSPre)*QSPreLive;        % Pre-buckling displacement vector for live loads
```

```
VSPreDead=inv(KSPre)*QSPreDead;       % Pre-buckling displacement vector for dead loads
```

%2.4 Call element end moments

```
RDead=KElPre*VElPreDead-QElPreDead;   % Nodal reaction vector for live loads
RLive=KElPre*VElPreLive-QElPreLive;       % Nodal reaction vector for dead loads
MDead(i,1)=-(RDead(2,1)+MDead(i,1));       % moment of the first node in element i (dead)
MDead(i,2)=-(RDead(4,1)+MDead(i,2));    % moment of the second node in element i (dead)
MLive(i,1)=-(RLive(2,1)+MLive(i,1));          % moment of the first node in element i (live)
MLive(i,2)=-(RLive(4,1)+MLive(i,2));      % moment of the second node in element i (live)
```

%3. BUCKLING ANALYSIS

%3.1 Build beam elastic and geometric stiffness matrix

%3.1.1 Create variables and matrices

```
aa=0;                                 % Used for counting number
nn=0;                                 % Used for counting number
KeS=zeros(4*NJ,4*NJ);                 % Global structural elastic stiffness matrix
KgSDead=zeros(4*NJ,4*NJ);             % Global geometric stiffness matrix for dead loads
KgSLive=zeros(4*NJ,4*NJ);             % Global geometric stiffness matrix for live loads
for i=1:NElBeam
```

%3.1.2 Extract relevant information for element i

```
    %3.1.2.1 Call transformed Eb and Ibyy,Cw
    % Call basic material and cross-section info
    MT=ElBeam(i,1);             % Material type for element i
    SecT=ElBeam(i,2);           % Cross-section type for element i
    Ew=MatBeam(MT,1);           % Modulus of elasticity of the web
    Ef=MatBeam(MT,3);           % Modulus of elasticity of the flanges
    Gw=MatBeam(MT,2);           % Shear modulus of the web
    Gf=MatBeam(MT,4);           % Shear modulus of the flanges
    Iwyy=SecBeam(SecT,1);       % Moment of inertia of the web about weak-axis
    Ifyy=SecBeam(SecT,5); % Moment of inertia of the flanges about weak-axis
    Jw=SecBeam(SecT,3);         % Saint-Venant torsional constant of the web
    Jf=SecBeam(SecT,7);         % Saint-Venant torsional constant of the flanges
    Iwww=SecBeam(SecT,2);       % Warping constant of the web
    Ifww=SecBeam(SecT,6);       % Warping constant of the flanges
    % Call transformed material and cross-section info
    Eb=Ef;                      % Transformed modulus of elasticity
    Gb=Gf;                      % Transformed shear modulus
```

```
    n1=Gw/Gf;                    % Ratio of the shear modulus
    n2=Ew/Ef;                    % Ratio of the modulus of elasticity
    Ibyy=Ifyy+n2*Iwyy;          %Transformed beam moment of inertia about weak-axis
    Jb=Jf+n1*Jw;               % Transformed beam Saint-Venant torsional constant
    Cw=Ifww+n2*Iwww;           % Transformed beam warping constant
     %3.1.2.2 Call beam element length
     if Coord(i+nn,1)==Coord(i+1+nn,1)
            Lb=Coord(i+1+nn,2)-Coord(i+nn,2);
     else
            nn=nn+1;
            Lb=Coord(i+1+nn,2)-Coord(i+nn,2);
     end
     %3.1.2.3 Call beam element connectivity vector
     if Coord(i+aa,1)==Coord(i+1+aa,1)
            bel=[i+aa,i+aa+1];         %bel is the left and right joints of element i
       else
            aa=aa+1;
            bel=[i+aa,i+aa+1];
       end
BeamElCon=[1+4*(bel(1,1)-1),2+4*(bel(1,1)-1),1+4*(bel(1,2)-1),2+4*(bel(1,2)-1),3+4*(bel(
1,1)-1),4+4*(bel(1,1)-1),3+4*(bel(1,2)-1),4+4*(bel(1,2)-1)];

          %3.1.3 Build beam element elastic stiffness matrix
[Ke]=CallBeamElementElasticStiffnessMatrix(Eb,Ibyy,Gb,Jb,Cw,Lb);
-----------------------------------------------------------------------------------------------------------
%Subroutine
function[Ke]=CallBeamElementElasticStiffnessMatrix(Eb,Ibyy,Gb,Jb,Cw,Lb)
% Build submatrix B1 (defined in Chapter 4)
B1=1/(Lb^3)*[12 6*Lb -12 6*Lb;
    6*Lb 4*Lb^2 -6*Lb 2*Lb^2;
    -12 -6*Lb 12 -6*Lb;
    6*Lb 2*Lb^2 -6*Lb 4*Lb^2];
% Build submatrix B2 (defined in Chapter 4)
B2=1/(30*Lb)*[36 3*Lb -36 3*Lb;
    3*Lb 4*Lb^2 -3*Lb -Lb^2;
    -36 -3*Lb 36 -3*Lb;
    3*Lb -Lb^2 -3*Lb 4*Lb^2];
A=Eb*Ibyy*B1;
zero=zeros(4,4);
B=Gb*Jb*B2+Eb*Cw*B1;
% Build beam element elastic stiffness matrix
Ke=[A zero;
```

```
    zero B];

    %3.1.4 Store all the loading info
[UDLLive,ClLive,CoordClLive]=StoreLoadInfo1(i,ElForce);
-----------------------------------------------------------------------------------------------------------------
%Subroutine
function[UDLLive,ClLive,CoordClLive]=StoreLoadInfo1(i,ElForce)
UDLLive=ElForce(i,1);       % UDL live
ClLive=ElForce(i,3);        % Live concentrated loads
CoordClLive=ElForce(i,4);  % Loading point of live concentrated loads

    %3.1.5 Build beam element geometric stiffness matrix for dead load
[KgDead]=CallBeamElementGeometricStiffnessMatrixDead(i,MDead,Lb);
-----------------------------------------------------------------------------------------------------------------
%Subroutine
function[KgDead]=CallBeamElementGeometricStiffnessMatrixDead(i,MDead,Lb)
% Extract moment for the first node of element i
M1=MDead(i,1);
% Extract moment for the second node of element i
M2=MDead(i,2);
% Build submatrix B4 (defined in Chapter 4)
B4=[(11*M1-M2)/(10*Lb) 9*M1/10-M2/5 -(11*M1-M2)/(10*Lb) M1/5+M2/10;
    M1/10 Lb*(3*M1-M2)/30 -M1/10 Lb*M2/30;
    -(M1-11*M2)/(10*Lb) M1/10+M2/5 (M1-11*M2)/(10*Lb) -M1/5+9*M2/10;
    -M2/10 -M1*Lb/30 M2/10 Lb*(M1-3*M2)/30];
zero=zeros(4,4);
% Build beam element geometric stiffness matrix for dead load
KgDead=[zero B4;
    (B4)' zero];

    %3.1.6 Build beam element geometric stiffness matrix for live load
[KgLive]=CallBeamElementGeometricStiffnessMatrixLive(i,MLive,Lb,UDLLive);
-----------------------------------------------------------------------------------------------------------------
%Subroutine
function[KgLive]=CallBeamElementGeometricStiffnessMatrixLive(i,MLive,Lb,UDLLive)
% Extract moment for the first node of element i
M1=MLive(i,1);
% Extract moment for the second node of element i
M2=MLive(i,2);
% Build submatrix B3 (defined in Chapter 4)
B3=Lb/420*[156 22*Lb 54 -13*Lb;
    22*Lb 4*Lb^2 13*Lb -3*Lb^2;
```

```
    54 13*Lb 156 -22*Lb;
    -13*Lb -3*Lb^2 -22*Lb 4*Lb^2];
% Build submatrix B4 (defined in Chapter 4)
B4=[(11*M1-M2)/(10*Lb) 9*M1/10-M2/5 -(11*M1-M2)/(10*Lb) M1/5+M2/10;
    M1/10 Lb*(3*M1-M2)/30 -M1/10 Lb*M2/30;
    -(M1-11*M2)/(10*Lb) M1/10+M2/5 (M1-11*M2)/(10*Lb) -M1/5+9*M2/10;
    -M2/10 -M1*Lb/30 M2/10 Lb*(M1-3*M2)/30];
     % Extract load height info from Excel
     [num]=xlsread('input2','Load height');
a=num(1,1);                    % load height
zero=zeros(4,4);
% Build beam element geometric stiffness matrix for live load
KgLive=[zero (B4)';
    B4 a*UDLLive*B3];

%3.1.7 Build structural elastic and geometric stiffness matrix
[KeS,KgSDead,KgSLive]=CallStructuralElasticGeometricMatrix(Ke,KgDead,KgLive,Beam
ElCon,KeS,KgSDead,KgSLive);
-------------------------------------------------------------------------------------------------------
%Subroutine
function[KeS,KgSDead,KgSLive]=CallStructuralElasticGeometricMatrix(Ke,KgDead,KgLiv
e,BeamElCon,KeS,KgSDead,KgSLive)
for i=1:8
    for j=1:8
KeS(BeamElCon(1,i),BeamElCon(1,j))=Ke(i,j)+KeS(BeamElCon(1,i),BeamElCon(1,j));
            % Structural elastic stiffness matrix
KgSDead(BeamElCon(1,i),BeamElCon(1,j))=KgDead(i,j)+KgSDead(BeamElCon(1,i),Beam
ElCon(1,j));   % Structural geometric stiffness matrix for live load
KgSLive(BeamElCon(1,i),BeamElCon(1,j))=KgLive(i,j)+KgSLive(BeamElCon(1,i),BeamEl
Con(1,j));   % Structural geometric stiffness matrix for dead load
    end
end
end


%3.2 Build structure elastic stiffness matrix
%3.2.1 Create variables and matrices
-------------------------------------------------------------------------------------------------------
nn=0;                          % Used for counting number
KeS1=zeros(4*NJ,4*NJ);    % Stiffness matrix for the deck bending action
KeS2=zeros(4*NJ,4*NJ);    % Stiffness matrix for the deck-joint assembly
for i=1:NElDeck
```

```
    %3.2.1.1 Read relavent info
    % Call basic material and cross-section info
    MT=ElDeck(i,1);         % Material type for element i
SecT=ElDeck(i,2);       % Cross-section type for element i
Ed=MatDeck(MT,1);   % Modulus of elasticity
k=MatDeck(MT,2);      % Lateral stiffness of the deck-joint assembly
Hd=SecDeck(SecT,1);  % Deck board thickness
b=SecDeck(SecT,2);    % Deck board width
h=SecDeck(SecT,3);    % Beam height (an indicator of the lateral restraint height)
% Call beam element span
        if Coord(i+nn,1)==Coord(i+1+nn,1)
            Lb=Coord(i+1+nn,2)-Coord(i+nn,2);
        else
            nn=nn+1;
            Lb=Coord(i+1+nn,2)-Coord(i+nn,2);
        end
    % Call the deck span
Ld=Coord(ElDeck(i,5),1)-Coord(ElDeck(i,3),1);

%3.2.2 Call deck element pre-buckling connectivity vector
-----------------------------------------------------------------------------------------------------------
DeckElCon=[3+4*(ElDeck(i,3)-1),4+4*(ElDeck(i,3)-1),3+4*(ElDeck(i,4)-1),4+4*(ElDeck(i,
4)-1),3+4*(ElDeck(i,5)-1),4+4*(ElDeck(i,5)-1),3+4*(ElDeck(i,6)-1),4+4*(ElDeck(i,6)-1)];

%3.2.3 Call spring element connectivity vector
-----------------------------------------------------------------------------------------------------------
SpringElCon=[1+4*(ElDeck(i,3)-1),2+4*(ElDeck(i,3)-1),1+4*(ElDeck(i,4)-1),2+4*(ElDeck(i
,4)-1),1+4*(ElDeck(i,5)-1),2+4*(ElDeck(i,5)-1),1+4*(ElDeck(i,6)-1),2+4*(ElDeck(i,6)-1),3+
4*(ElDeck(i,3)-1),4+4*(ElDeck(i,3)-1),3+4*(ElDeck(i,4)-1),4+4*(ElDeck(i,4)-1),3+4*(ElDe
ck(i,5)-1),4+4*(ElDeck(i,5)-1),3+4*(ElDeck(i,6)-1),4+4*(ElDeck(i,6)-1)];

    %3.2.3 Build deck element elastic stiffness matrix
[Kd]=CallDeckElementElasticMatrix(Ed,Ld,Lb,Hd);
-----------------------------------------------------------------------------------------------------------
    % Subroutine
function[Kd]=CallDeckElementElasticMatrix(Ed,Ld,Lb,Hd)
B3=Lb/420*[156 22*Lb 54 -13*Lb;
    22*Lb 4*Lb^2 13*Lb -3*Lb^2;
    54 13*Lb 156 -22*Lb;
    -13*Lb -3*Lb^2 -22*Lb 4*Lb^2];
Kd1=4*Ed*Hd^3/(12*Ld)*B3;
Kd2=2*Ed*Hd^3/(12*Ld)*B3;
```

```
Kd=[Kd1 Kd2;
    Kd2 Kd1];

    %3.2.4 Build deck-joint stiffness matrix
[KSp]=CallSpringStiffnessMatrix(k,b,Lb,h);
-----------------------------------------------------------------------------------------------------------
    % Subroutine
function[KSp]=CallSpringStiffnessMatrix(k,b,Lb,h)
B3=Lb/420*[156 22*Lb 54 -13*Lb;
    22*Lb 4*Lb^2 13*Lb -3*Lb^2;
    54 13*Lb 156 -22*Lb;
    -13*Lb -3*Lb^2 -22*Lb 4*Lb^2];
KSp=k/b*[B3 -B3 h/2*B3' -h/2*B3';
    -B3' B3 -h/2*B3' h/2*B3';
    h/2*B3 -h/2*B3 h^2/4*B3 -h^2/4*B3;
    -h/2*B3 h/2*B3 -h^2/4*B3' h^2/4*B3];

%3.2.5 Build structure elastic stiffness matrix
-----------------------------------------------------------------------------------------------------------
KeS=KeS+KeS1;

%3.3 Enforce buckling support conditions
[KeS,KgSDead,KgSLive]=CallEnforceBoundarycondition(NSupLT,SupCodeBucklin
g,KeS,KgSDead,KgSLive);
-----------------------------------------------------------------------------------------------------------
% Subroutine
function[KeS,KgSDead,KgSLive]=CallEnforceBoundarycondition(NSupLT,SupCodeBucklin
g,KeS,KgSDead,KgSLive)
nn=0;                           % Used for counting number
for i=1:NSupLT
    for j=2:5
        if SupCodeBuckling(i,j)==1
            nn=nn+1;                    % Number of DoF restrained.
            dof(nn,1)=1+4*(SupCodeBuckling(i,1)-1)+j-2; % Vector with boundary info
        end
    end
end
% Enforce boundary conditions
for h=1:nn
    KeS(dof(h,1),:)=0;
    KeS(:,dof(h,1))=0;
    KeS(dof(h,1),dof(h,1))=1;
```

```
    KgSDead(dof(h,1),:)=0;
    KgSDead(:,dof(h,1))=0;
    KgSLive(dof(h,1),:)=0;
    KgSLive(:,dof(h,1))=0;
end

%3.4 Getting eigen-value and eigen-vector
[V,D]=eig((KeS+KgSDead),-KgSLive);
% D is the matrix containing eigen-value, V is matrix containing eigen-vector
```

Sample Output

Case Number 2 (Chapter 5)

Critical moment= 245 kNm

Buckling amplitude for beam 1:

z coordinate (m)	Lateral disp.	Angle of twist
0.0	0.00	0.00
1.0	0.42	0.42
2.0	0.81	0.81
3.0	1.00	1.00
4.0	0.81	0.81
5.0	0.42	0.42
6.0	0.00	0.00